2006

Analytical Potential Of Polymerized Liposomes Bound To Lanthanide Ions For Qualitative And Quantitative Analysis Of Proteins

Marina Santos
University of Central Florida

ANALYTICAL POTENTIAL OF POLYMERIZED LIPOSOMES BOUND TO LANTHANIDE IONS FOR QUALITATIVE AND QUANTITATIVE ANALYSIS OF PROTEINS

by

MARINA SANTOS
B.S. Universidad Nacional de Rosario, Argentina, 2001

A dissertation submitted in partial fulfillment of the requirements
for the degree of Doctor of Philosophy
in the Department of Chemistry
in the College of Sciences
at the University of Central Florida
Orlando, Florida

Fall Term
2006

Major Professor: Andres Campiglia

ABSTRACT

One of the intriguing features of biological systems is the prevalence of highly selective and often very strong interactions among different cellular components. Such interactions play a variety of organizational, mechanical, and physiological roles at the cellular and organism levels. Antigen-antibody complexes are representative examples of highly selective and potent interactions involving proteins. The marked specificity of protein-antibody complexes have led to a wide range of applications in cellular and molecular biology related research. They have become an integral research tool in the present genomic and proteomic era. Unfortunately, the production of selective tools based on antigen-antibody interactions requires cumbersome protocols.

The long term goal of this project explores the possibility of manipulating liposomes to serve as the chemical receptors ("artificial antibodies") against selected proteins. Cellular lipids (e.g., lipid rafts) are known to facilitate highly selective binding of proteins on cell membranes. The binding of proteins to cell membranes can be envisaged to be modulated via interactions between polar (charged) and non-polar head groups of lipids and the complementary amino acid residues of proteins. Their interaction is facilitated by a combination of van der Waals, electrostatic, hydrogen bonding and hydrophobic forces. A further interesting aspect of the above interaction is the "fluidity" of the membrane resident lipids, which can migrate from other regions to further enhance the complementary interactions of proteins on the initially "docked" membrane surface. With these features in mind, the end goal of this project is expected to deliver lipid-based chemical receptors "synthetically" designed against proteins to function as "artificial

antibodies". Protein sensing will be accomplished with lipid receptors assembled in templated polymerized liposomes.

The research presented here specifically focus on the analytical aspects of protein sensing via polymerized liposome vesicles. Lanthanide ions (Eu^{3+} and Tb^{3+}) are incorporated into polymerized liposome with the expectation to "report" quantitative and qualitative information on the interacting protein. Our proposition is to extract quantitative and qualitative information from the luminescence intensity and the luminescence lifetime of the lanthanide ion, respectively. A thorough investigation is presented regarding the analytical potential of these two parameters for protein sensing. Two chemometic approaches - namely partial least squares (PLS-1) and artificial neural networks (ANN) - are compared towards quantitative and qualitative analysis of proteins in binary mixtures.

ACKNOWLEDGMENTS

A special thanks to

My adviser, Dr. Andres D. Campiglia, for his guidance and support to succeed in the graduate research.

My committee members, Drs. K.D. Belfield, M.F. Quigley, T.L. Selby, and M. Sigman.

The members of Dr. Campiglia's research group: S. Yu, Dr. A.J. Bystol, M.M. Rex, Dr. A.F. Arruda, J.L. Grimland, H. Wang, and K. Vatsavai.

Dr. S. Mallik, S. Nadi, Dr. M.K. Haldar, and Dr. B.C. Roy for providing the complexes and liposomes samples.

Dr. H.C. Goicoechea for his input in the chemometrics studies.

And the Chemistry Department of University of Central Florida and the National Institute of General Medical Sciences and the National Science Foundation for financial support.

TABLE OF CONTENTS

LIST OF FIGURES

LIST OF TABLES

LIST OF ACRONYMS/ABBREVIATIONS

α……Confidence interval

A……Absorption

AFOM……Analytical Figures of Merit

Å……Angstrom (10^{-10} meters)

ANN……Artificial Neural Network

4As……4 Aminosalilicylic acid

5As……5 Aminosalilicylic acid

4As-EDTA-Tb^{3+}……4-Aminosalicylic acid ethylenediaminetetraacetate terbium(III)

5As-EDTA-Eu^{3+}……5-Aminosalicylic acid ethylenediaminetetraacetate europium(III)

CA……Carbonic Anhydrase

cps……Counts per Second

^{o}C……Degrees Celsius

EDTA……Ethylenediaminetetraacetic acid

ET……Energy Transfer

Eu……Europium

F……Fluorescence

g……Grams

HAS……Human Serum Albumin

IDA……Iminodiacetic acid

ICCD……Intensified charge fiber-coupled device

IC……..……..……Internal Conversion

ISC…….……..Intersystem Crossing

LOD……..…Limit of Detection

LDR……..Linear Dynamic Range

M……..……Molar

mL……...……..Milliliters (10^{-3} L)

nm……..……..…...Nanometer (10^{-9} meter)

Nd:YAG…….....……Neodymium:Yttrium-Aluminum-Garnet

NTA.....Nitrilotriacetic acid

N…….....Number of statistical samples

ppm…..……...……..Parts per million

PLS…..…….….Partial Least Squares

PMT…..……...…..Photomultiplier tube

PRESS.…….……..Prediction Error Sum of Squares

PCA…….…….....……..…Principal Component Analysis

R…….....……..…Correlation coefficient

RLS……...…….Rayleigh Light Scattering

RSD…….……..…Relative Standard Deviation

s…….……...……....……Seconds

S/B.……...……...…Signal to Background ratio

Std. Dv. ……..……...Standard Deviation

S…….…...……...……...……Singlet State

SS…….……..……Steady-State

TR…….……..……...…Time-Resolved

TREEM…….……..….Time-Resolved Excitation Emission Matrix

T…….…….....…….Triplet State

UV…….…….....……....Ultraviolet

VR……....……..……...…….....Vibrational Relaxation

vis…....……....……...Visible

CHAPTER 1. INTRODUCTION

Detection of peptides and proteins is important for diagnosis of diseases[1] and sensing of toxins,[2] bacteria, [3] and viruses.[4] The development of sensing schemes capable of recognizing specific proteins in complex biological matrixes remains an analytical challenge.[5-8] The limitations of popular clinical and laboratory tests have been extensively discussed in the literature.[9] The Lowry assay (1951) is often-cited for general use protein assay.[10] For some time it was the method of choice for accurate protein determination for cell fractions, chromatography fractions, enzyme preparations, and so on. This procedure is particularly sensitive because it employs two color-forming reactions (the Biuret reaction followed by the reduction of the Folin-Ciocalteu reagent). Despite its popularity, the Lowry assay presents many disadvantages.[11] Particularly, it is sensitive to interferences by many other compounds. In an attempt to overcome some of the problems of the method, other assays for protein have been proposed, such as the Bradford assay (1976), which relies on the protein binding to organic dyes with strong absorption in the ultraviolet (UV) and visible (vis) regions of the spectrum.[12] There are several disadvantages in the employment of the Bradford method, including different binding stoichiometry between the dye (Coomassie brilliant blue G-250) and different proteins,[11,13] and nonlinearity of color yield versus total protein content.[14] Most importantly, classical approaches do not address an inherent limitation of the assays, which is the measurement of absorption in the UV-vis range of the spectrum.[5] Spectroscopic measurements in the UV-vis are prone to strong matrix interference. Absorption and fluorescence from concomitants can certainly deteriorate limits of detection, reproducibility, and accuracy of analysis.[5]

Recent efforts concerning simple protein assays have been based on synchronous fluorescence spectroscopy,[9] Rayleigh light scattering (RLS)[15,16] spectroscopy, and near – infrared[17,18] spectroscopy. Fluorescence assays[9] rely on the spectral response of an organic fluorescence tag chemically attached to nanoparticles. Wavelength shifts on the fluorescence spectrum of the tag and intensity variations provide qualitative and quantitative information on the interacting protein, respectively. RLS methods are based on a similar principle but extract their information from synchronous spectra, i.e. spectra recorded at zero nm difference between excitation and emission wavelengths.[15] The near-infrared approach[17,18] takes advantage of vibrationally resolved spectra with fingerprint information for protein identification. Because infrared transitions provide inherently weak spectral bands, peak assignment for qualitative and quantitative purposes is made possible with chemometric approaches that minimize spectral interference from sample contaminants. Although these approaches are rapid, simple and highly sensitive, their selectivity for the direct and accurate determination of target proteins in complex samples is still an open question.

Our approach to protein detection takes advantage of the luminescence properties of lanthanide ions, particularly Eu^{3+} and Tb^{3+}, incorporated into polymerized liposomes. The long-lived luminescence of Eu^{3+} and Tb^{3+} is a good match to time-resolved (TR) techniques, which discriminate against the well-known short-lived fluorescence background of biological samples. The polymerized liposomes offer a lipophilic platform for protein interaction with the lanthanide ion.[19] The expectation from the lanthanide ion is to report qualitative and quantitative information on the interacting protein(s). Quantitative analysis is based on the linear relationship between the luminescence signal of the liposome and protein concentration. Qualitative analysis is based on the luminescence lifetime of the liposome. Distinct luminescence lifetimes upon

protein-liposome interaction make feasible the qualitative analysis of binary mixtures of proteins by using chemometric approaches.

1.1 General properties of lanthanides

The lanthanide ions are essentially spherical, and their *4f* orbitals may be partially filled.[20] The *4f* orbitals are, for the most part, not available for chemical bonding and are sufficiently shielded from the environment by the outer core 5*s* and 5*p* electrons. Therefore, stabilization due to crystal field effects is rarely more than a few hundred cm^{-1}.[20] Eu^{3+} and Tb^{3+} posses large ionic radii (0.95 Å and 0.938 Å) meaning that the charge to radius ratio (ionic potential) is relatively low which results in a very low polarizing ability. This, naturally, is reflected in the predominantly ionic character in the metal-ligand bonds. A second major effect of the large ionic radii is to affect the coordination number of the lanthanide complexes. These two factors finally result in complexes which generally have coordination numbers in excess of six. In fact, the most common co-ordination numbers of lanthanides are eight and nine.[20]

1.2 Luminescence of lanthanides in solution

The majority of transition metal ions absorb light in the UV-vis range of the electromagnetic spectrum.[21] A strong coupling of their *d*-electron excited states with the environment via the ligand field offers an efficient de-excitation mechanism, therefore only a few can return to the ground state through photon emission.[21] Conversely, all of the trivalent lanthanide ions above lanthanum are known to luminesce. The most important difference from other transition metals is that lanthanide's excited states involve promotion of one of the *4f*

electrons, and these electrons are shielded by the presence of electrons in the 5th and, for several, the 6th shell as well.[21]

The energy of the $4f^n$ configuration of a lanthanide ion is a result of the interelectronic repulsion, spin-orbit coupling, and the coordinating environment (ligand field).[21] Electronic transitions between *4f* levels are forbidden by the Laporte rule because they involve no change in parity. Nevertheless, strong spin-orbit interaction and interaction of the ligand field causing mixing of the electronic states make these transitions possible, with commonly weak molar extinction coefficients.[21]

Figure 1.1 shows the energy level diagram for Eu^{3+} and Tb^{3+}. Both lanthanide ions have energy gaps that allow emission in the vis region of the spectrum.[22] Their emission patterns reflect the probability of the various transitions. For Eu^{3+} ions, the major allowed transitions are from the $^5D_0$ to the ^7F manifold, and they occur within the 570-730 nm region of the electromagnetic spectrum. The strongest transitions are the $^5D_0 \rightarrow {}^7F_1$ (~ 594 nm) and $^5D_0 \rightarrow {}^7F_2$ (~ 616 nm), whose relative intensities are very sensitive to the ligand environment. The $^5D_0 \rightarrow {}^7F_{0,3,5}$ transitions are severely prohibited and are either weak or unobservable.[22]

The lowest lying level of the first excited-term multiplet of Tb^{3+} is $^5D_4$. Transitions between the $^5D_4$ and the $^7F_6$, $^7F_5$, $^7F_4$, and $^7F_3$ levels usually give rise to four emission bands in the 450-650 nm spectral region .[22]

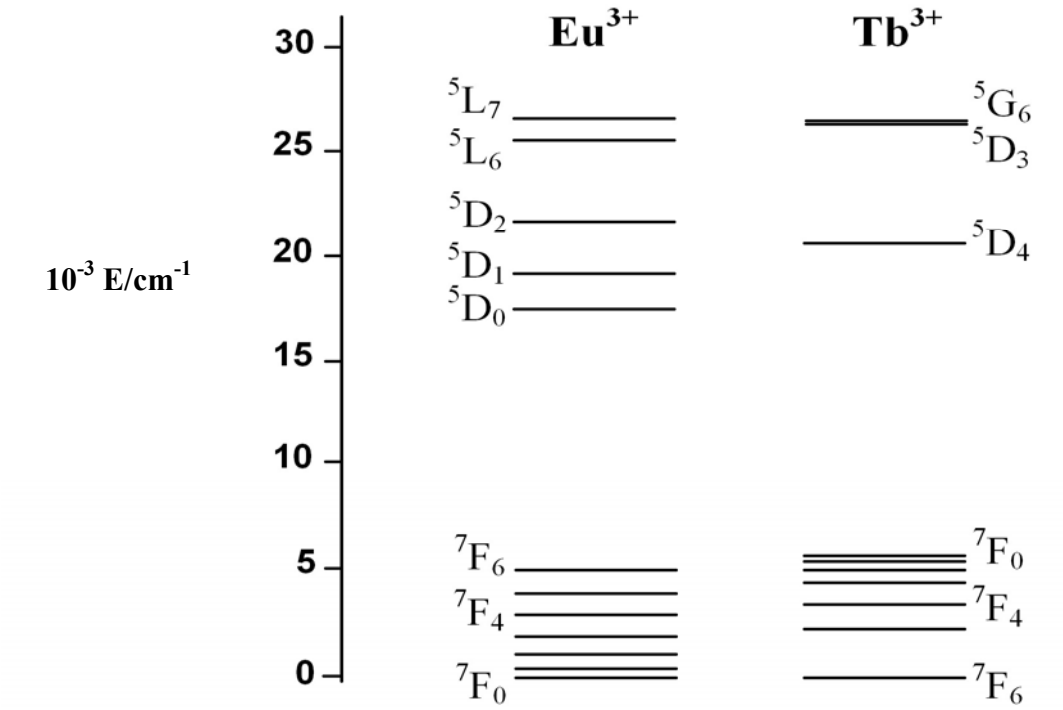

Figure 1.1 The lower energy levels of Eu^{3+} and Tb^{3+}.

1.3 Luminescence of lanthanides in biological samples

Biological samples exhibit short-lived fluorescence emission compared to the long luminescence lifetimes that may be observed for Eu^{3+} and Tb^{3+}. The long-lived emissions of lanthanide ions allow the use of TR techniques in which measurement of emission is started after an initial delay (Figure 1.2). During this delay time all the background fluorescence and light scattering dissipate.[21,23] The luminescence decay is distinctly reproducible, therefore the measured emission intensity over the integration time (t_g) is directly proportional to the concentration of lanthanide. Technically, any luminescent molecule possessing an appropriate long phosphorescent lifetime could be used for this purpose. Nevertheless, deoxygenated solutions and low temperatures are usually required in order to observe the long-lived

phosphorescence emission. On the contrary, the long-lived luminescence of lanthanides can be observed in the presence of oxygen at room temperature.[23,24]

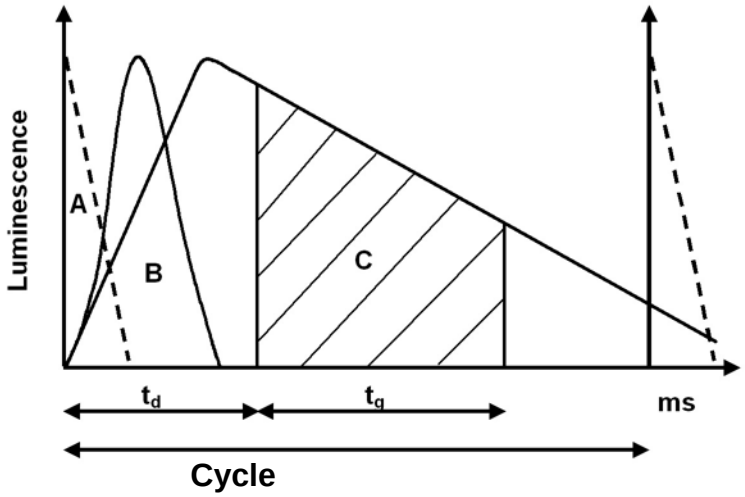

Figure 1.2. Representation of a cycle of a pulsed-source TR spectrofluorimeter.

Source pulse (A); short-lived fluorescence emission (B); long-lived luminescence emission (C); t_d, delay time; t_g, gate time.

Other characteristics that encourage the use of lanthanides to analyze biological samples is that the lanthanide's emission bands are predominantly narrow and they hardly shift upon environmental changes. In addition, because large Stokes shifts are observed in the luminescence of lanthanides, spectral overlap between its emission bands with absorption bands from other components of the sample is unlikely.[23]

1.4 Sensitized emission

Offsetting the advantage of time-resolved capability and spectral regions with potentially lower interference is the fact that lanthanide emission is quite weak as a result of low molar

extinction coefficients (in general lower than 1 M^{-1} cm^{-1}). The low magnitude of these coefficients is because the lanthanide's absorption involves states of the same f^n configuration. This results in excited states that are not readily populated. Sensitized emission supplies a practical solution to this setback.[22]

Essentially, a ligand incorporates a chromophore (antenna) which strongly absorbs energy at an appropriate wavelength and transfers its excitation energy to the metal ion which, in accepting this energy, becomes excited to the emissive state. If the molar absorption coefficient of the antenna is high and the energy transfer process occurs efficiently, the "effective" molar absorption coefficient of the metal is greatly increased and intense luminescence from the lanthanide occurs.[21]

The energy transfer process is favored by a short distance between the cation and the antenna. Two types of processes can be observed: *Intramolecular energy transfer* takes place when the antenna is chelated to the lanthanide ion. *Intermolecular energy transfer* occurs when a non-chelated organic molecule in solution transfers its energy to the lanthanide ion.[22]

The energy transfer process (Figure 1.3) begins with the absorption of a photon by the antenna. Upon absorption of electromagnetic radiation (A), the organic molecule can pass from the ground state to a higher energy excited state (S_1, S_2). Then the excited molecule typically releases the extra vibrational energy to reach the lowest vibrational level of the first excited state (S_1) through vibrational relaxation (VR).[24] Normally, the excited molecule at this point has three possibilities: return to the ground state through internal conversion (IC) without the emission of a photon; by the emission of a photon in a process called fluorescence (F); or undergo an intersystem crossing (ISC) phenomenon and pass to the triplet state (T).[24] In the presence of lanthanides, there are two possibilities of energy transfer from the organic molecule to the

lanthanide: from its singlet state (ET(s)) and from its triplet state (ET(t)).[25] For the energy transfer process to be effectively accomplished, parallel radiant and non-radiant transitions should be minimized.[21]

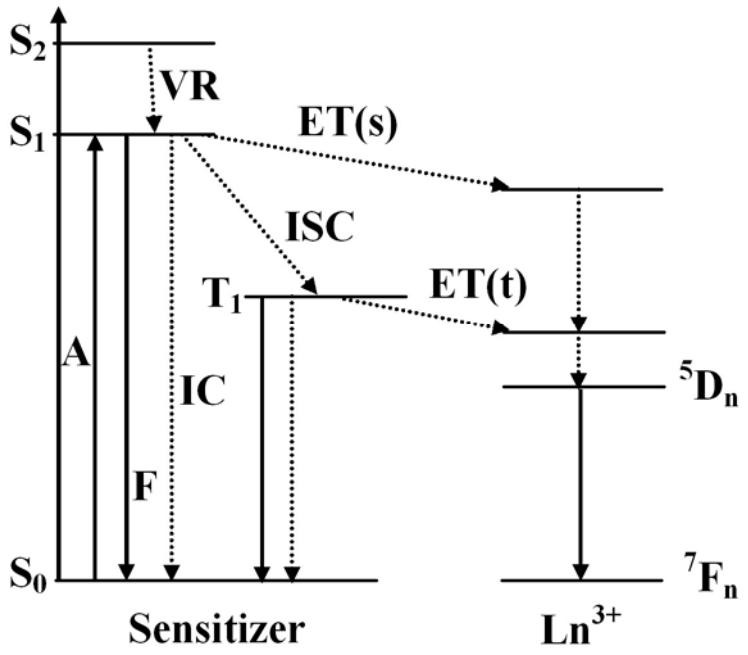

Figure 1.3. Possible energy transfer pathways.

The recommended selection criterion for intramolecular energy transfer between an organic sensitizer and a lanthanide ion is the observation of the fluorescence spectra of the antenna overlapping the excitation spectra of the lanthanide.[26] Experimentally, the occurrence of energy transfer (contrasting to direct lanthanide ion excitation) may well be explored by recording a luminescence excitation spectrum, in which the emission intensity at a given wavelength is monitored as a function of the excitation wavelength.[23] The selected emission intensity coincides with the emission maximum wavelength of the metal (*e.g.* 616 nm for Eu^{3+},

545 nm for Tb^{3+}). The resultant excitation spectrum shows the band or bands responsible for lanthanide luminescence. When exciting the lanthanide at this excitation wavelength in the absence of the antenna, its luminescence intensity is much lower (if any) than in the presence of the sensitizer.

1.5 Polymerized liposomes for protein sensing

Liposomes are spherical, bilayer assemblies of lipids with aqueous interiors and exteriors (Figure 1.4).[28] They can be prepared in a variety of sizes, and compounds can be encapsulated in the aqueous interior. Because of the ease of preparation and biocompatibility, liposomes have found many medical and non-medical applications.[29,30] Most of the medical applications are in drug delivery, especially when active targeting and triggered release are needed.[29,31]

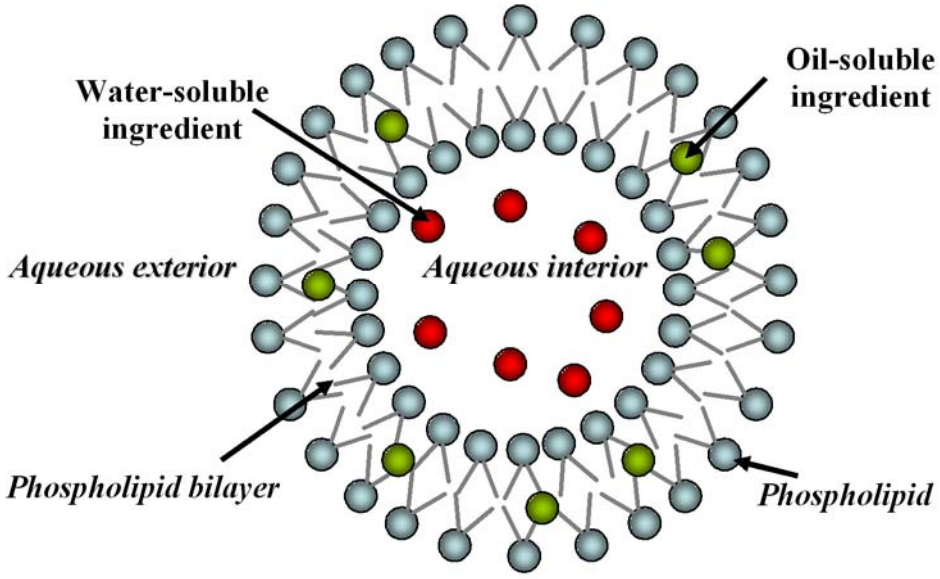

Figure 1.4. Schematic of a liposome.

Liposome-based protein sensing systems often use non-polymerizable liposomes[2] and rely on organic fluorophores. Polymerized liposomes with lanthanide ions have been extensively used as magnetic resonance contrast agents,[32] but their potential to detect proteins remains unexplored. Unlike unpolymerized vesicles, proteins cannot insert into the lipid bilayer of polymerized liposomes. Instead, they interact with the outer lipid layer of the vesicle via metal-ligand[33,34] and receptor-ligand[35,36] interactions.

The lipids composing polymerized liposomes usually contain diacetylene in two acyl chains.[37] Upon UV light (254 nm) irradiation at 0^{o}C, diacetylenes link together and form a polymer backbone made up of conjugated single and multiple carbon bonds. The polymerization is monitored by observing a reduction of the absorption for the dialkyne (240 nm). The resultant polymerized liposomes are stable at room temperature for more than a month.[38]

Because polymerized liposomes are appreciably more stable than their non-polymerized counterparts, they provide more robust platforms for protein sensing. We investigate the detection of proteins using luminescence property of lanthanide ions on the surface of polymerized liposomes (Figure 1.5).[38] Many lanthanide ions are incorporated on the surface of the liposomes. For simplicity's sake, only one lanthanide ion is shown on Figure 1.5.

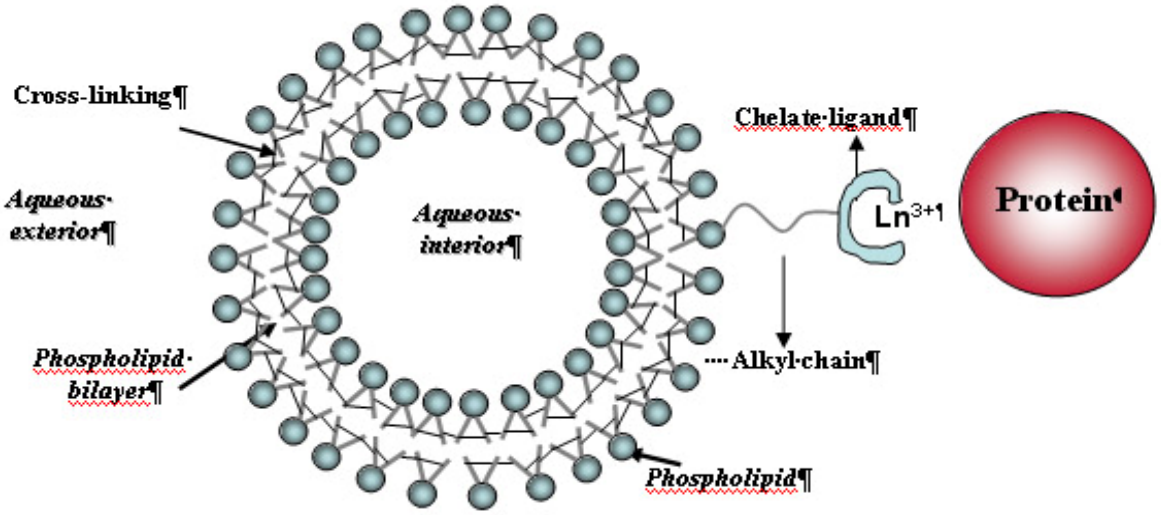

Figure 1.5. Schematic of a polymerized liposome incorporating lanthanide ions.

Sizes of chelate ligand, lanthanide, and protein had been magnified for clarity.

1.6 Multivariate calibration

1.6.1 Introduction

Univariate signals are analytical responses that are measured in an instrumental method as a function of a unique controlled variable. Univariate calibration is based upon the building of a relationship between two variables, **x** and **y**, such that **x** is employed to predict **y**. Multivariate signals are measured as a function of two or more controlled variables. Therefore, the information that might be obtained from univariate signals is limited compared to the greater possibilities that multivariate signals have.[39,40]

Applying multivariate calibration methods,[39,40] it is possible to obtain quantitative information from non-selective data, allowing the simultaneous determination of several components in complex matrices.[41-46] Univariate methods usually require complex processes

previous to the acquisition of signal (generally separation procedures). These time-consuming processes might cause the contamination of samples, and in most cases the quantitative determination of only one component from the complex matrix is possible. Alternatively, multivariate calibration methods allow the analysis of more than one compound of interest in multifaceted real systems with a more direct approach. Sample pretreatment is narrowed to a minimum consequently reducing the time of analysis, both aspects of great importance in routine or control analysis on a large quantity of analogous samples.[47]

The common procedures in multivariate calibration are based in the production and storage of signals belonging to a group of well-known samples that contain the same compounds that are desired to be determined; optimization of the model of calculus using appropriate variables that affect the system and finally, prediction of the problem samples of unknown concentration.[39,48]

Different types of analytical signals can be used: absorption spectra, molecular excitation or emission, chromatographic signals, etc. Such signals are mathematically manipulated in order to obtain the necessary information about the concentration of the components. This process is called ***calibration***.[39,48]

A model of calculus that satisfies the prediction expected from real samples should lean on an adequate set of calibration.[39,48] Such calibration set ought to contain mixtures of samples of known concentration and the concentrations of the compounds should encompass the possible unknowns. During the calibration process, the number and concentration of every component that will be determined should be specified in each one of the calibration samples. Also, the region of signals that will be used in the analysis should be selected. Once the calibration model is created, samples of unknown concentration can be resolved. It is not necessary to specify

either the content or the nature of interferences present in the sample because its influence on the corresponding analytical signals will be implicitly gathered in the calculus model, making possible its modulation if they were present in the real samples to analyze.[39,48]

Initially, a behavior pattern between two groups of variables, ***y = f(x)***, is desired in the calibration stage. The purpose is to find the relationship between them through a mathematical model that should fit the group of known-concentration samples, the calibration set. Such set must generate correct results and in order to do that, it has to contain at least as many samples as components to be determined, and usually, many more samples. Using mixtures of components in the construction of the calibration set makes possible the modulation of certain interactions in solution through a multivariate method.[39]

The ***prediction*** stage consists on the prediction of the value of the independent variables in a group of samples, prediction set, after obtaining the corresponding dependent variables.[39]

1.6.2 Calibration methods

1.6.2.1 Principal components analysis

Principal Component Analysis (PCA) is a useful statistical technique for finding patterns in data of high dimension, and expressing them in such a way as to highlight their similarities and differences.[49-51] The application of PCA to spectral decomposition can be summarized indicating the steps performed over the calibration set. First, the mean spectrum is calculated by averaging the intensity values at each wavelength of the samples of the calibration set. Then, the mean spectrum is subtracted from each spectrum of the calibration set. This produces a data set whose mean is zero. These difference spectra receive the name of *loading vectors.* The

covariance matrix of the data set is calculated and the eigenvectors and eigenvalues of the matrix are obtained. These are rather important, as they provide information about the patterns in the data. The eigenvector with the highest eigenvalue is the principal component of the data set and corresponds to the greatest variance in the data set.[49-51]

In general, once eigenvectors are found from the covariance matrix, the next step is to order them by eigenvalue, highest to lowest. The components of lesser significance (low eigenvalues) can be ignored. If some components are left out, the final data set will have lesser dimensions than the original. A *feature vector* is constructed by taking the eigenvectors that are desirable to retain, and forming a matrix with these eigenvectors in the columns.[49-51]

The new data set is derived by taking the transpose of the *feature vector* and multiplying it on the left of the original data set, transposed. This gives the original data solely in terms of the chosen vectors. The eigenvectors are the weightings which, when applied to the original data, obtain *scores* for the observations. A large positive or negative value (score) indicates a variable that is correlated, either in a positive or a negative way, with the component. The resulting spectra replace the original data and after that, the first step comes again and the whole process is repeated. Thus, any spectrum of a sample can be recreated and at the end, the spectra can be represented by their own *scores* instead of the data.[49-51]

The difference between the original spectrum and the spectrum reconstructed is the "residuum" spectrum. When the residuum is summed across the wavelength, a number is obtained: the residual.[49-51] The following method, Partial Least Squares (PLS), utilizes a step of PCA in the spectral decomposition.

1.6.2.2 Partial least squares regression

PLS has become the standard for multivariate calibration because of the quality of the calibration models, the ease of implementation, and the availability of commercial software.[52-54] In addition, PLS uses full data points, which is critical for the spectroscopic resolution of complex mixtures of analytes. It allows a rapid determination of components, usually with no need for prior separation.[48]

The PLS regression method is based in the analysis using PCA, but PLS modeling relies on a simultaneous fit of both response and concentration matrix.[48] Basically, the PLS algorithm finds components from the concentration matrix that are also relevant for the signal matrix. The calibration spectra can be represented for either the PCA or PLS model as follows[55]:

$$\mathbf{A} = \mathbf{TB} + \mathbf{E_A} \tag{1.1}$$

where **A** is the $m \times n$ matrix of calibration spectra. **T** is an $m \times h$ matrix of intensities (or scores) in the new coordinate system of the h PLS or PCA *loading vectors* for the m sample spectra. **B** is a $h \times n$ matrix with the rows of **B** being the new PLS or PCA basis set of h *loading vectors*. $\mathbf{E_A}$ is the $m \times n$ matrix of spectral residuals not fit by the best PLS model. The intensities in the new coordinate system are treated as linearly related to concentrations. The new set of *loading vectors* is the result of linear combinations of the original calibration spectra. The amounts (i.e., intensities) of every *loading vector* that are necessary to rebuild each calibration spectrum are the *scores*.[55]

The spectral intensities (**T**) in the new coordinate system can be related to concentrations with a separate inverse least-squares analysis. The following set of equations is solved by least squares[55]:

$$\mathbf{c} = \mathbf{T}\mathbf{v} + \mathbf{e_c} \tag{1.2}$$

Here **c** is the $m \times 1$ vector of concentrations of the analyte of interest in the m calibration samples, **T** is the matrix of scores (intensities) from PLS or PCA spectral decomposition in equation (1.1), **v** is the $h \times 1$ vector of coefficients relating the scores to the concentrations, and $\mathbf{e_c}$ is the $m \times 1$ vector vector of concentration residuals not fit by the model.[55]

The least-squares solution for **v** has the form:

$$\mathbf{v} = (\mathbf{T'T})^{-1}\mathbf{T'c} \tag{1.3}$$

The PLS algorithm obtains loading vectors in order that more predictive information is positioned in the first factors by using concentration information to obtain the decomposition of the spectral matrix **A** in equation (1.1). Concentration-dependent *loading vectors* are produced (**B**) and the calculated scores (**T**) are subsequently associated to the concentrations or concentration residuals after each *loading vector* is computed. As a result, in theory, superior predictive capacity is forced into the early PLS *loading vectors*.[55]

1.6.2.3 PLS validation.

One of the hardest steps in using PLS is determining the right number of *loading vectors* to employ to model the data. As more vectors are calculated, they are arranged by the degree of importance to the model. Eventually the *loading vectors* will start to model the system noise.[48]

The former vectors in the model are presumably to be the ones associated to the components of interest, while later vectors usually have less information that is valuable for predicting concentration.[55] In fact, if these vectors are included in the model, the predictions can actually be worse than if they were ignored altogether. Thus, decomposing spectra with these procedures and opting for the correct amount of loading vectors is a very successful way of filtering out noise. Models that incorporate more vectors than are in fact required to predict the constituent concentrations are known as *overfit*.[55] On the other hand, if too few vectors are used to build the model, the prediction accuracy for unknown samples will deteriorate since not enough terms are being used to model all the spectral variations that compose the constituents of interest. Models that do not have enough factors in them are called *underfit*.[55] Hence, it is of chief importance to define a model that contains enough vectors to properly model the components of interest without adding too much contribution from the noise.

Several statistical criteria can be applied in order to avoid *over-* and *underfitting*. Most specialized bibliography suggests the determination of a prediction error sum of squares (PRESS) for every possible *loading vector*. Tracking the PRESS value the optimum number of components to use can be established[55]:

$$\text{PRESS} = \sum_{j=1}^{m}\sum_{i=1}^{l}\left(\hat{C}_{i,j} - C_{ij}\right)^2 \qquad (1.4)$$

In the above equation, m is the number of samples in the calibration set; l is the number of components in the mixture, $\hat{C}_{i,j}$ is the matrix of predicted sample concentrations from the model; and $C_{i,j}$ is the matrix of known concentrations of the samples. The smaller the PRESS value, the better the model is capable to predict the concentrations of the calibrated constituents.[55]

Experimentally, there are several methods that can be used to calculate the PRESS value. The *cross validation* procedure is one of the most effectives[48]:

1) A number of samples (generally one) are selected, and the corresponding spectra (spectrum) and concentration data are eliminated from the calibration set. The *loading vector* counter is set to i=1.
2) The remaining samples of the calibration set are used to execute the decomposition and calibration calculations for *loading vector* 1.
3) The concentration(s) of the left out sample(s) are predicted by means of the calibration equation from Step 2 and PRESS(i) is calculated.
4) The *loading vector* counter is incremented (i = i+1) and the calculations are repeated from Step 2 until all desired *loading vectors* (i = f) have been calculated and predicted.
5) The previously removed sample data is placed back into the training set and a different sample (or group) is selected. Step 1 is performed again and the calculations repeated. As each sample is left out, the calculated squared residual error is added to all the previous PRESS values. The process is repeated until all samples have been removed and predicted at least once.

By calculating the PRESS value for a model using all possible *loading vectors* (i.e., first with 1 *loading vector*, then 2, 3, etc.) and plotting the results a very clear trend should emerge.[55] Employing the number of factors (h^*) which yields a minimum in PRESS can lead to some overfitting. A good criterion to select the best model engages the contrast of PRESS from models with fewer than h^* factors. The chosen model is the one with the smallest number of factors such that PRESS for that model is not significantly greater than PRESS for the model with h^* factors (the **F** statistic is used to make the significance determination).[55] Application of this criterion yields more cautious PLS models using fewer factors and alleviates the overffiting setback.[55]

Cross validation is the only validation technique that can provide complete outlier detection for the calibration data set.[48] Given that each sample is removed from the models during the cross validation process, it is possible to calculate how well the spectrum matches the model by calculating the spectral reconstruction and comparing it to the original calibration spectrum (via the spectral residual). If the predicted concentrations for a single sample are far off and the spectrum does not match the model very well but the rest of the data works just fine, the sample is probably an outlier. Recognizing and eliminating outlier samples from the calibration set should always improve the predictive capability of the model.[48]

1.6.2.4 Artificial neural network (ANN)

ANN can be described as a comparison with a black box encompassing plentiful inputs and outputs which maneuver by means of a large number of mostly connected simple arithmetic units.[56-57] The method works best if the dependence between inputs and outputs is non-linear.[58] ANN estimate relationships between the input variables (independent variables) and the output

variables (dependent variables).[58-60] The information is distributed among multiple cells (nodes) and connections between the cells (weights). Figure 1.6 displays a model with four input variables x_1, x_2, x_3, x_4 and a single output variable y.[60]

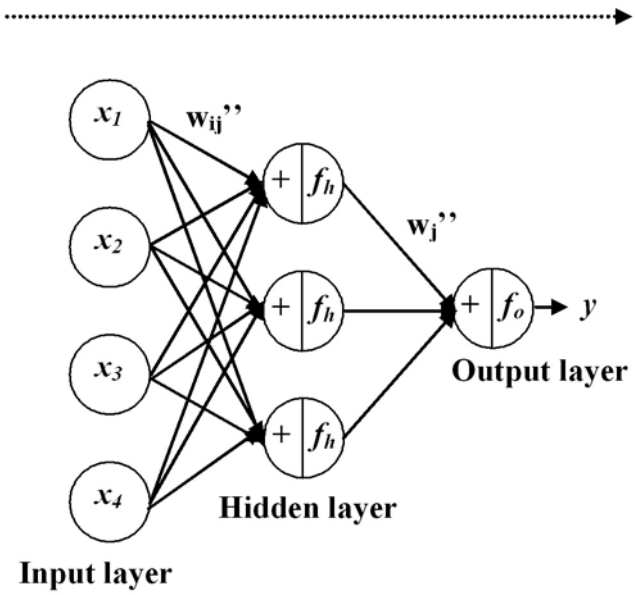

Figure 1.6. Forward Pass in ANN training.

The independent variables are offered to the ANN at the input layer and subsequently weighted by the connections w_{ij}' among the input and hidden layer. Hidden layer nodes accept simultaneously weighted signals from input nodes perform two subsequent tasks: first, a summation of the weighted inputs; and second, a projection of this sum on a transfer function f_h, to create and activation.[60] Consecutively, hidden nodes activations are weighted by the connections w_j'' involving the hidden and output layer and forwarded towards the nodes of the output layer.[60-62] Likewise to hidden nodes, output nodes execute a summation of arriving weighted signals and project the sum on their particular transfer function f_o. Figure 1.6 shows a

single dependent variable *y* that is modeled and the output layer has only one node. The output of this node can be expressed as[60]:

$$\hat{y} = f_o\left[\theta'' + \sum_{j=1}^{nh} w_j'' f_h\left[\sum_{i=1}^{nd} w_{ij}' x_i + \theta'\right]\right] \tag{1.5}$$

Here, *nd* and *nh* are the number of input variables and hidden nodes, respectively, θ' and θ'' are the biases. ANN are defined by sets of adjustable parameters (w'_{ij}, w''_j, θ', and θ'') defined by an algorithm, not by the user. These parameters are determined with an iterative procedure named "training". First, initial random values are ascribed to these adjustable parameters, and then training begins occurring in two steps.[60] Initially, a forward pass (Figure 1.6) is carried out in the course of the ANN with a set of training samples with known experimental response *y*. After the pass, the error between experimental and expected responses is computed and employed to tune every weight of the ANN, in a back-propagation step[60] (Figure 1.7). After that, a new forward pass is achieved with the training samples and the optimized parameters. The entire procedure is repeated until an acceptable low error is attained.[60]

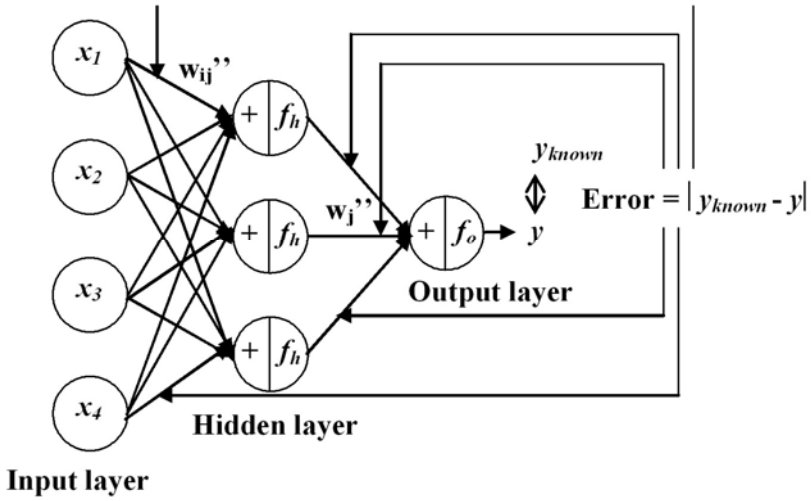

Figure 1.7. Error back-propagation in ANN training.

If the output function is a binary threshold function, the output has simply two values: zero or one.[58-62] Nevertheless, the transfer function most commonly used is of sigmoidal shape. Whatever the form of the transfer function is selected, it is used for all nodes in the network, in spite of where they are positioned or how they are connected with other neurons, and this function does not change during the training.[60]

CHAPTER 2. MATERIALS AND METHODS

2.1 Instrumentation

Preliminary collection of excitation and emission spectra were carried out with a commercial spectrofluorimeter using standard quartz cuvettes (1 cm x 1 cm). No sample de-oxygenation was attempted. For steady state (SS) measurements, the excitation source was a continuous wave 75 W Xenon lamp with broadband illumination from 200 nm to 2,000 nm. Detection was made with a photomultiplier tube with wavelength range from 185 to 650 nm. For time-resolved (TR) measurements, the excitation source was a pulsed 75 W Xenon lamp (wavelength range from 200 to 2,000 nm), variable repetition rate from 0 to 100 pulses per second, and a pulse width of approximately 3 μs. Detection was made with a gated analog photomultiplier tube (PMT, Model 1527). Its spectral response extended from 185 to 900 nm. SS and TR spectra were collected with excitation and emission monochromators having the same reciprocal linear dispersion (4 $nm.mm^{-1}$) and accuracy (±1 nm with 0.25 nm resolution). Their 1200 grooves/mm gratings were blazed at 300 and 400 nm, respectively. The instrument was computer controlled using commercial software specifically designed for the system.

Samples were excited at several excitation wavelengths. Excitation at 266nm was accomplished with the 4^{th} harmonic of a 10 Hz Nd:YAG Q-switched solid state laser. Excitation above 270 was carried out directing the output of a tunable dye laser through a KDP frequency-doubling crystal. The dye laser was operated on Rhodamine 6G (Exciton, Inc.) and it was pumped with the second harmonic of the Nd:YAG laser. Excitation between 310-330nm was made with the dye laser operating on DCM (Exciton, Inc.). Luminescence was detected with a multi-channel detector consisting of a front-illuminated intensified charge fiber-coupled device

(ICCD). The minimum gate time (full width at half maximum) of the intensifier was 2 ns. The CCD had the following specifications: active area = 690 x 256 pixels (26 mm^2 pixel size photocathode), dark current = 0.002 electrons/pixels, and readout noise = 4 electrons at 20 KHz. The ICCD was mounted at the exit focal plane of a spectrograph equipped with a 1200 grooves/mm grating blazed at 500 nm. The system was used in the external trigger mode. The gating parameters (gate delay, gate width, and the gate step) were controlled with a digital delay generator via a GPIB interface. Custom software was developed in-house for complete instrumental control and data collection.

2.2 Procedures

Measurements with the spectrofluorimeter were made with standard cuvettes (1 x 1 cm). Luminescence lifetimes were measured with the aid of a fiber optic probe and a laser system mounted in our laboratory.[63] The probe assembly consisted of one excitation and six collection fibers fed into a 1.25 m long section of copper tubing. All the fibers were 3 m long and 500 μm core diameter silica-clad silica with polyimide buffer coating. At the analysis end, the excitation and emission fibers were arranged in a conventional six-around-one configuration, bundled with vacuum epoxy and fed into a metal sleeve for mechanical support. The copper tubing was flared stopping a swage nut tapped to allow for the threading of a 0.75 mL polypropylene sample vial. At the instrument end, the excitation fiber was positioned in an ST connection and aligned with the beam of the tunable dye laser while the emission fibers were bundled with vacuum epoxy in a slit configuration, fed into a metal sleeve and aligned with the entrance slit of the spectrometer.

Lifetime determination followed a three-step procedure[63]: (1) collection of full sample and background wavelength-time matrices; (2) subtraction of background decay curve from the luminescence decay curve at the target wavelengths of the sensor; (3) fitting the background corrected data to single exponential decays. The decay curve data were collected with a minimum 150 μs interval between opening of the ICCD gate and the rising edge of the laser pulse, which was sufficient to avoid the need to consider convolution of the laser pulse with the analyte signal (laser pulse width = 5 ns). In addition, the 150 μs delay completely removed the fluorescence of the sample matrix from the measurement. Fitted decay curves ($y = y_0 + A_1 \exp^{-(x-x0)t_1}$) were obtained with Origin software (version 5; Microcal Software) by fixing y_0 and x_0 at a value of zero. For chemometric analysis, all spectra were saved in ASCII format and transferred to a PC AMD 1200 MHz for subsequent manipulation. All calculations were done using MATLAB 6.0.[64] Routines for ANN were written in our laboratory following previously known algorithms.[65] PLS-1 was implemented using the MVC1 MATLAB toolbox.[65]

2.3 Reagents

All reagents and solvents were purchased from commercial suppliers and used without further purification. Nanopure water was used throughout. Europium (III) chloride hexahydrate and Terbium (III) chloride hexahydrate were obtained from Aldrich (Milwaukee, WI). Ethylenediaminetetraacetic acid (EDTA), Nitrilotriacetic acid (NTA), HEPES, Human Serum Albumin, Thermolysin, γ-globulins, α-amylase, Concanavalin A, and Carbonic Anhydrase were purchased from Sigma (Milwaukee, WI). Deuterium Oxide (D_2O) was obtained from Acros Organics (Geel, Belgium). The organic solvents used in the synthesis were of high performance

liquid chromatography (HPLC) grade. Anhydrous solvents were obtained by distillation of the HPLC-grade solvents over CaH_2.

2.4 Synthesis of 5-aminosalicylic acid ethylenediaminetetraacetate europium (III) (5As-EDTA-Eu^{3+}) and 4-aminosalicylic acid ethylenediaminetetraacetate terbium (III) (5As-EDTA-Tb^{3+})

The synthetic steps of these complexes were fully described in the literature.[66] These compounds were received in solid state from Dr. Sanku Mallik's group (Department of Chemistry and Molecular Biology, North Dakota State University, Fargo, ND). The chemical structures of the complexes can be found in Appendix C.

2.5 Synthesis of polymerized liposomes

The synthetic steps of the liposome samples were fully described in the literature.[5,38] Liposomes were prepared from Eu^{3+} complexes of synthesized lipids (10 wt %) having oligoethylene glycols as spacers and EDTA as the metal-chelating headgroup[5,38] and the commercially available polymerizable phosphocholine PC1 (90 wt %) in 25 mM HEPES buffer, pH 7.0. The liposomes were polymerized at 0^oC with UV light (254 nm), and the polymerization was followed by UV-vis spectrometry.[5,38] Transmission electron microscopic studies indicated that the liposome structures are retained after polymerization.

Liposome samples were received in liquid state from Dr. Sanku Mallik's group (Department of Chemistry and Molecular Biology, North Dakota State University, Fargo, ND). The chemical structures of the lipids constituting the liposomes can be found in Appendix C.

CHAPTER 3. Eu^{3+} AND Tb^{3+} COMPLEXES: LUMINESCENT PROPERTIES AND ABILITY TO ANALIZE PROTEINS

3.1 Introduction

The lanthanide ions, particularly those on the center of the series, samarium, europium, terbium, and dysprosium, form complexes that often emit visible radiation (luminescence) when excited with UV-vis radiation. Opposed to europium and terbium complexes, which present lifetimes in general longer than 100 μs, samarium and dysprosium complexes in solution exhibit lifetimes usually shorter than 75 μs.[20] Since time discrimination often reduces fluorescence background of biological concomitants, working with lanthanide complexes that present longer lifetimes is convenient.[21] In this chapter, we investigate the luminescent properties of Eu^{3+} and Tb^{3+}, and their potential for qualitative and quantitative analysis of proteins.

3.2 Spectral characterization of Eu^{3+} and Tb^{3+} complexes

Figure 3.1 shows the TR excitation and luminescence spectra of Eu^{3+} (A), NTA-Eu^{3+} (B) and EDTA-Eu^{3+} (C); in HEPES buffer (pH = 7). The luminescence bands are characteristic of Eu^{3+} and correspond to the various electronic transitions that occur from the $^5D_0$ to the ^7F manifold. The two intense peaks at 593 and 616 nm result from the transitions $^5D_0 \rightarrow {}^7F_1$ and $^5D_0 \rightarrow {}^7F_2$, respectively. The other peaks result from the transitions $^5D_0 \rightarrow {}^7F_0$ (581 nm), $^5D_0 \rightarrow {}^7F_3$ (653 nm), and $^5D_0 \rightarrow {}^7F_4$ (694 nm).[26]

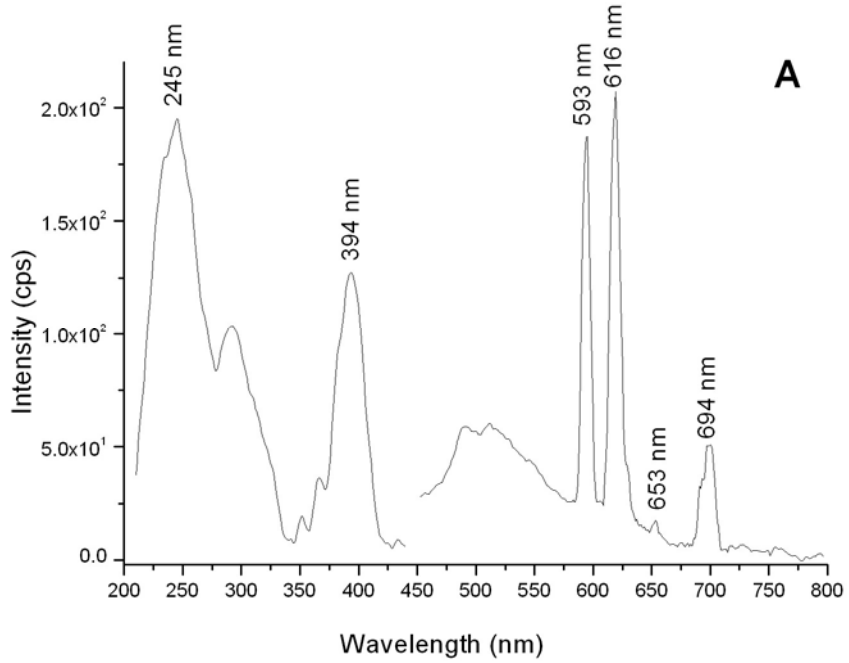
A
245 nm
394 nm
593 nm
616 nm
653 nm
694 nm
Intensity (cps)
Wavelength (nm)

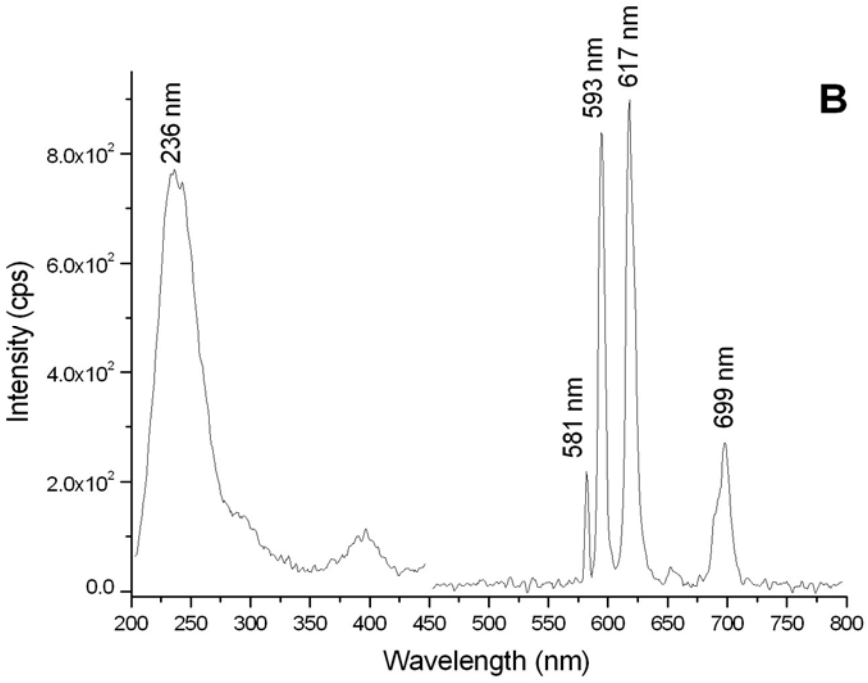
B
236 nm
581 nm
593 nm
617 nm
699 nm
Intensity (cps)
Wavelength (nm)

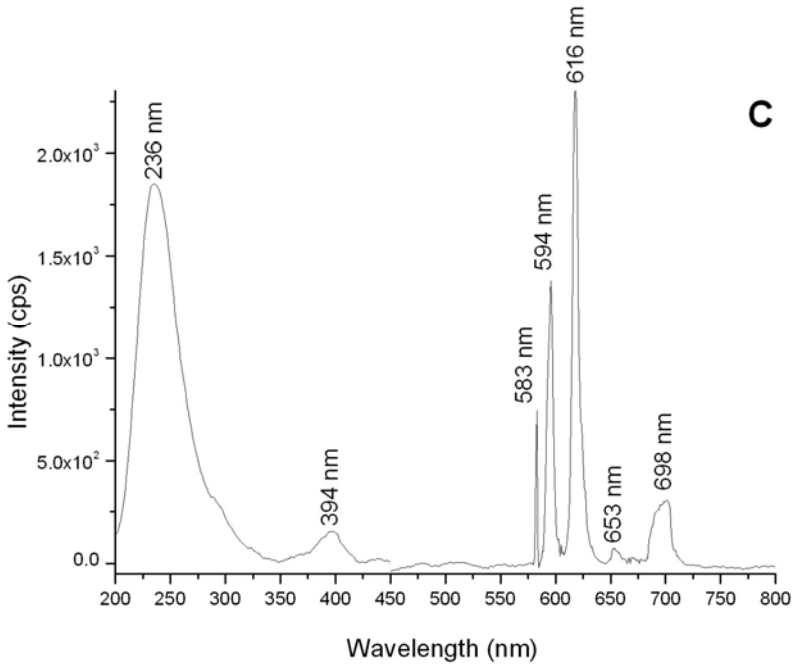

Figure 3.1. TR excitation and emission spectra recorded from 10^{-3} M Eu^{3+} (A), 10^{-3} M NTA-Eu^{3+} (B), and 10^{-3} M EDTA-Eu^{3+} (C) solutions.

All solutions were prepared in 25 mM HEPES. Chelate-Eu^{3+} solutions were prepared dissolving equal moles of EDTA (s) or NTA (s) and $EuCl_3.(H_2O)_6$ (s). Excitation/emission band-pass were 40/5 nm (A), 15/5 nm (B), and 5/5 nm (C), respectively. Other acquisition parameters were 150 μs delay and 1000 μs integration time. A cutoff filter was used at 450 nm to avoid second-order emission. Excitation spectra (200-450 nm) were recorded monitoring the luminescence intensity at 615 nm. Emission spectra (450-800 nm) were recorded using maximum excitation wavelengths.

Figure 3.2 displays the time-resolved excitation and luminescence spectra of Tb^{3+} (A), NTA-Tb^{3+} (B) and EDTA-Tb^{3+} (C); in HEPES buffer. The luminescence bands are attributed to Tb^{3+} transitions that take place from the $^5D_4$ to the ^7F manifold. The peaks result from the transitions $^5D_4 \rightarrow {}^7F_6$ (488 nm), $^5D_4 \rightarrow {}^7F_5$ (547 nm), $^5D_4 \rightarrow {}^7F_4$ (584 nm), and $^5D_4 \rightarrow {}^7F_3$ (622 nm).[26]

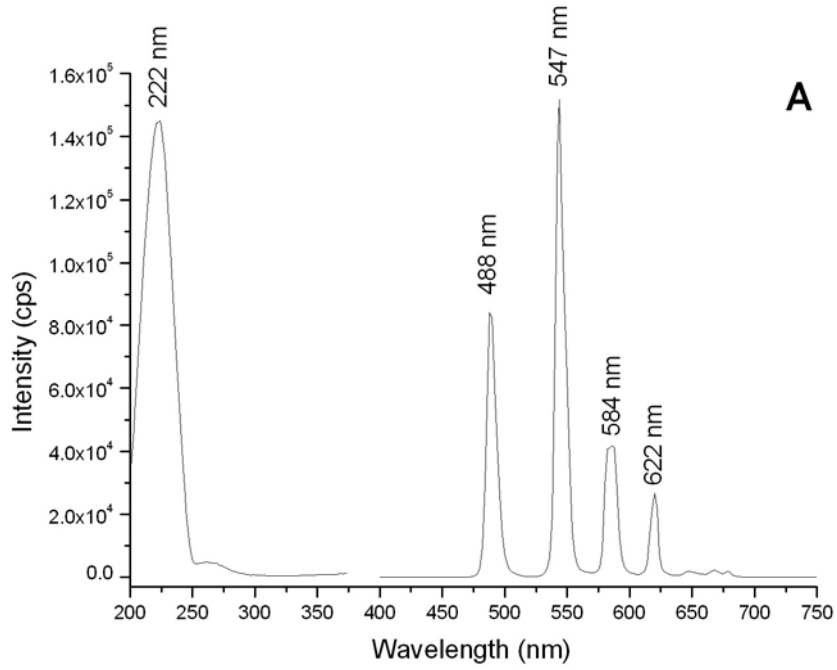
A
222 nm
488 nm
547 nm
584 nm
622 nm
Intensity (cps)
Wavelength (nm)
1.6x10^5
1.4x10^5
1.2x10^5
1.0x10^5
8.0x10^4
6.0x10^4
4.0x10^4
2.0x10^4
0.0
200 250 300 350 400 450 500 550 600 650 700 750

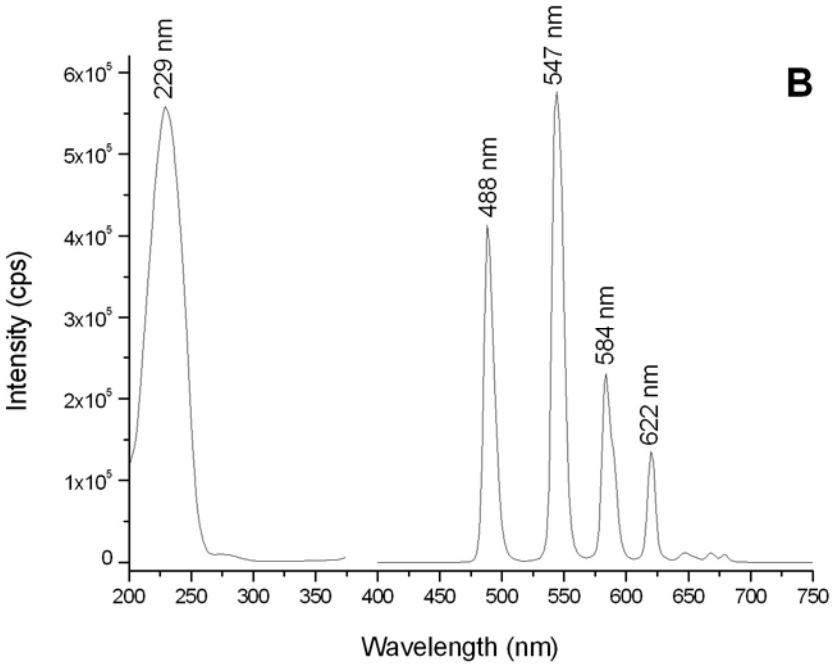
B
229 nm
488 nm
547 nm
584 nm
622 nm
Intensity (cps)
Wavelength (nm)
6x10^5
5x10^5
4x10^5
3x10^5
2x10^5
1x10^5
0
200 250 300 350 400 450 500 550 600 650 700 750

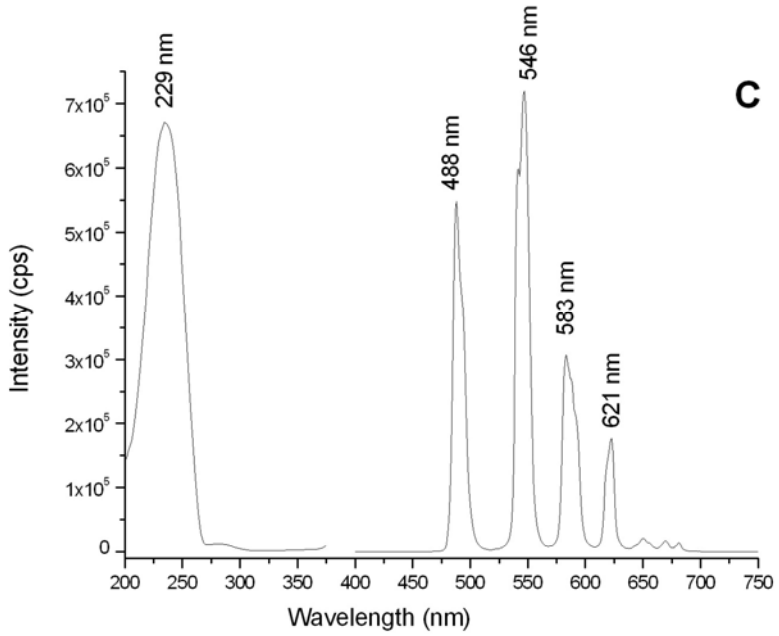

Figure 3.2. TR excitation and emission spectra recorded from 10^{-3} M Tb^{3+} (A), 10^{-3} M NTA-Tb^{3+} (B), and 10^{-3} M EDTA-Tb^{3+} (C) solutions.

All solutions were prepared in 25 mM HEPES. Chelate-Tb^{3+} solutions were prepared dissolving equal moles of EDTA (s) or NTA (s) and $TbCl_3.(H_2O)_6$ (s). Spectra were recorded using 10 and 1 nm excitation and emission band-pass, respectively. Other acquisition parameters were 150 μs delay and 1000 μs integration time. A cutoff filter was used at 400 nm to avoid second-order emission. Excitation spectra (200-375 nm) were recorded monitoring the luminescence intensity at 547 nm. Emission spectra (400-750 nm) were recorded using excitation maximum wavelengths.

The emission intensities of the NTA-Eu^{3+} and EDTA-Eu^{3+} complexes are 4.5 and 28 times the intensity of aqueous Eu^{3+}, respectively. The emission intensities of the NTA-Tb^{3+} and EDTA-Tb^{3+} complexes are 3.8 and 4.7 times the intensity of aqueous Tb^{3+}, respectively. The enhancements in luminescence intensity upon complexation are due to the removal of water molecules from the primary coordination sphere of the lanthanide ion.[26] In both cases, EDTA produces a higher luminescence enhancement than NTA. While EDTA is a hexadentate ligand

and removes six water molecules from the lanthanide's first coordination sphere, NTA is a tetradentate ligand and only removes four water molecules.

3.3 Number of water molecules coordinated to Eu^{3+} and Tb^{3+} complexes

The lifetime of the $^5D_0$ (Eu^{3+}) and $^5D_4$ (Tb^{3+}) levels can be strongly affected by the surrounding of the ion. Vibronic coupling with the O-H oscillators of coordinated water molecules provides an easy path for the radiationless depopulation of these levels. The rate of depopulation is directly proportional to the number of coordinated water molecules. Hence, measurement of the lifetime of the $^5D_0$ (Eu^{3+}) and $^5D_4$ (Tb^{3+}) levels provides information on the number of coordinated water molecules.[26]

Several processes contribute to the de-excitation of an excited-state ion. The reciprocal of the excited-state lifetime (τ^{-1}_{obs}) is the sum of individual rate constants of all the de-excitation processes. In aqueous solution, it can be expressed as:

$$\tau^{-1}_{obs} = \tau^{-1}_{nat} + \tau^{-1}_{OH} + \tau^{-1}_{nonrad} \qquad (3.1)$$

where τ^{-1}_{nat} is the natural rate constant for the emission of photons, τ^{-1}_{OH} is the rate constant of the non-radiative energy transfer to the O-H oscillators in the first coordination sphere, and τ^{-1}_{nonrad} represents the rate constant of non-radiative energy loss by all other pathways.[26]

For Eu^{3+} and Tb^{3+}, the value of τ^{-1}_{OH} is greater than the other rate constant values. Replacement of the O-H oscillators by O-D ones in deuterated media, makes the vibronic coupling of the $^5D_0$ and $^5D_4$ levels to the O-D oscillators much less efficient. As a result, the

luminescence lifetime of the excited state becomes longer.[26] In H_2O-D_2O mixtures, τ^{-1}_{obs} varies linearly with the mole fraction of H_2O (see Figure 3.3). The difference in the effects of H_2O and D_2O upon luminescence lifetimes provides information on the number of water molecules coordinated to Eu^{3+}. This number can be calculated with the following equation:

$$q = A_{LN}(\tau_{H2O}^{-1} - \tau_{D2O}^{-1}) \qquad (3.2)$$

where q is the number of water molecules in the first coordination sphere of the lanthanide ion, A_{LN} is a proportionality constant (1.05 for Eu^{3+}, and 4.2 for Tb^{3+}), and τ_{H2O} and τ_{D2O} are the luminescence lifetimes of the ion in H_2O and D_2O, respectively.[26]

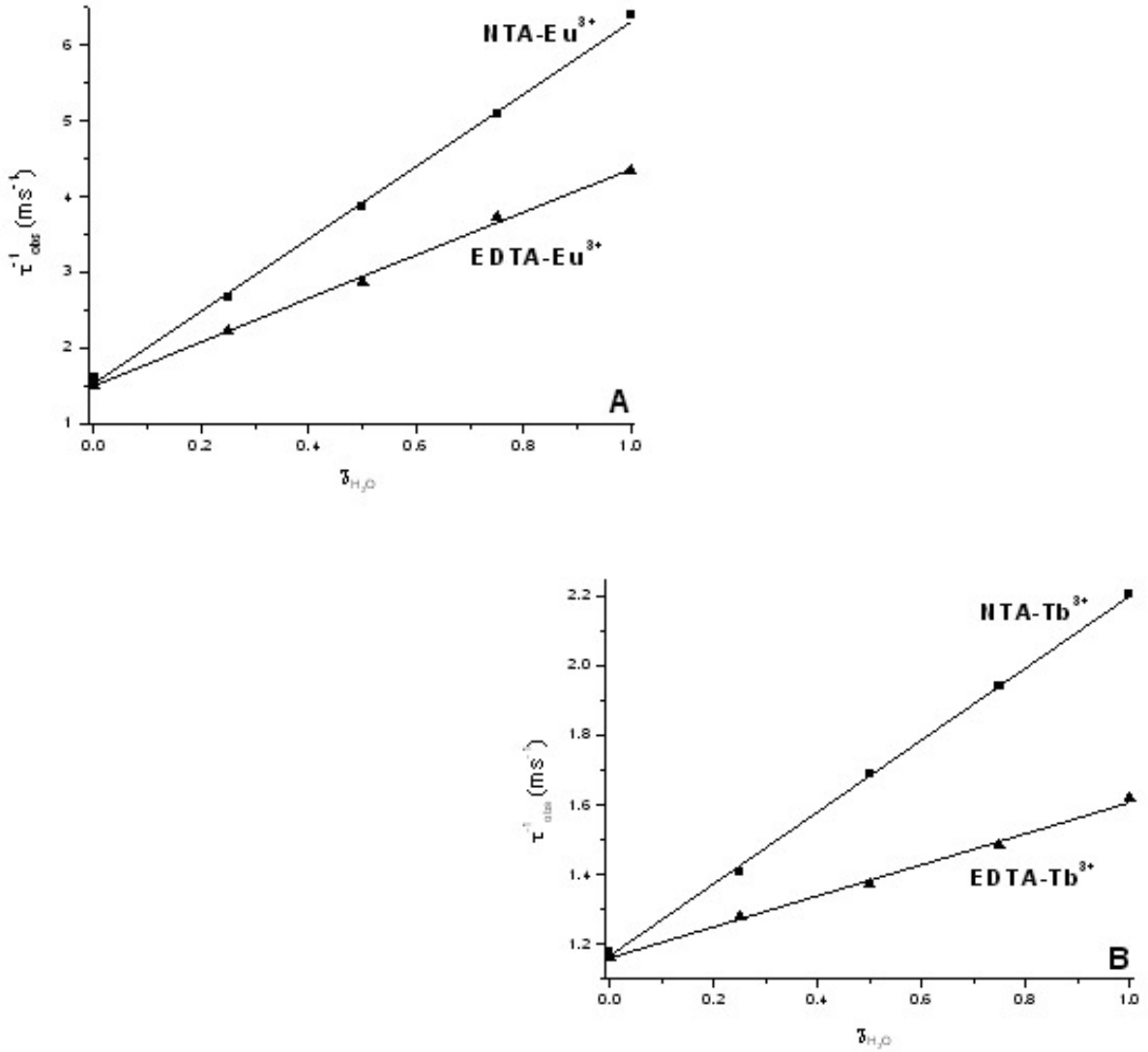

Figure 3.3. Reciprocal luminescence lifetime (τ^{-1}) in μs^{-1} as a function of mole fraction of water (χ_{H2O}) in D_20-H_20 mixtures of chelate-Eu^{3+} (A), and chelate-Tb^{3+} (B) solutions.

All samples were prepared in a 25 mM HEPES buffer solution by mixing the corresponding amounts of H_2O and D_2O. Chelate complexes were prepared by mixing equal moles of EDTA (s) or NTA (s) and $LnCl_3.(H_2O)_6$ (s). Final chelate-lanthanide^{3+} concentrations were 1×10^{-3}M. Luminescence lifetimes were measured using $\lambda_{exc}/\lambda_{em}$ = 266/616 nm (A), $\lambda_{exc}/\lambda_{em}$ = 266/547 nm (B). Other experimental parameters for wavelength-time matrix collection were: time delay = 0.3 ms, gate width = 1 ms (A), 2 ms (B), gate step = 0.02 ms, number of accumulations per spectrum = 100 laser pulses, number of kinetic series per wavelength-time matrix = 40, slit width of spectrograph: 10 mm.

It is a well-known fact that Eu^{3+} and Tb^{3+} can accommodate up to eight or nine molecules of water in its inner coordination sphere (q = 8 or 9). The obtained numbers of coordinated water molecules for the NTA-lanthanide^{3+} and EDTA-lanthanide^{3+} complexes coincide with the fact that NTA is a tetradentate ligand and EDTA is a hexadentate ligand (see Table 3.1).

Table 3.1. Number of water molecules (q) coordinated to the chelate:lanthanide^{3+} complexes.

Complex	q
NTA-Eu^{3+}	5.02
EDTA-Eu^{3+}	2.97
NTA-Tb^{3+}	4.3
EDTA-Tb^{3+}	1.92

3.4 Model protein: *Thermolysin*

3.4.1 Lanthanide ion: Eu^{3+}

The feasibility of using Eu^{3+} as a luminescent probe for qualitative and quantitative analysis of proteins was first investigated with Thermolysin. Previous knowledge of the binding of lanthanide ions to Thermolysin made this endoproteinase the selected protein to model the sensor.[26] The X-ray structure of thermolysin reveals the binding of a Zn^{2+} ion at the active site of the protein and four structural Ca^{2+} ions.[26] Zn^{2+}, which is required for biological activity, can be

replaced by other divalent ions such as Co^{2+}, with a resulting enhancement of activity. Either one or three Ca^{2+} ions can be replaced by trivalent lanthanide ions without alteration on activity. X-ray crystallographic techniques had shown that trivalent lanthanide ions can substitute isomorphously for divalent calcium in Thermolysin.[26]

The minimum concentration of Eu^{3+} in aqueous solvent that produces a luminescence signal strong enough for reproducible lifetime measurements is 1×10^{-3} M. Thermolysin can be dissolved up to 0.69 gr/L and still obtain a see-through solution. This concentration of protein gives approximately 6×10^{-5} moles of binding sites per liter of solution. When aqueous Eu^{3+} is mixed with thermolysin (final concentrations: 1×10^{-3} M and 0.69 gr/L, respectively), there is no change in the intensity nor the lifetime of the lanthanide. These observations can be explained by noticing that most of the Eu^{3+} is still free in solution (in one liter: 1×10^{-3} moles of Eu^{3+} - 6×10^{-5} moles of binding sites = 9.4×10^{-4} moles of Eu^{3+} free in solution).

In order to measure reproducible signals from lower lanthanide concentrations we used a chelate bound to Eu^{3+}. In this case, one would not expect the complex to occupy a binding site of the protein. The dimensions of the protein site are not big enough to host such a voluminous guest. Instead, we expected electrostatic interaction between the lanthanide ion and functional groups of residues of the protein. Eighteen batch titrations of EDTA-Eu^{3+} and NTA-Eu^{3+} were performed with Thermolysin at three fixed concentrations of chelate-Eu^{3+}: 5×10^{-6} M, 2×10^{-5} M, and 2×10^{-4} M. Luminescence intensities were monitored at three excitation wavelengths: 266, 280 and 394 nm. Excitation at 266 nm was selected because it provides a convenient wavelength for a Nd:YAG laser, which is currently available in our laboratory. Excitation at 280 nm was investigated as a possible means to promote energy transfer from the protein to the lanthanide

ion. Many proteins show maximum absorption at 280 nm (see Appendix A). Protein excitation at 280 promotes strong fluorescence emission between 300 and 400 nm (see Appendix B), i.e. a wavelength region that overlaps with excitation bands of Eu^{3+} and Tb^{3+}. Excitation at 394 nm was selected because it corresponds to a maximum in the excitation spectrum of Eu^{3+} (see Figure 3.1).

As expected, excitation at 266 and 280 nm promoted strong inner filter effects. These were corrected with the expression[24]:

$$F_{corr} = F_{obs} \times \text{antilog}\,[(A_{ex} + A_{em})/2] \qquad (3.3)$$

where F_{corr} and F_{obs} are the corrected and observed fluorescence intensities, and A_{ex} and A_{em} are the UV absorbance values of the protein at the excitation and emission wavelengths, respectively. Since proteins do not absorb light at wavelengths higher than 320 nm, excitation at 394 nm, did not require protein absorption correction.

Figure 3.4 shows the titration curve of Thermolysin obtained with 5×10^{-6} M NTA-Eu^{3+} (A) and 5×10^{-6} M EDTA-Eu^{3+}(B). Both curves were built upon excitation at 266 nm. All experiments were performed in batch (25 mM HEPES) and signal intensities were measured after 15 min of protein mixing. As expected, no spectral shift of the lanthanide luminescence was observed upon protein interaction. The EDTA-Eu^{3+} system only showed a linear correlation at concentrations of protein below 0.0035 gr/L (see Figure 3.4 C). The NTA-Eu^{3+} system showed linearity over the entire protein concentration range (Figure 3.4 A). Similar results were obtained with other chelate-Eu^{3+} concentrations.

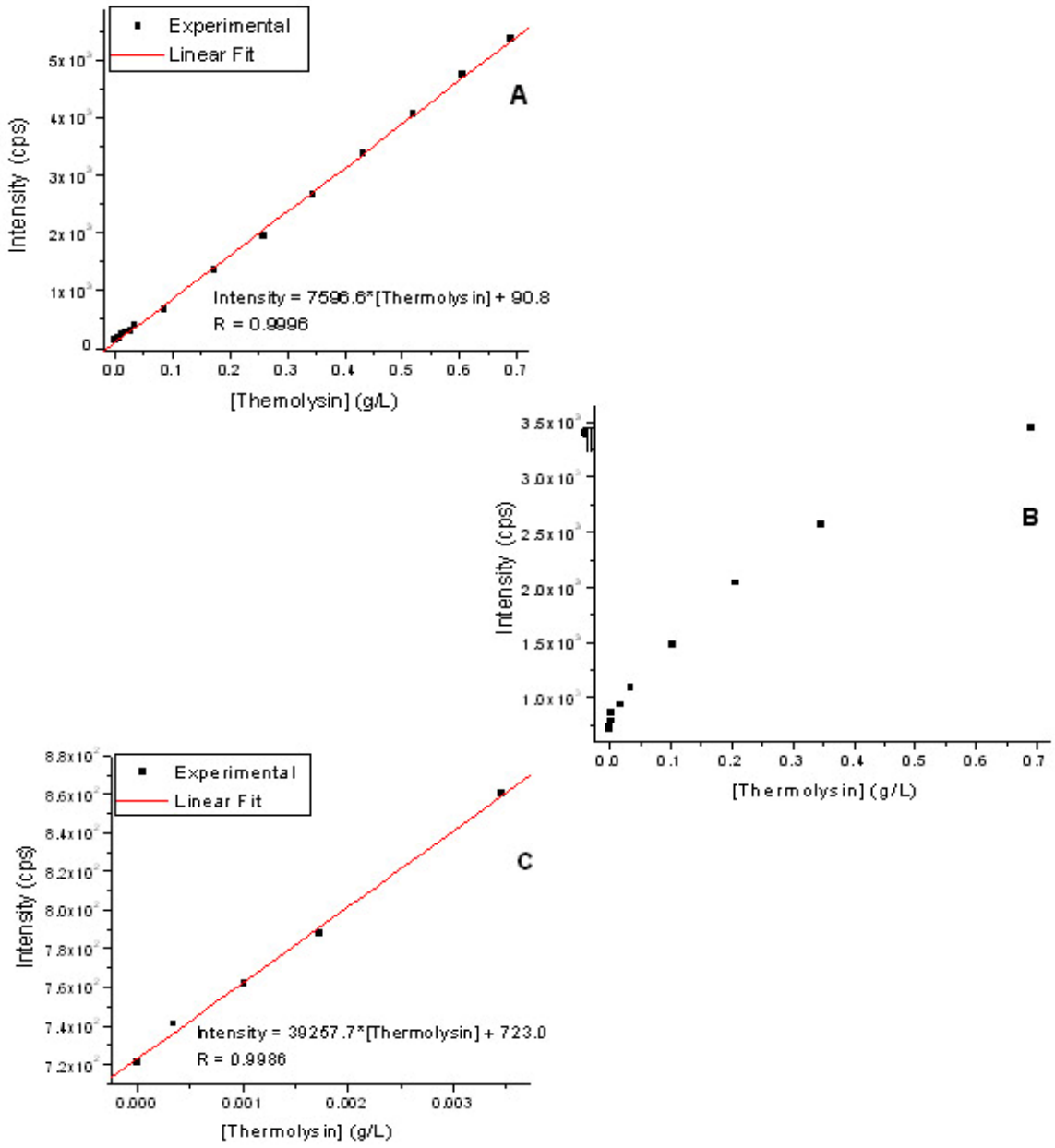

Figure 3.4. Titration curves for Thermolysin obtained with 5×10^{-6} M NTA-Eu^{3+} (A) and 5×10^{-6} M EDTA-Eu^{3+} (B,C).

Intensity measurements were done at $\lambda_{exc}/\lambda_{em}$ = 266/616 nm using 150 μs and 1000 μs delay and gate times, respectively. Spectra were recorded using 40 and 4 nm excitation and emission band-pass, respectively. A cutoff filter was used at 450 nm to avoid second-order emission.

Tables 3.2 and 3.3 summarize the analytical figures of merit (AFOM) obtained with the two chelates. The luminescence intensities plotted in the calibration graphs are the averages of individual measurements taken from three aliquots of the same working solution. The linear dynamic ranges (LDR) of the calibration curves were based on at least five protein concentrations. LDR extended from limit of detection (LOD) to the upper linear concentration, i.e. the concentration at which the calibration curve heads off linearity. The LOD were calculated with the following equation:

$$LOD = 3s_R/m \tag{3.4}$$

where m is the slope of the calibration curve and s_R is the standard deviation of 16 measurements of the reference signal, i.e. the luminescence intensity of the chelate-Eu^{3+} in the absence of protein. On the basis of LOD, Tables 3.2 and 3.3 show that 5×10^{-6} M EDTA-Eu^{3+} (λ_{exc}: 266 nm) provides a LOD one order of magnitude better.

Table 3.2. AFOM[a] obtained with the EDTA-Eu^{3+} probe.

[EDTA-Eu^{3+}] (M)	λ_{exc}: 266 nm		λ_{exc}: 280 nm		λ_{exc}: 394 nm	
	LDR (g/L)	LOD (g/L)	LDR (g/L)	LOD (g/L)	LDR (g/L)	LOD (g/L)
5×10^{-6}	0.0008-0.0356	0.0008	0.0090-0.1041	0.0090	0.0239-0.1041	0.0239
2×10^{-5}	0.0165-0.3462	0.0165	0.0301-0.3462	0.0301	—[b]	
2×10^{-4}	0.0458-0.3462	0.0458	0.0342-0.3462	0.0342	—[b]	

[a] Measurements were made in 25 mM HEPES. λ_{em} was 616 nm. Delay and gate times were 0.15 and 1 ms, respectively. A cutoff filter was used at 450 nm to avoid second-order emission. [b]No change in the lanthanide's luminescence was observed upon protein addition.

Table 3.3. AFOM[a] obtained with the NTA-Eu^{3+} probe.

[NTA-Eu^{3+}] (M)	λ_{exc}: 266 nm		λ_{exc}: 280 nm		λ_{exc}: 394 nm	
	LDR (g/L)	LOD (g/L)	LDR (g/L)	LOD (g/L)	LDR (g/L)	LOD (g/L)
5×10^{-6}	0.004-0.692	0.004	0.007-0.692	0.007	0.024-0.173	0.0239
2×10^{-5}	0.006-0.692	0.006	0.008-0.692	0.008	—[b]	
2×10^{-4}	0.005-0.623	0.005	0.010-0.623	0.010	—[b]	

[a] Measurements were made in 25 mM HEPES. λ_{em} was 616 nm. Delay and gate times were 0.15 and 1 ms, respectively. A cutoff filter was used at 450 nm to avoid second-order emission. [b] No change in the lanthanide's luminescence was observed upon protein addition.

As previously mentioned, protein interaction with the lanthanide ion causes no spectral shift that could be used for qualitative analysis. On the other hand, the replacement of O-H oscillators by the O-D variety causes a significant change in the luminescence lifetime of lanthanide complexes (Figure 3.3). Assuming a similar effect upon protein binding, the possibility of using luminescence lifetime for protein identification was investigated.

Lifetime measurements were performed along the entire titration curves. Figure 3.5 shows typical examples of the observed results for $5x10^{-6}$ M EDTA-Eu^{3+} and $5x10^{-6}$ M NTA-Eu^{3+}. Excitation was performed at 266nm. As the lifetime value is based on the ratio of two intensity measurements, correction for protein absorption is not necessary. In both cases, lifetime values increased with increasing protein concentration to reach an asymptotic limit. The plateau of lifetime values is attributed to a protein concentration range where the complete titration of lanthanide ions has occurred. This assumption is supported with additional experimental evidence showing well behaved single exponential luminescence decays. However, single exponential decays were also observed for Thermolysin concentrations below the asymptotic limit. As the examples shown in Figure 3.6, all luminescence decays presented single exponential decays within the studied concentration ranges. Table 3.4 summarizes the lifetime values collected at each data point of Figure 3.5 A and B. Clearly, the lifetime values of both complexes get longer as Thermolysin concentration increases towards the asymptotic limit. This behavior is similar to the one observed in H_2O:D_2O studies. Apparently, protein interaction with the complex replaces H_2O molecules with heavier protein oscillators in the inner coordination sphere of the lanthanide ion. The single exponential decays observed above the asymptotic protein concentrations were somehow expected and attributed to one or a combination of the following reason(s): (a) only one type of microenvironment surrounding the lanthanide ion; (b)

only one type of microenvironment significantly contributes to the observed lifetime; and/or (c) the different microenvironments surrounding the lanthanide ion provide very similar lifetimes with instrumentally undistinguishable values. On the other hand, our expectation below the asymptotic protein concentration was the observation of multi-exponential decays. As a result of the partial titration of the lanthanide ion, we expected to observe at least a bi-exponential decay with a short and a long component corresponding to the populations of "free" and "protein-bound" lanthanide ions, respectively. As shown in Tables 3.4 and 3.5, the difference in lifetime values of the first two data points in Figures 3.5 A and 3.5 B are 122.2 μs (EDTA-Eu^{3+}) and 83.7 μs (NTA-Eu^{3+}), i.e. well above the time resolution of our instrumental set-up (5 ns). Another interesting fact emerges when one compares the two complexes with regards to the lifetime differences in the absence and the presence of Thermolysin at its highest concentration, i.e. the first and last data points in Figures 3.5 A and 3.5 B. The lifetime difference values, i.e. $\Delta\tau_{EDTA} = 299.3 \pm 15.8$ μs and $\Delta\tau_{NTA} = 272.9 \pm 17.5$ μs are statistically equivalent ($\alpha = 0.05$, $N_1 = N_2 = 6$).[53] Based on the larger number of available sites for protein interaction, and assuming that one protein molecule can interact with more than one lanthanide ion, we expected to observe a larger lifetime difference for NTA-Eu^{3+}. Our expectation was based on the results of the H_2O:D_2O studies, where the replacement of 5 H_2O molecules (NTA-Eu^{3+}) led to a much larger lifetime difference than the replacement of 3 H_2O molecules (EDTA-Eu^{3+}). In the case of Thermolysin, a number of available sites larger than 3 appears to make no difference. At present we have no conclusive explanation for the observed phenomena. For the purpose at hand, i.e. to evaluate the feasibility of protein sensing on the bases of lifetime measurements, EDTA-Eu^{3+} and NTA-Eu^{3+} appear to be robust luminescence probes with simple exponential decays for lifetime analysis. Future studies focused on EDTA-Eu^{3+}. Our choice was based on the binding

constants of EDTA-Eu^{3+} (~ 10^{18})[68] and NTA-Eu^{3+} (~ 10^{14}).[68] A stronger binding constant should preserve the physical integrity of the probe in the presence of potentially competing ions and/or proteins.

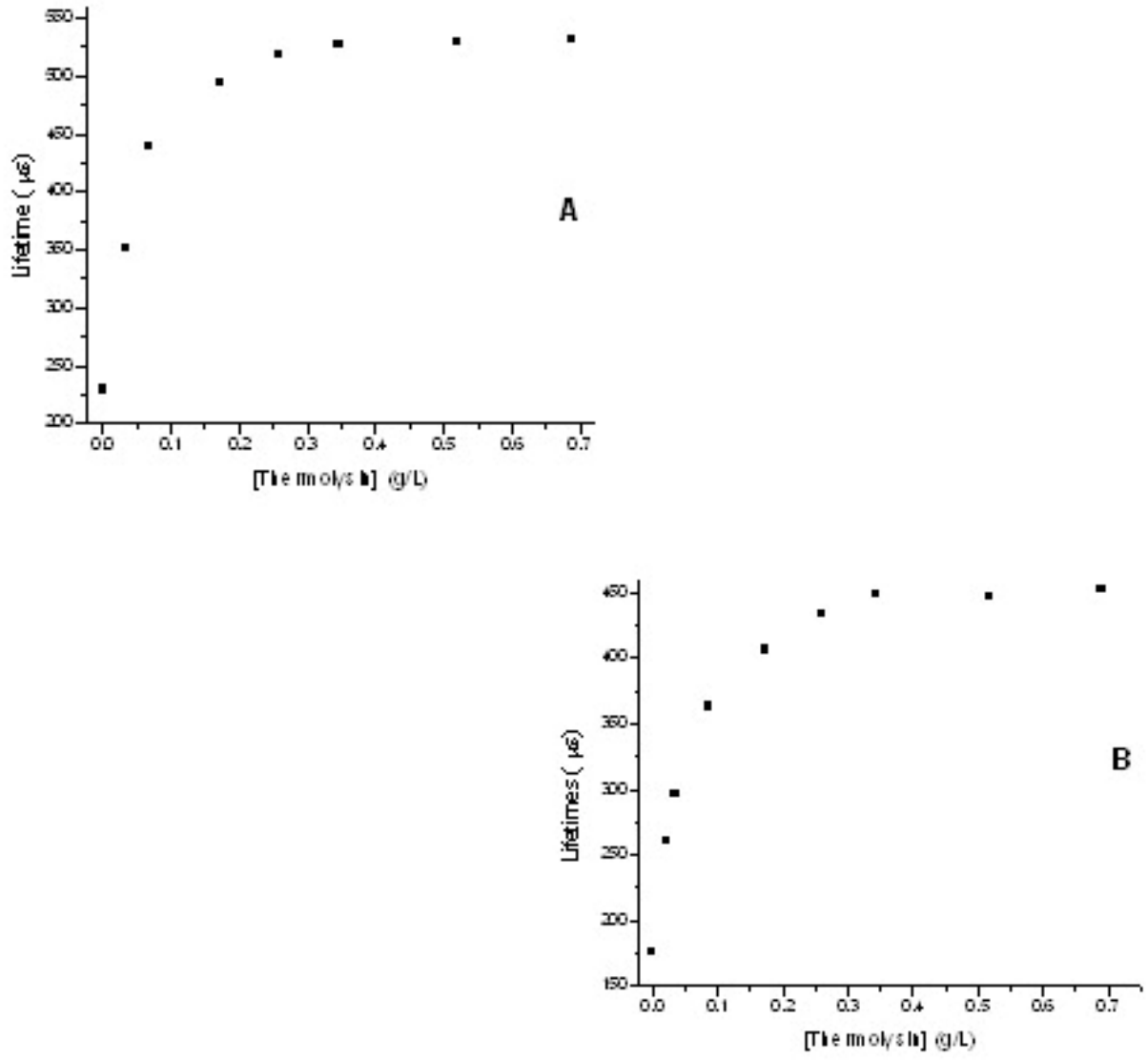

Figure 3.5. Titration curves for Thermolysin obtained with 5×10^{-6} M EDTA-Eu^{3+} (A) and 5×10^{-6} M NTA-Eu^{3+} (B).

Experimental parameters for wavelength-time matrix collection were the following: $\lambda_{exc}/\lambda_{em}$ = 266/616 nm, time delay = 0.3 ms, gate width = 1 ms, gate step = 0.02 ms, number of accumulations per spectrum = 100 laser pulses, number of kinetic series per wavelength-time matrix = 40, slit width of spectrograph: 10 mm.

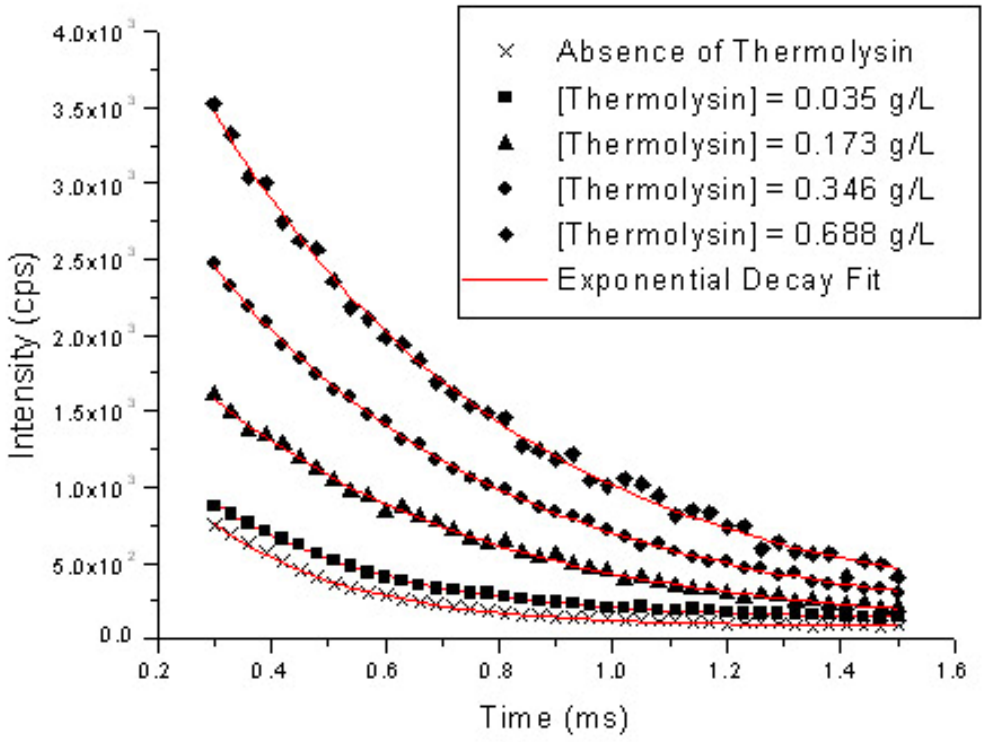

Figure 3.6. Fitted luminescence decay curves for 5×10^{-6} M EDTA-Eu^{3+} in 25 mM HEPES (×) and in the presence of Thermolysin at: 0.035 g/L (■), 0.173 g/L (▲), 0.346 g/L (●), and 0.688 g/L (♦).

Experimental parameters for wavelength-time matrix collection were the following: $\lambda_{exc}/\lambda_{em}$ = 266/616 nm, time delay = 0.3 ms, gate width = 1 ms, gate step = 0.03 ms, number of accumulations per spectrum = 100 laser pulses, number of kinetic series per wavelength-time matrix = 40, slit width of spectrograph: 10 mm.

Table 3.4. Lifetime decays obtained with the EDTA-Eu^{3+} probe.

[Thermolysin] (g/L)	Lifetimes (μs)	RSD (%)	
—	229.7 ± 11.0	4.8	t_{exp} = 19.39
0.035	351.9 ± 10.9	3.1	t_{exp} = 15.45
0.069	439.6 ± 8.6	1.9	t_{exp} = 8.42
0.173	493.8 ± 13.2	2.7	t_{exp} = 2.61
0.259	518 ± 18.4	3.6	t_{exp} = 0.91
0.346	526.9 ± 15.2	2.9	t_{exp} = 0.19
0.519	528.9 ± 21.3	4.0	t_{exp} = 0.24
0.689	531.6 ± 11.4	2.1	

$t_{tabulated}$ = 1.94 ($N_1 = N_2 = 6$, $\alpha = 0.05$).[53]

Table 3.5. Lifetime decays obtained with the NTA-Eu^{3+} probe.

[Thermolysin] (g/L)	Lifetimes (μs)	RSD (%)	
—	176.6 ± 7.9	4.5	
0.021	260.3 ± 11.4	4.4	t_{exp} = 14.75
0.035	296.3 ± 13.6	4.6	t_{exp} = 4.96
0.086	363.1 ± 15.3	4.2	t_{exp} = 7.98
0.173	406.2 ± 10.9	2.6	t_{exp} = 5.61
0.259	434.2 ± 16.7	3.9	t_{exp} = 2.43
0.344	449.1 ± 13.8	2.9	t_{exp} = 1.68
0.519	446.5 ± 11.7	2.5	t_{exp} = 0.35
0.690	452.6 ± 16.1	3.6	t_{exp} = 0.73

$t_{tabulated}$ = 1.94 ($N_1 = N_2 = 6$, $\alpha = 0.05$).[53]

3.4.2 Qualitative and quantitative potential of EDTA-Eu^{3+} for Carbonic Anhydrase (CA) and Human Serum Albumin (HSA).

Similar titrations were performed with CA and HSA. Although their concentration levels in human physiological fluids have been correlated to anomalies such as diabetes, malnutrition, and liver diseases,[79,80] the main reason for their choice was their commercial availability. Figures 3.7 and 3.8 show the titration curves obtained with 5×10^{-6} M EDTA-Eu^{3+}. Experiments were performed in batch (25 mM HEPES) and signal intensities were measured after 15 min of protein

mixing. Undoubtedly, there is a direct correlation between the luminescence intensity and protein concentration. The attained AFOM are shown in Table 3.6.

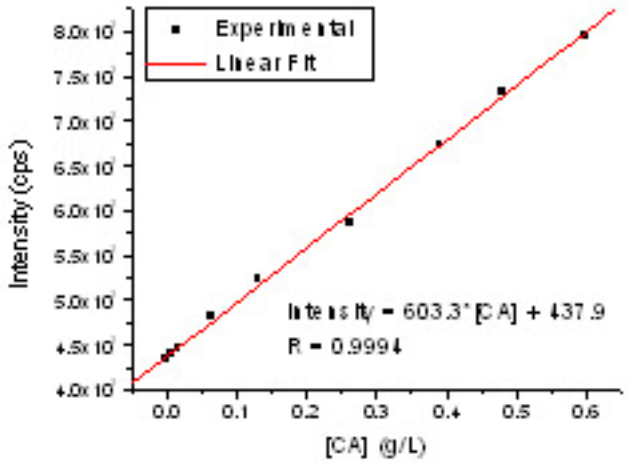

Figure 3.7. Calibration curve for CA obtained with 5×10^{-6} M EDTA-Eu^{3+} in 25 mM HEPES buffer.

Intensity measurements were done at λexc/ λem = 266/616 nm using 150 μs and 1000 μs delay and gate times, respectively. Spectra were recorded using 40 and 5 nm excitation and emission band-pass, respectively. A cutoff filter was used at 450 nm to avoid second-order emission.

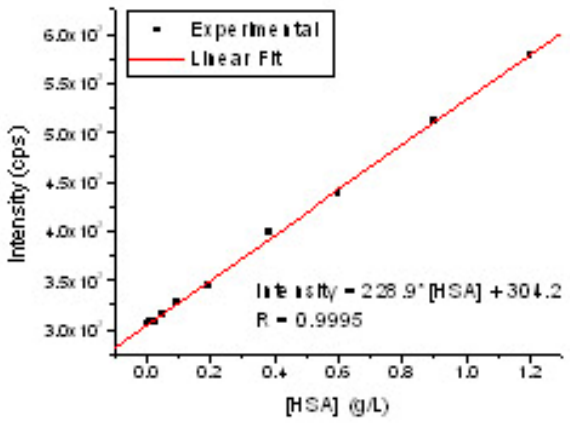

Figure 3.8. Calibration curve for HSA obtained with 5×10^{-6} M EDTA-Eu^{3+} in 25 mM HEPES buffer.

Intensity measurements were done at λexc/ λem = 266/616 nm using 150 μs and 1000 μs delay and gate times, respectively. Spectra were recorded using 40 and 4 nm excitation and emission band-pass, respectively. A cutoff filter was used at 450 nm to avoid second-order emission.

Table 3.6. AFOM[a] obtained with EDTA-Eu^{3+} for CA and HSA.

Protein	LDR (mg/L)	R	LOD (mg/L)
CA	49.2 – 597.0	0.9994	49.2
HSA	65.8 – 1200.0	0.9996	65.8

[a]Measurements were performed under instrumental conditions stated in Figures 3.7 and 3.8.

Similar to Thermolysin, lifetime measurements along the titration curve provided single exponential decays at all concentration levels. Lifetimes increased with increasing protein concentrations to asymptotic limits. Table 3.7 compares the reference lifetime (absence of protein) to the lifetimes in the presence of the two proteins at the asymptotic limit. For a confidence level of 95 % ($\alpha = 0.05$, $N_1 = N_2 = 6$)[53], the reference value was statistically different from the lifetime in the presence of the two proteins. The lifetime in the presence of CA was

statistically equivalent ($\alpha = 0.05$, $N_1 = N_2 = 6$) to the lifetime in the presence of HSA. The inability to differentiate between these two proteins shows the need for an additional parameter to improve the selectivity of the proposed sensor toward a target protein.

Table 3.7. Comparison of luminescence lifetimes measured with EDTA-Eu^{3+} in the absence and the presence of proteins.

Protein[a]	Lifetimes[b] (μs)	RSD (%)
—	229.8 ± 8.5	3.7
CA	280.5 ± 10.4	3.7
HSA	269.7 ± 12.4	4.6

[a]Protein solutions were mixed with 5×10^{-6} M EDTA-Eu^{3+} complex to provide the following final concentrations: 1.2 g/L CA, and 0.6 g/L AB. All solutions were prepared in 25 mM HEPES. [b]Lifetimes are the average values of six measurements taken from six aliquots of sample solution. All measurements were made at at λ_{exc}/ λ_{em} = 266/616 nm, time delay = 0.3 ms, gate width = 1 ms, gate step = 0.03 ms, number of accumulations per spectrum = 100 laser pulses, number of kinetic series per wavelength-time matrix = 40, slit width of spectrograph: 10 mm.

3.4.3 Lanthanide ion: Tb^{3+}

Similar studies to those performed with Eu^{3+} (see Section 3.3.1) were carried out with Tb^{3+}. The minimum concentration of Tb^{3+} in aqueous solvent that provides reproducible lifetime values is 1×10^{-3} M. When this concentration of Tb^{3+} is mixed with 0.69 g/L of Thermolysin in HEPES buffer (pH = 7), no change is observed in the intensity or the lifetime of the lanthanide ion. This is the same result that was obtained with 1×10^{-3} M Eu^{3+}. Consequently, we decided to

chelate Tb^{3+} with EDTA and NTA to enhance the luminescence signal of the lanthanide in solution.

The selected working concentrations for further studies were 3×10^{-7} M EDTA-Tb^{3+} and 1×10^{-7} M NTA-Tb^{3+}. These concentrations provide a signal to background ratio (S/B) equivalent to 5×10^{-6} M in EDTA-Eu^{3+} and NTA-Eu^{3+}, respectively. Batch titrations of chelate-Tb^{3+} were performed at only two excitation wavelengths -266 and 280 nm- because Tb^{3+} does not present a strong excitation band above 320 nm. Figure 3.9 shows the titration curve of Thermolysin obtained with 3×10^{-7} M EDTA-Tb^{3+} (A) and 1×10^{-7} M EDTA-Tb^{3+} (B) exciting at 266 nm. The experiments were performed in batch (25 mM HEPES) and signal intensities were measured after 15 min of protein mixing. The linear relationship between the luminescence intensity and protein concentration clearly appears at lower protein concentration levels (see Figure 3.9 C and D). Similar linear relationships were also obtained for the titrations performed upon excitation at 280 nm. Table 3.8 summarizes the AFOM obtained for these systems. LDR and LOD were calculated as explained in Section 3.3.1. EDTA-Tb^{3+} and NTA-Tb^{3+} are able to detect amounts of Thermolysin that are three and four orders of magnitude lower than their Eu^{3+} counterparts (see Tables 3.2 and 3.3).

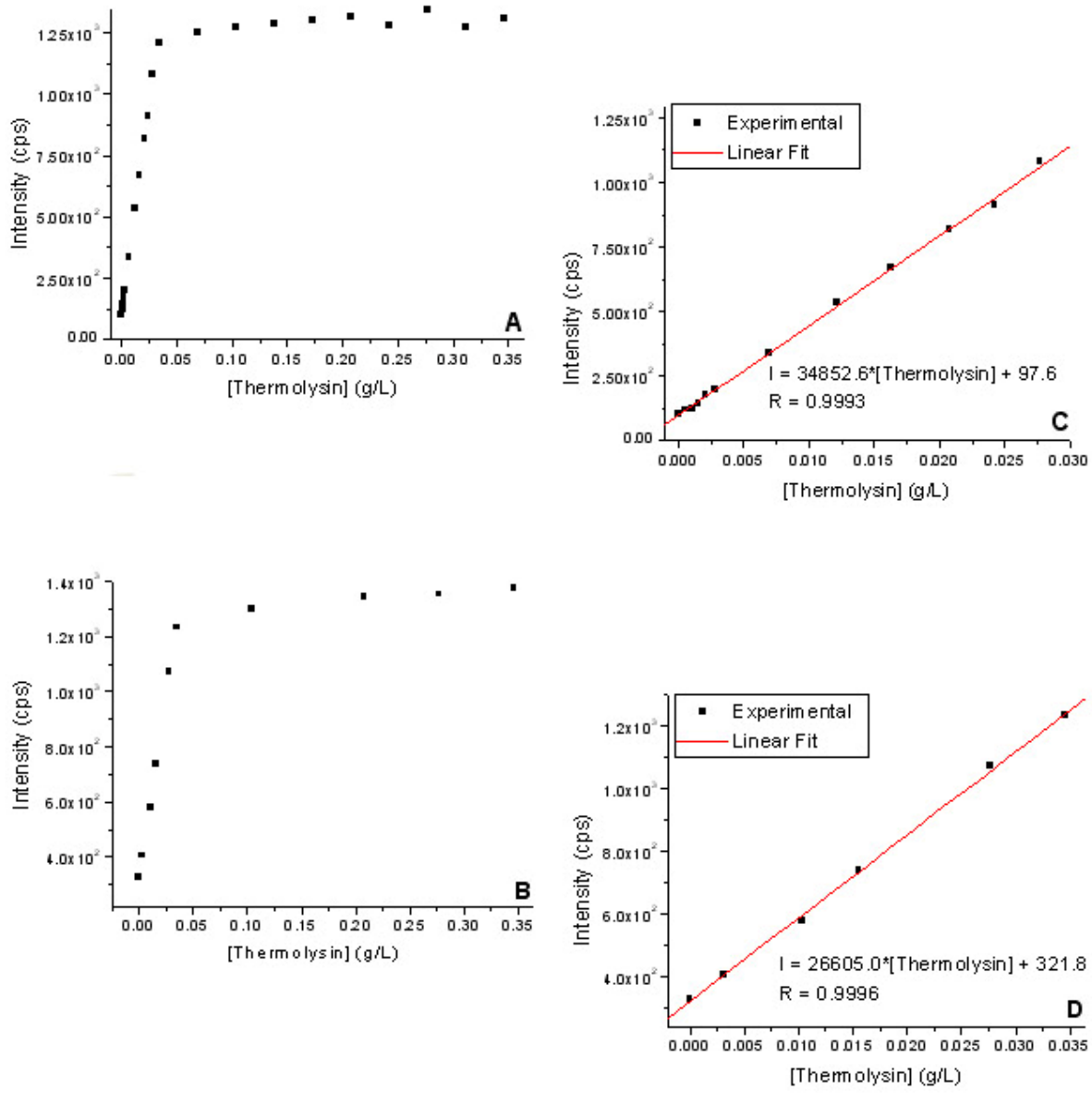

Figure 3.9. Titration curves for Thermolysin obtained with 3×10^{-7} M EDTA-Tb^{3+} (A,C) and 1×10^{-7} M NTA-Tb^{3+} (B,D).

Intensity measurements were done at $\lambda_{exc}/\lambda_{em}$ = 266/547 nm using 150 μs and 1000 μs delay and gate times, respectively. Spectra were recorded using 40 and 4 nm excitation and emission band-pass, respectively. A cutoff filter was used at 400 nm to avoid second-order emission.

Table 3.8 AFOM[a] otained with the chelate-Tb^{3+} sensor.

	λ_{exc}: 266 nm		λ_{exc}: 280 nm	
	LDR (mg/L)	**LOD (mg/L)**	**LDR (mg/L)**	**LOD (mg/L)**
EDTA-Tb^{3+}	0.170-27.681	0.170	0.929-27.681	0.929
NTA-Tb^{3+}	0.293-34.321	0.293	0.702-34.321	0.702

[a]**Measurements were performed under instrumental conditions stated in Figure 3.9.**

Figure 3.10 shows the lifetime measurements performed along the titration curve for EDTA-Tb^{3+} (A) and NTA-Tb^{3+} (B). Similar to the results obtained with Eu^{3+}, single exponential decays with excellent statistical fittings were observed at all protein concentrations. The lifetime increases asymptotically with increasing protein concentration. The differences between lifetime measurements in the asymptotic part of the curve and in the absence of protein are 990.8 and 592.6 μs for EDTA-Tb^{3+} and NTA-Tb^{3+}, respectively. This is the main difference between the behavior of Tb^{3+} and Eu^{3+}. EDTA-Eu^{3+} and NTA-Eu^{3+} showed statistically equivalent lifetime differences. The larger difference in lifetime values that EDTA-Tb^{3+} showed in the presence and absence of protein compared to NTA-Tb^{3+} was unexpected. Our H_2O-D_2O studies "pointed" in the opposite direction. At present we have no explanation for the observed results. For protein sensing on the basis of lifetime analysis of both systems are useful. Similar to Eu^{3+}, the criterion we used to select EDTA was the larger value of the EDTA-Tb^{3+} binding constant. Binding constant values have been reported in the literature[68] as log *K* EDTA-Tb^{3+} = 17.98, and log *K* NTA-Tb^{3+} = 11.31. The larger binding constant should provide superior stability for the lanthanide probe.

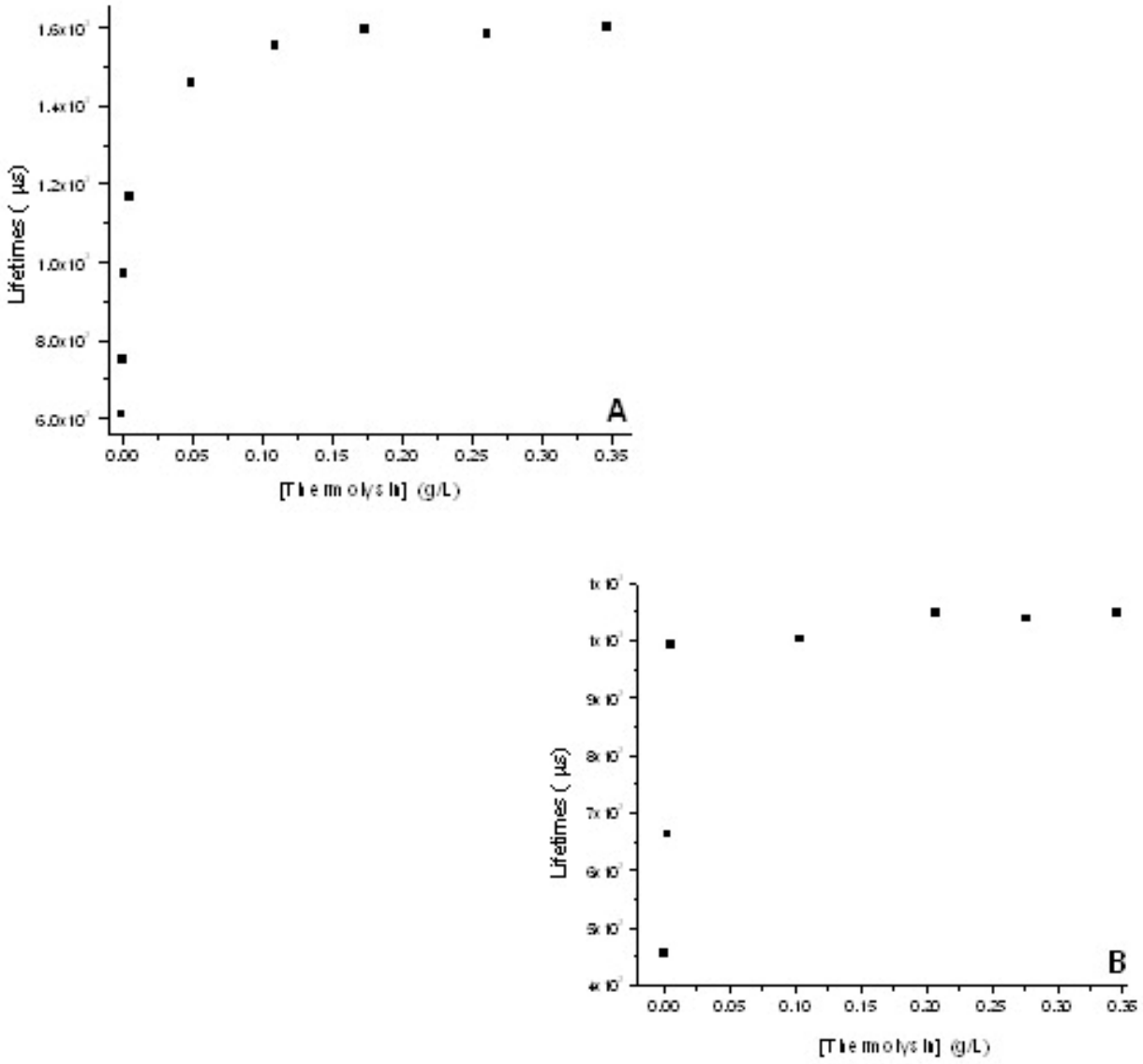

Figure 3.10. Titration curves for Thermolysin obtained with 3×10^{-7} M EDTA-Tb^{3+} (A) and 1×10^{-7} M NTA-Tb^{3+} (B).

Experimental parameters for wavelength-time matrix collection were the following: λexç/λem = 266/547 nm, time delay = 0.3 ms, gate width = 2 ms, gate step = 0.02 ms, number of accumulations per spectrum = 100 laser pulses, number of kinetic series per wavelength-time matrix = 40, slit width of spectrograph: 10 mm.

3.4.4 EDTA-Tb^{3+} sensor for α-amylase and Concanavalin A

Batch titrations of CA and HSA were unsuccessfully attempted with 3×10^{-7} M EDTA-Tb^{3+}. No change in luminescence intensity or luminescence lifetime was noticed. Attributing our observations to the lack of protein-Tb^{3+} interaction, two new proteins, namely α-amylase and Concanavalin A were tested. These two proteins, which are commercially available, have shown binding to Tb^{3+}.[81,82] Figure 11 A and B shows their titration curves with 3×10^{-7} M EDTA-Tb^{3+}. The experiments were performed in batch (25 mM HEPES) and signal intensities were measured after 15 min of protein mixing. At concentrations of protein below 0.085 g/L, the correlation between the luminescence intensity and protein concentration is linear (see Figure 3.11 C and D). The LDR of the calibration curves, the correlation coefficients, and the LOD are shown in Table 3.9.

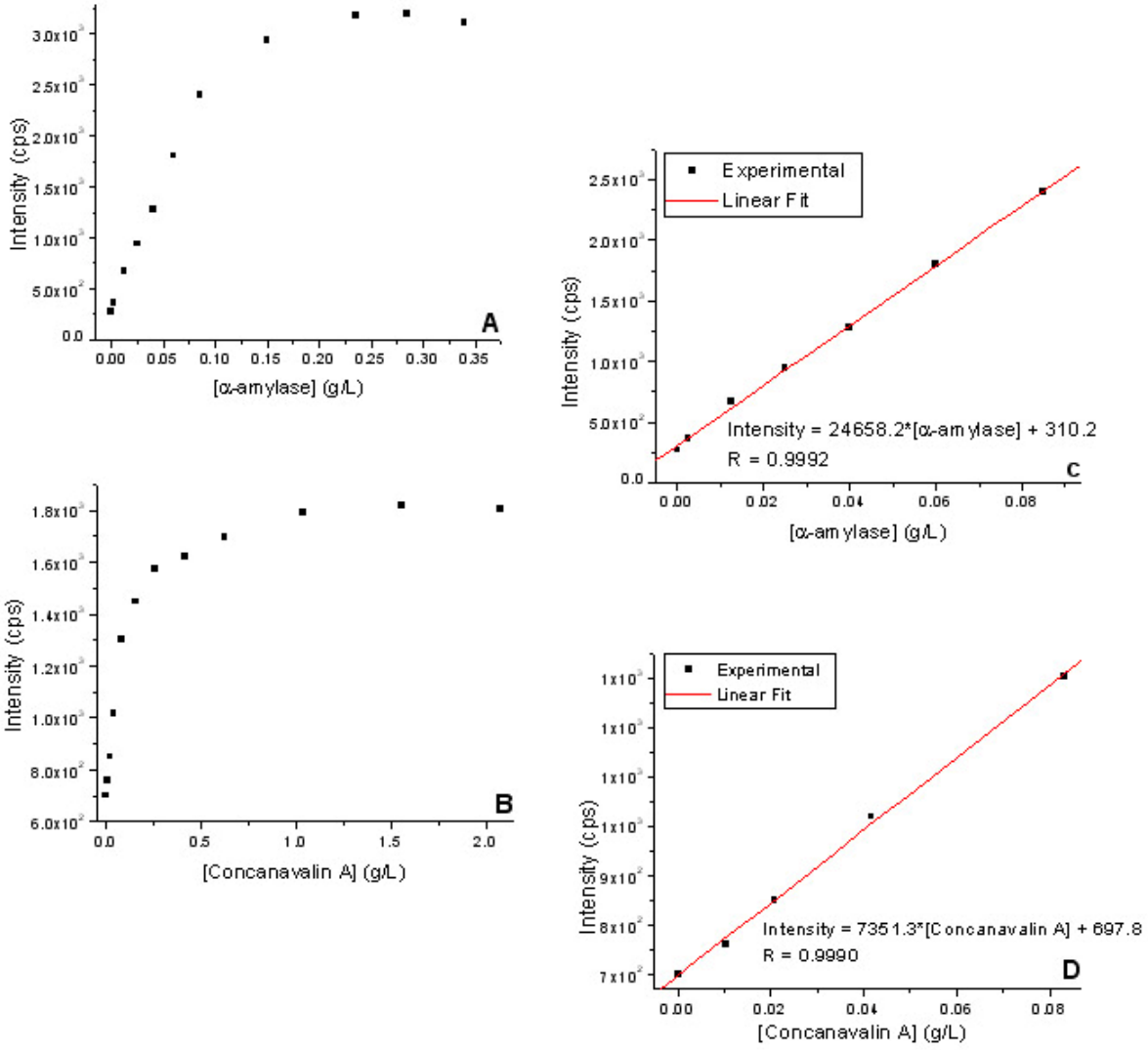

Figure 3.11. Titration curves for α-amylase (A,C) and Concanavalin A (B,D) obtained with 3×10^{-7} M EDTA-Tb^{3+}.

Intensity measurements were done at $\lambda_{exc}/\lambda_{em}$ = 266/545 nm using 150 μs and 1000 μs delay and gate times, respectively. Spectra for α-amylase were recorded using 40 and 3 nm excitation and emission band-pass, respectively. Spectra for Concanavalin A were recorded using 40 and 7 nm excitation and emission band-pass, respectively. A cutoff filter was used at 400 nm to avoid second-order emission. All intensity measurements were corrected for protein absorption.

Table 3.9. AFOM[a] obtained for α-amylase and Concanavalin A with EDTA-Tb^{3+}.

Protein	LDR (mg/L)	R	LOD (mg/L)
α-amylase	0.102 – 85.012	0.9992	0.102
Concanavalin A	0.156 – 83.285	0.9990	0.156

[a] Measurements were performed under instrumental conditions stated in Figure 3.11.

Lifetime measurements were performed along the titration curves. The statistical fittings provided single exponential decays at all studied concentrations. The lifetime values increased with increasing protein concentration to an asymptotic limit. Table 3.10 compares the reference lifetime (absence of protein) to the lifetimes in the presence of the two proteins at the asymptotic limit. For a confidence level of 95 % ($\alpha = 0.05$, $N_1 = N_2 = 6$)[53], the reference value, was statistically different from the lifetime in the presence of the two proteins. This fact demonstrates that the lifetime of the complex is sufficiently sensitive to detect the presence of these two proteins. The lifetime in the presence of α-amylase was statistically different ($\alpha = 0.05$, $N_1 = N_2 = 6$) from the lifetime in the presence of Concanavalin A, which proves the utility of this sensor to differentiate between these two proteins.

Table 3.10. Comparison of luminescence lifetimes measured with EDTA-Tb^{3+} in the absence and the presence of proteins.

Protein[a]	Lifetimes[b] (μs)	RSD (%)
—	598.9 ± 34.1	5.7
α-amylase	656.2 ± 23.2	3.5
Concanavalin A	757.5 ± 24.1	3.2

[a]Protein solutions were mixed with 3×10^{-7} M complex to provide the following final concentrations: 0.5 g/L α-amylase and 0.26 g/L Concanavalin A. All solutions were prepared in 25 mM HEPES.
[b]Lifetimes are the average values of six measurements taken from six aliquots of sample solution. Experimental parameters for wavelength-time matrix collection were the following: $\lambda_{exc}/\lambda_{em}$ = 266/547 nm, time delay = 0.3 ms, gate width = 2 ms, gate step = 0.02 ms, number of accumulations per spectrum = 100 laser pulses, number of kinetic series per wavelength-time matrix = 40, slit width of spectrograph: 10 mm.

3.5 Conclusions

This chapter demonstrates the feasibility of using the luminescence response of EDTA-Eu^{3+} and EDTA-Tb^{3+} to monitor protein concentrations in aqueous media. Protein interaction enhances the luminescence signal of both lanthanide ions. The observed luminescence enhancements are attributed to the removal of water molecules from the first coordination sphere of the lanthanide ion. There is a linear correlation between the concentration of the complex and the minimum protein concentration detected with the probe. Our LOD were of the same order of magnitude as those previously reported with the most sensitive methods.[15-17]

The luminescence decays, which followed well-behaved single exponential decays in the presence and the absence of proteins, provided a selective parameter for protein identification on the basis of lifetime analysis. EDTA-Tb^{3+} is not sensitive to the presence of CA and HSA, but its

usefulness was demonstrated with Thermolysin, α-amylase and Concanavalin A. The lifetimes obtained with these three proteins were all statistically different, which shows the feasibility of using EDTA-Tb^{3+} to monitor one of these proteins in the presence of the other two. The lack of sensitivity of EDTA-Tb^{3+} to monitor HSA and CA encourages the search for a protein sensor with a wider scope.

The EDTA-Eu^{3+} complex is sensitive to the presence of Thermolysin, CA, and HSA. The lifetime of EDTA-Eu^{3+} in the presence of Thermolysin is statistically different to its lifetime in the presence of HSA and CA. This proves the capability of EDTA-Eu^{3+} to monitor Thermolysin in the presence of HSA and/or CA. On the other hand, the lifetime values of HSA and CA were statistically equivalent. The fact that two of the target proteins showed statistically equivalent lifetimes demonstrates the need for additional selectivity.

CHAPTER 4. EVALUATION OF TWO LANTHANIDE COMPLEXES (5-AMINOSALYCILIC ACID-EDTA-Eu^{3+} AND 4-AMINOSALYCILIC ACID-EDTA-Tb^{3+}) FOR QUALITATIVE AND QUANTITATIVE ANALYSIS OF TARGET PROTEINS

4.1 Introduction

As previously shown, the luminescence of lanthanide ions is quite weak as a result of low molar extinction coefficients in aqueous solvents.[22] Water molecules strongly bind to the lanthanide ion and quench its luminescence via weak vibronic coupling with the vibrational states of the O-H oscillators. Significant enhancements for analytical use were obtained with chelating agents (NTA and EDTA) that remove water molecules from the lanthanide's primary coordination sphere. Coordination of a chelating agent to the lanthanide ion also provides the possibility of attaching a sensitizer (or antenna) to further enhance the luminescence of the lanthanide ion. Sensitizers are typically organic molecules that strongly absorb and transfer excitation energy to the metal ion, thereby overcoming the inherently weak absorption of the lanthanide ion.[22] The present Chapter explores the possibility of using sensitizers to promote energy transfer to Eu^{3+} and Tb^{3+} and obtain useful parameters for the qualification and quantification of proteins.

4.2 Spectral characterization of 5-aminosalicylic acid ethylenediaminetetraacetate europium(III) (5As-EDTA-Eu^{3+}) and 4-aminosalicylic acid ethylenediaminetetraacetate terbium(III) (4As-EDTA-Tb^{3+}) complexes

EDTA was chosen as the chelating agent because it forms tightly bound complexes with Eu^{3+} and Tb^{3+}.[68] Strong bonding assures the physical integrity of the probes in the presence of

potentially competing ions and/or proteins. 4-Aminosalicylic acid (4As) and 5-aminosalicylic acid (5As) were chosen as the antennas for Tb^{3+} and Eu^{3+} because their fluorescence spectra overlap the excitation spectra of the respective EDTA complexes (Figures 4.1 and 4.2). This is a recommended selection criterion for intramolecular energy transfer between an organic sensitizer and a lanthanide ion.[26] In addition, 4As and 5As present maximum excitation wavelengths above the main wavelength range of protein absorption.

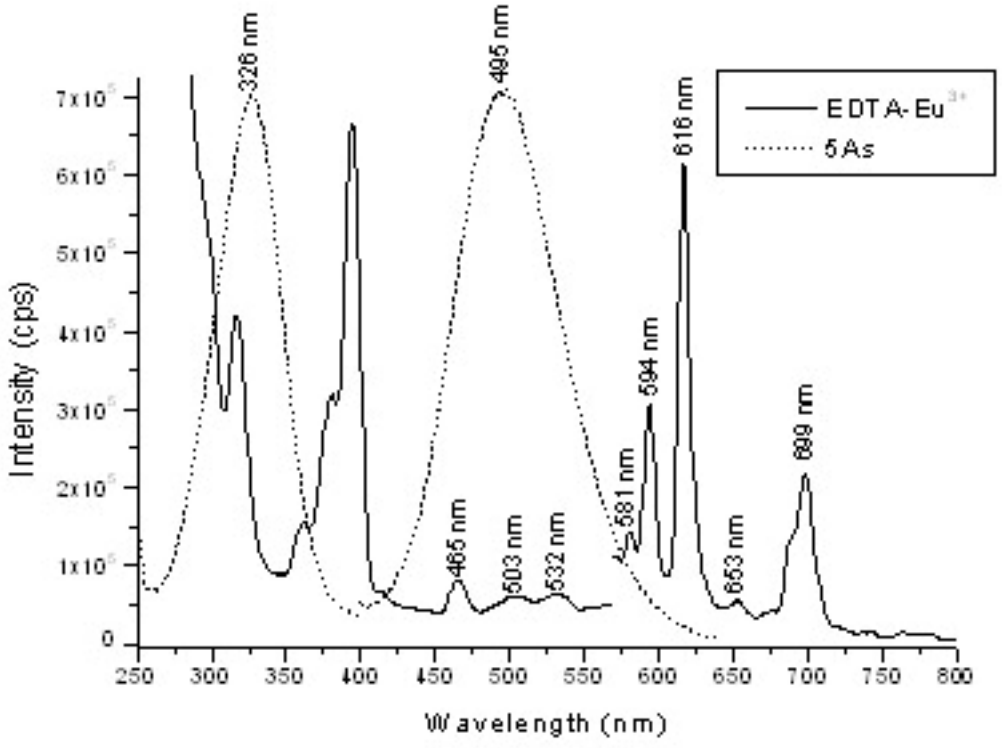

Figure 4.1. Overlap of the fluorescence emission of 5As (···) with the excitation peaks of EDTA-Eu^{3+} (—). Excitation and fluorescence spectra of 1×10^{-5} M 5As were recorded under SS conditions using 2 nm excitation and emission band-pass at $\lambda_{exc}/\lambda_{em}$ = 326/495 nm. Excitation and luminescence spectra of 5×10^{-6} M EDTA-Eu^{3+} were recorded under TR conditions. Instrumental parameters were as follows: $\lambda_{exc}/\lambda_{em}$ = 394/616 nm, delay time = 0.15 ms, gate time = 1 ms, excitation and emission band-pass: 40 and 5 nm, respectively. A cutoff filter was used at 550 nm to avoid second-order emission.

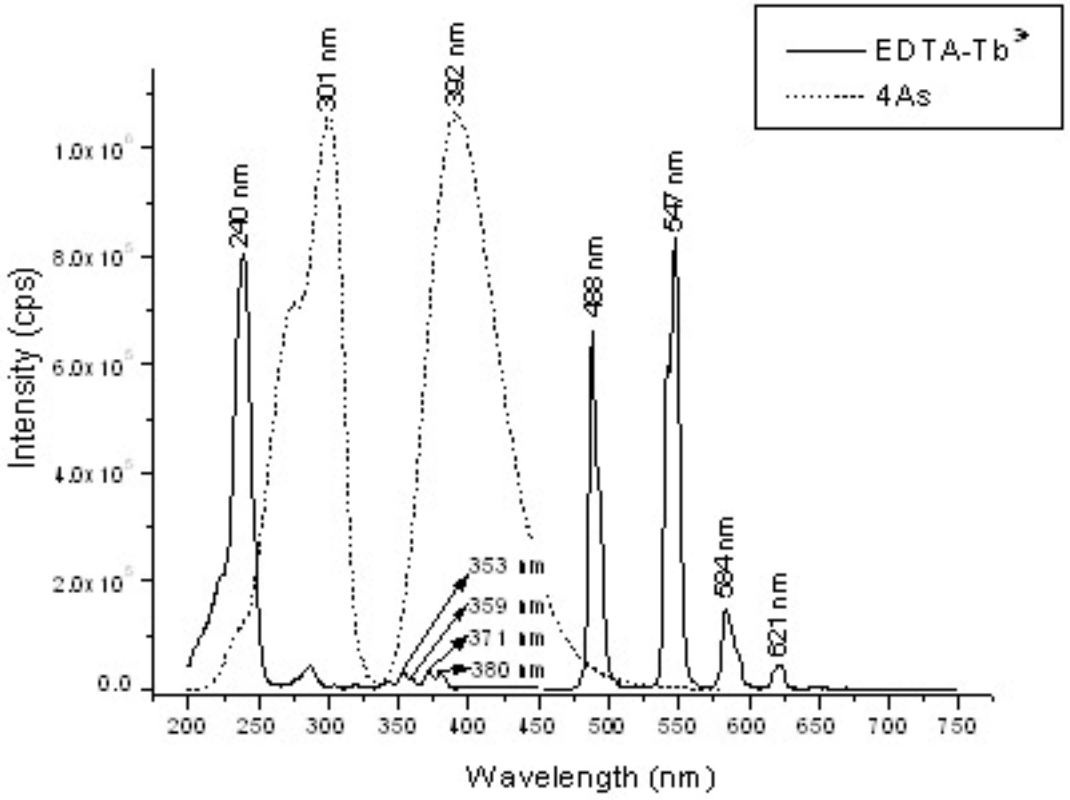

Figure 4.2. Overlap of the fluorescence emission of 4As (···) with the excitation peaks of EDTA-Tb^{3+} (—). Excitation and fluorescence spectra of 1×10^{-5} M 4As were recorded under SS conditions using 2 nm excitation and emission band-pass at $\lambda_{exc}/\lambda_{em}$ = 301/392 nm. Excitation and luminescence spectra of 3×10^{-7}M EDTA-Tb^{3+} were recorded under TR conditions. Instrumental parameters were as follows: $\lambda_{exc}/\lambda_{em}$ = 238/547 nm, delay time = 0.15 ms, gate time = 1 ms, excitation and emission band-pass: 40 and 3 nm, respectively. A cutoff filter was used at 450 nm to avoid second-order emission.

Figure 4.3 shows the SS (A) and the TR (B) excitation and luminescence spectra of 5As-EDTA-Eu^{3+}. The broad emission band in the SS spectrum of 5As-EDTA-Eu^{3+} corresponds to the fluorescence contribution of the antenna. The luminescence of Eu^{3+} appears only in the TR spectrum of the complex. A 150-μs delay after the excitation pulse removes the fluorescence contribution from 5As and provides a reference signal solely based on the luminescence of Eu^{3+}.

When the sample is excited at wavelengths away from protein absorption (λ_{exc} > 320 nm), the emission intensity of the 5As-EDTA-Eu^{3+} is approximately 10 times higher than the one from of EDTA-Eu^{3+}. This is attributed to energy transfer from 5As to Eu^{3+}.

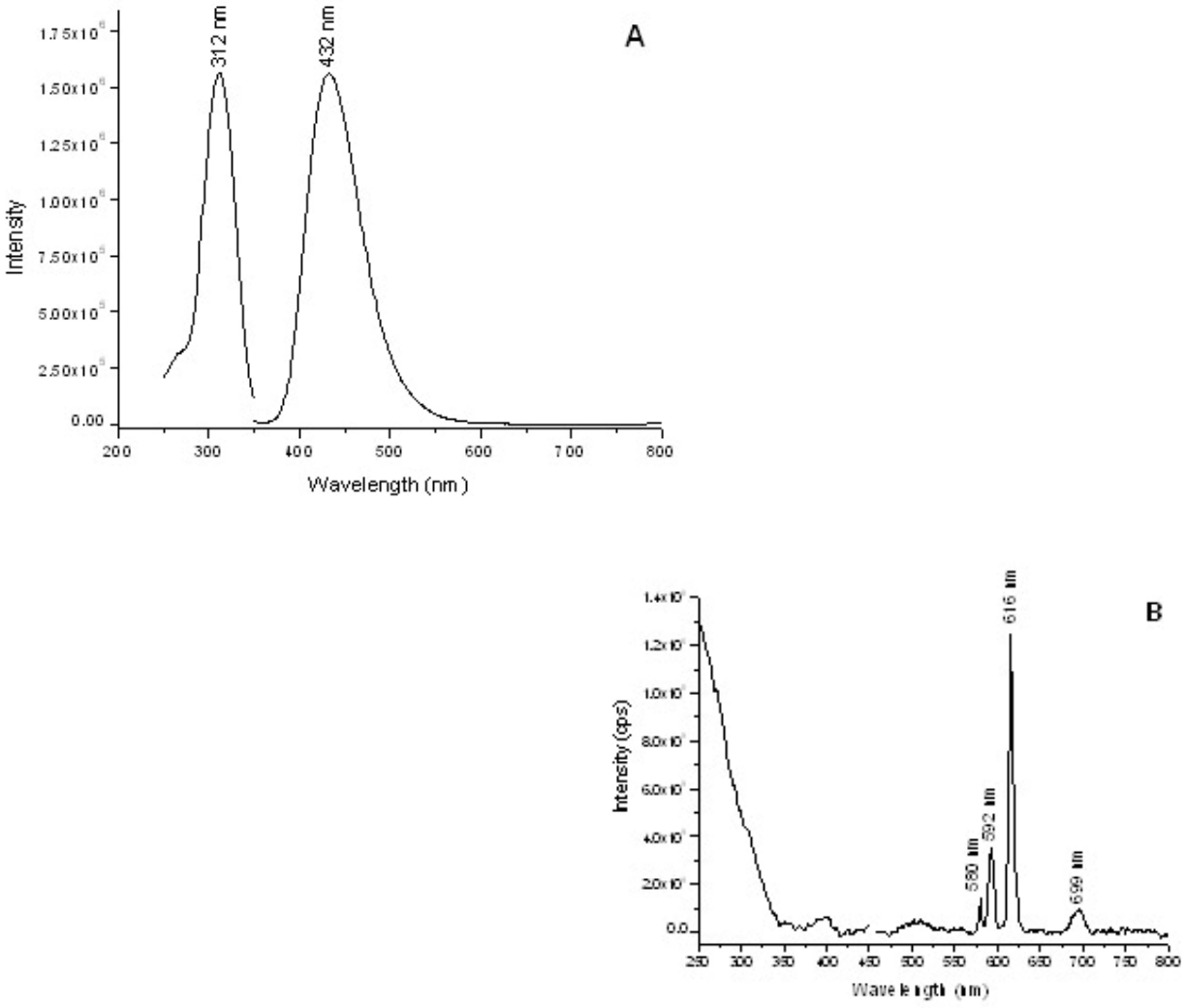

Figure 4.3. Excitation and fluorescence spectra of 1.0×10^{-5} M 5As-EDTA-Eu^{3+} in 25 mM HEPES recorded under SS (A) and TR (B) conditions.

(A) Excitation and emission band-pass were 4 nm at $\lambda_{exc}/\lambda_{em}$ = 311/432 nm. (B) Excitation and emission band-pass were 15 and 2 nm, respectively at $\lambda_{exc}/\lambda_{em}$ = 266/616 nm. Other parameters: delay time = 0.15 ms, gate time = 1 ms. A cutoff filter at 450 nm was used to avoid second-order emission.

Figure 4.4 shows the SS excitation and luminescence spectra of 4As-EDTA-Tb^{3+}. The four sharp peaks that appear in the luminescence spectrum of the complex correspond to characteristic electronic transitions of the lanthanide ion. Upon sample excitation at 310 nm, the luminescence intensity of 4As-EDTA-Tb^{3+} is approximately 1.4×10^2 higher than the one from EDTA-Tb^{3+}. This is attributed to energy transfer from 4As to Tb^{3+}. In this case, the luminescence enhancement promoted by energy transfer is much higher than the one observed from 5As to Eu^{3+}. The luminescence intensity from 4As-EDTA-Tb^{3+} is so strong that no time discrimination is required in order to observe Tb^{3+} characteristic emission bands.

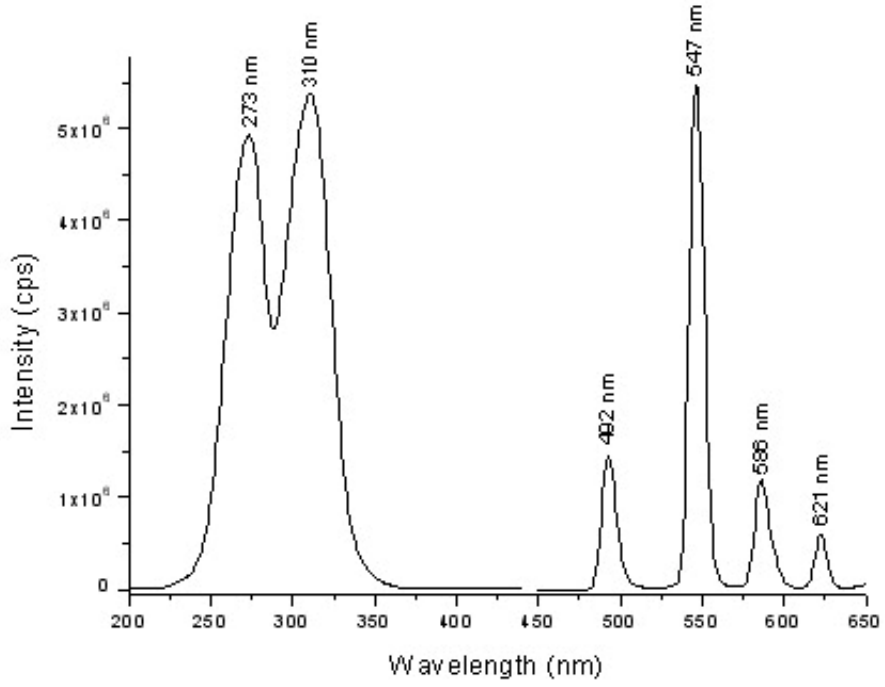

Figure 4.4. Excitation and luminescence spectra of 1.0×10^{-5} M 4As-EDTA-Tb^{3+} in 25 mM HEPES.

Spectra were recorded under SS conditions using 2 nm excitation and emission band-pass at $\lambda_{exc}/\lambda_{em}$ = 310/547 nm. A cutoff filter at 450 nm was used to avoid second-order emission.

4.3 Number of water molecules coordinated to 5As-EDTA-Eu^{3+} and 4As-EDTA-Tb^{3+} complexes

Similarly to the behaviour observed for EDTA-Eu^{3+} and EDTA-Tb^{3+} in H_2O-D_2O mixtures, τ^{-1}_{obs} varies linearly with the mole fraction of H_2O for the 5As-EDTA-Eu^{3+} (Figure 4.5 A) and 5As-EDTA-Tb^{3+} (Figure 4.5 B) complexes. All measurements were made at the maximum excitation and emission wavelengths of the complexes; i.e., λ_{exc}/ λ_{em} = 312/616 nm for 5As-EDTA-Eu^{3+} and λ_{exc}/ λ_{em} = 310/547 nm for 4As-EDTA-Tb^{3+}. All data points plotted in the graphs are the averages of six independent measurements. The number of coordinated water molecules calculated with equation 3.2 were 3.06 (5As-EDTA-Eu^{3+}) and 2.95 (4As-EDTA-Tb^{3+}). In both cases, the maximum number of available sites for protein-metal interaction can then be approximated to three. These numbers are in agreement with the facts that EDTA was synthesized to coordinate five sites of the lanthanide ion, and that Eu^{3+} and Tb^{3+} can take up to eight or nine water molecules in their first coordination sphere.

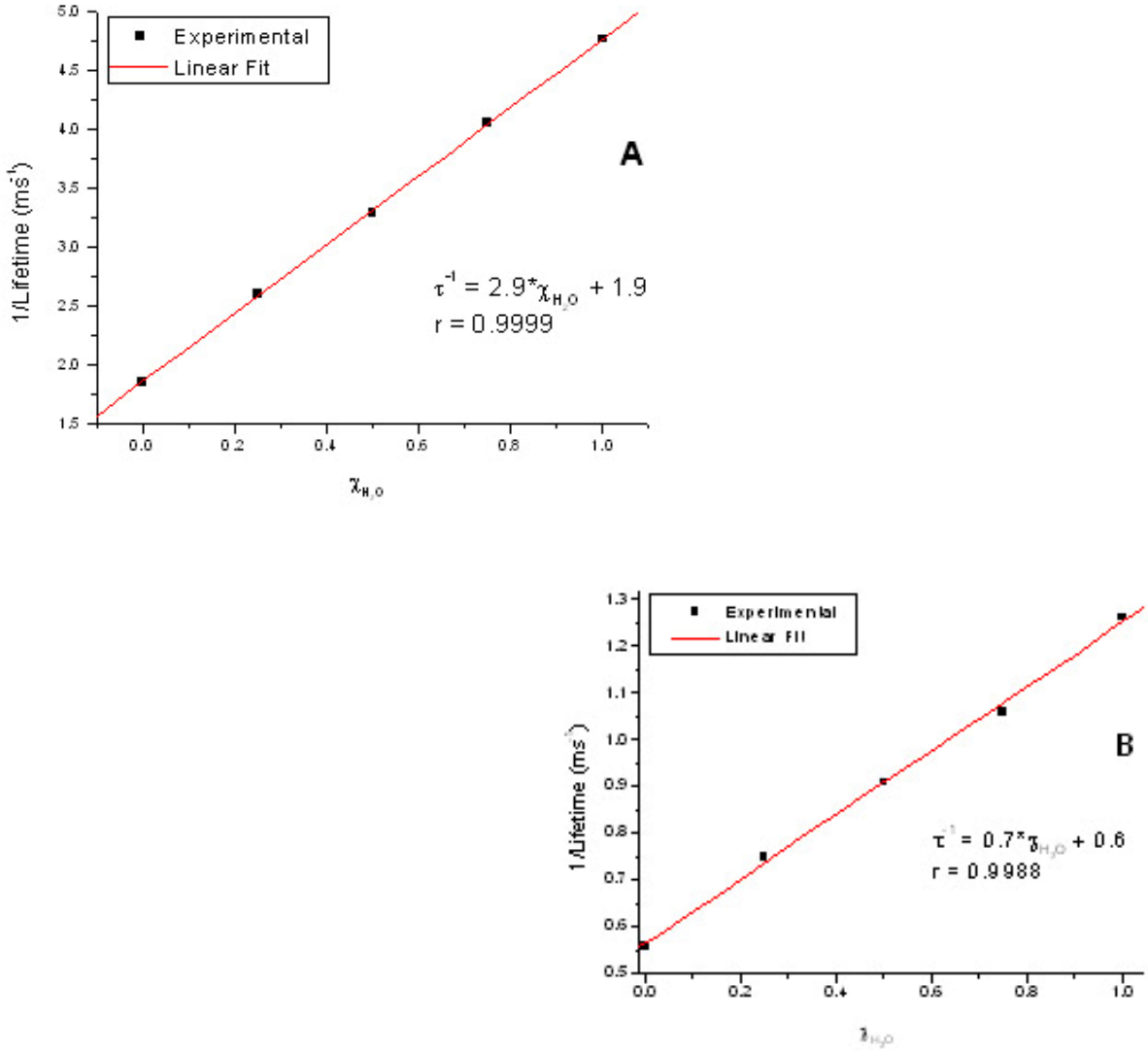

Figure 4.5. Reciprocal luminescence lifetime (τ^{-1}) in ms^{-1} as a function of mole fraction of water (χ_{H2O}) in D_2O-H_2O mixture in 5×10^{-6} M 5As-EDTA-Eu^{3+} (A) and 2×10^{-9} M 4As-EDTA-Tb^{3+} (B).

All samples were prepared in a 25 mM HEPES buffer solution by mixing the corresponding amounts of H_2O and D_2O. Luminescence lifetimes were measured using $\lambda_{exc}/\lambda_{em}$ = 312/616 nm (A), $\lambda_{exc}/\lambda_{em}$ = 310/547 nm (B). Other experimental parameters for wavelength-time matrix collection were: time delay = 0.3 ms, gate width = 1 ms, gate step = 0.02 ms, number of accumulations per spectrum = 100 laser pulses, number of kinetic series per wavelength-time matrix = 40, slit width of spectrograph: 10 mm.

4.4 Quantitative potential for protein analysis

The working concentrations of lanthanide complexes were selected considering the direct correlation that exists between lanthanide complex concentration and protein concentration. The smaller amounts of protein are only detected with the lower complex concentrations (Tables 3.2 and 3.3). The selected working concentrations were 2×10^{-9} M (4As-EDTA-Tb^{3+}) and 5×10^{-6} M (5As-EDTA-Eu^{3+}). These concentrations provide good reproducibility of intensity and lifetime measurements with negligible contribution of instrumental noise. The lower concentration of 4As-EDTA-Tb^{3+} reflects the higher luminescence enhancement promoted by the energy transfer between 4As and Tb^{3+}. Although this complex is potentially more sensitive than 5As-EDTA-Eu^{3+}, its luminescence signal in the presence of proteins decays considerably upon irradiation time in the sample compartment of the spectrofluorimeter. For quantitative analysis, which is based on luminescence intensity, this behavior is not a problem because the analyst can always measure reproducible signals by setting a constant number of excitation pulses. On the other end, it becomes a problem when measuring luminescence decays because it provides inaccurate lifetime values. Since the present approach basis qualitative analysis on lifetime measurements, the 4As-EDTA-Tb^{3+} complex was dropped for further investigations.

Figure 4.6 shows the calibration curve of HSA obtained with 5×10^{-6} M 5As-EDTA-Eu^{3+}. The experiments were performed in batch (25 mM HEPES) and signal intensities were measured after 15 min of protein mixing. The excitation wavelength was 320 nm, so there was no need for protein absorption correction. Clearly, there is direct correlation between the luminescence intensity of the complex and HSA concentration. Linear relationships were also obtained with CA and γ-globulins. Table 4.1 summarizes the AFOM obtained for these three proteins. The luminescence intensities plotted in the calibration graphs were the averages of

individual measurements taken from three aliquots of the same working solution. The LDR of the calibration curves were based on at least five protein concentrations. A straightforward comparison with reported LOD by other methods is difficult because different instrumental setups and experimental and mathematical approaches have been used for their determination. However, we can safely state that the obtained LOD are of the same order of magnitude as those previously reported with the most sensitive methods.[15-17]

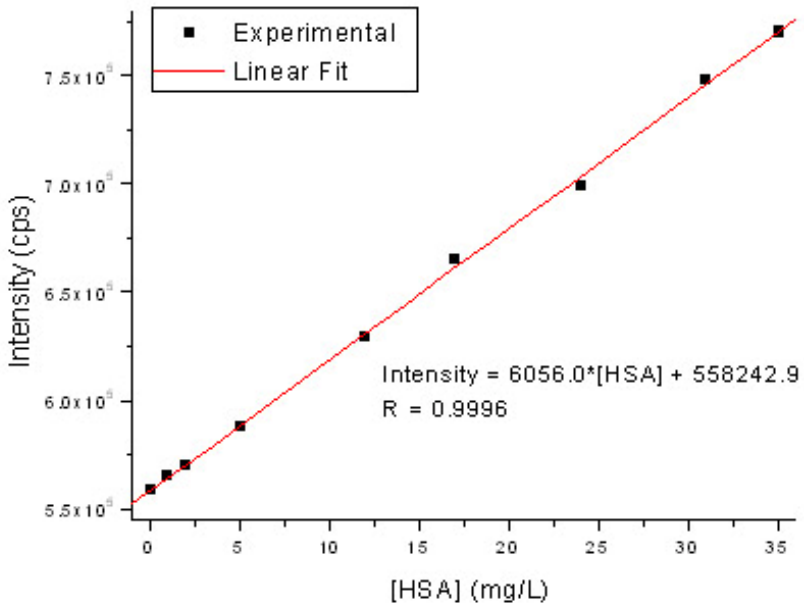

Figure 4.6. Calibration curve for HSA obtained with 5×10^{-6} M 5As-EDTA-Eu^{3+} in 25 mM HEPES.

Intensity measurements were done at $\lambda_{exc}/\lambda_{em}$ = 320/615 nm using 0.15 and 1 ms delay and gate times, respectively. Excitation and emission band-pass were 9 nm. A cutoff filter was used at 400 nm to avoid second order emission.

Table 4.1. AFOM[a] for three proteins obtained with 5As-EDTA-Eu^{3+}.

Protein	LDR (mg/L)	R	LOD (mg/L)
HSA	3.7 – 35.0	0.9992	3.7
CA	13.8 – 615.5	0.9996	13.8
γ-globulins	8.0 – 392.9	0.9998	8.0

[a] Measurements were made in 25 mM HEPES using excitation and emission wavelengths of 320 and 616 nm, respectively. Delay and gate times were 0.15 and 1 ms, respectively. A cutoff filter was used at 450 nm to avoid second-order emission.

4.5 Qualitative potential of 5As-EDTA-Eu^{3+}

The possibility of using the luminescence lifetime of 5As-EDTA-Eu^{3+} for protein identification was investigated with batch experiments carried out in 25 mM HEPES. All measurements were performed with a 5×10^{-6} M final concentration of 5As-EDTA-Eu^{3+} in the analytical sample. The exponential decays were collected at $\lambda_{exc}/\lambda_{em}$ = 312/616 nm after 15 min of protein mixing. Figure 4.7 shows typical decays in the absence and presence of HSA. Single exponential decays with excellent fittings were also observed in the absence and in the presence of CA and γ-globulins.

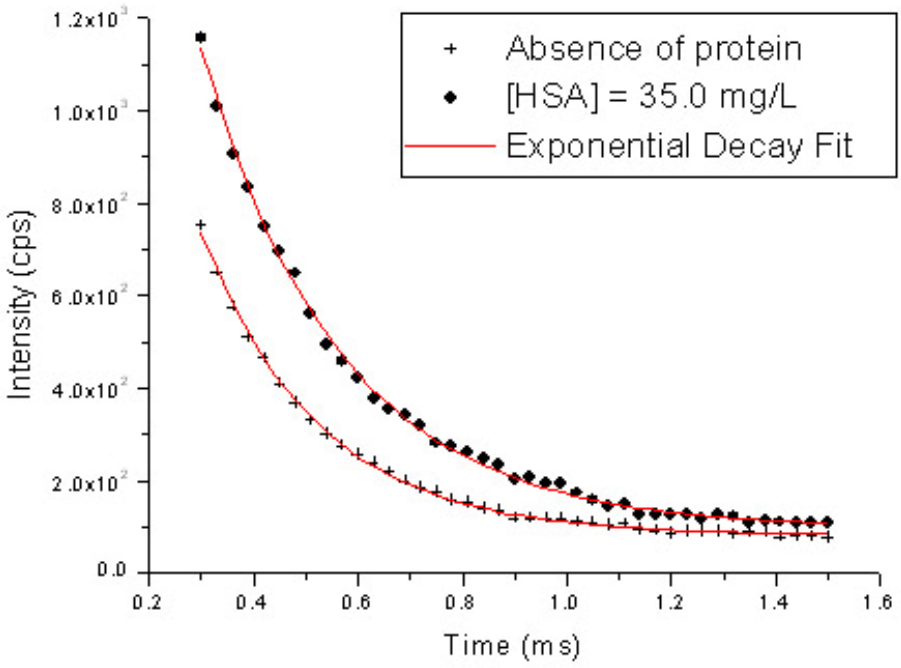

Figure 4.7.Fitted luminescence decay curves for 5×10^{-6} M 5As-EDTA-Eu^{3+} in 25 mM HEPES (x) and in the presence of 35.0 mg/L HSA (●).

Experimental parameters for wavelength-time matrix collection were the following: $\lambda_{exc}/\lambda_{em}$ = 312/616 nm, time delay = 0.3 ms, gate width = 1 ms, gate step = 0.03 ms, number of accumulations per spectrum = 100 laser pulses, number of kinetic series per wavelength-time matrix = 40, slit width of spectrograph: 5 mm.

Table 4.2 compares the reference lifetime (absence of protein) to the lifetimes in the presence of the three proteins. For a confidence level of 95% ($\alpha = 0.05$; $N_1 = N_2 = 6$),[53] the reference value was statistically different from the lifetime in the presence of the three proteins, demonstrating that the lifetime of the complex is sufficiently sensitive to detect the presence of these proteins. The lifetime in the presence of CA was significantly different ($\alpha = 0.05$; $N_1 = N_2 = 6$)[53] from the lifetimes in the presence of the other two proteins. The same is true for HSA and γ-globulins, which demonstrates the possibility of using the complex to identify any one of these proteins in the presence of the other two. The lifetimes in the presence of the three proteins are

significantly longer than the lifetime in the absence of proteins. This is in agreement with the luminescence enhancement observed upon protein interaction with the complex and the assumption that their interactions substitute the O-H oscillators of water molecules with lower-frequency oscillators in the inner coordination sphere of Eu^{3+}. The difference in lifetime values may be ascribed to structural differences of the three proteins.[17,18] Although HSA and CA have both α helix and β sheet structure, CA has mostly β sheet structure. γ-Globulins has only β sheet structure. HSA and CA are hydrophilic types of proteins and γ-globulins is a hydrophobic type of protein.[17,18]

Table 4.2. Comparison of luminescence lifetimes measured with 5As-EDTA-Eu^{3+} in the absence and the presence of proteins.

Protein[a]	Lifetimes[b] (μs)	RSD (%)
—	210 ± 5	2.4
HSA	288 ± 6	2.1
CA	259 ± 5	1.9
γ–globulins	232 ± 6	2.8

[a]Protein solutions were mixed with 5×10^{-6} M 5As-EDTA-Eu^{3+} to provide the following final concentrations: 35.0 mg/L HSA, 615.5 mg/L CA, and 392.9 mg/L γ-globulins. All solutions were prepared in 25 mM HEPES.
[b]Lifetimes are the average values of six measurements taken from six aliquots of sample solution. Experimental parameters for wavelength-time matrix collection were the following: $\lambda_{exc}/\lambda_{em}$ = 312/616 nm, time delay = 0.3 ms, gate width = 1 ms, gate step = 0.03 ms, number of accumulations per spectrum = 100 laser pulses, number of kinetic series per wavelength-time matrix = 40, slit width of spectrograph: 5 mm.

4.6 Conclusions

The two lanthanide complexes present the appropriate spectral characteristics for the purpose at hand. Strong absorption from biological matrixes typically occurs below 300 nm. The broad excitation spectra of 4As-EDTA-Tb^{3+} and 5As-EDTA-Eu^{3+} provide ample opportunity for finding an appropriate excitation wavelength with reduced primary inner filter effects. The experiments were performed upon sample excitation at their maximum excitation wavelengths, but longer excitation wavelengths can certainly promote efficient energy transfer and reproducible reference signals. In both complexes, EDTA takes five coordination sites in the first coordination sphere of the lanthanide ion, forming tightly bound complexes. This is important to retain the physical integrity of the probe upon protein interaction.

There is a linear correlation between the concentration of the complex and the minimum protein concentration detected with the probe. The higher luminescence intensity of 4As-EDTA-Tb^{3+} provides a minimum working concentration-i.e. a complex concentration that still produces a reproducible reference signal-approximately three orders of magnitude lower than the working concentration of 5As-EDTA-Eu^{3+}. This fact makes 4As-EDTA-Tb^{3+} the more sensitive probe. Unfortunately, its luminescence intensity decays considerably upon sample excitation and makes it unsuitable for accurate lifetime analysis. On the other hand, 5As-EDTA-Eu^{3+} turned out to be a valuable probe for liposome-protein interaction. Based on its luminescence intensity, it was possible to quantify CA, HSA, and γ-globulins. This shows an improvement over the EDTA-Eu^{3+} system. The presence of the sensitizer made possible the determination of γ-globulins. The concentration ranges examined in the present study cover the concentration values typically found for HSA, CA and γ-globulins in clinical tests of human blood serum.[66] Our LOD were of the same order of magnitude as those previously reported with the most sensitive methods.[15-17]

The luminescence decay of 5As-EDTA-Eu^{3+} followed well-behaved single exponential decays in the presence and the absence of proteins. It provides a selective parameter for protein identification on the bases of lifetime analysis via a simple mathematical treatment. The statistically different lifetime values demonstrate the selectivity of 5As-EDTA-Eu^{3+} towards HSA, CA, and γ-globulins. However, for the analysis of matrixes with higher complexity-such as those typically found in physiological fluids an additional parameter for selectivity might be necessary to reduce potential interference from other proteins.

CHAPTER 5. LIPOSOME INCORPORATING "5As-EDTA-Eu^{3+}" AS LUMINESCENT PROBES FOR QUALITATIVE AND QUANTITATIVE ANALYSIS OF PROTEINS

5.1 Introduction

This chapter investigates the sensing potential of 5As-EDTA-Eu^{3+} incorporated into polymerized liposomes. The lipophilic character of polymerized liposomes is expected to provide an appropriate platform for protein interaction with the lanthanide ion. The potential of polymerized liposomes as pre-concentrating vesicles for protein analysis is evaluated with HSA, CA, and γ-globulins.

5.2 Spectral characterization of liposomes incorporating 5As-EDTA-Eu^{3+} complex

Figure 5.1 A depicts the SS excitation and emission spectra of the complex 5As-EDTA-Eu^{3+} incorporated into the liposome. Its comparison to Figure 4.3 A shows broader excitation and emission bands and red-shifts in both wavelength maxima. These changes are attributed to the fluorescence contribution from the backbone of the polymerized liposomes. Similar to the unbound complex, the luminescence of Eu^{3+} does not appear in the SS spectrum of the polymerized liposome. It only appears in the TR spectrum (Figure 5.1 B). A 150 μs delay removes the fluorescence contribution from the antenna and the liposomes providing a probe that relies only on the emission wavelengths of Eu^{3+}.

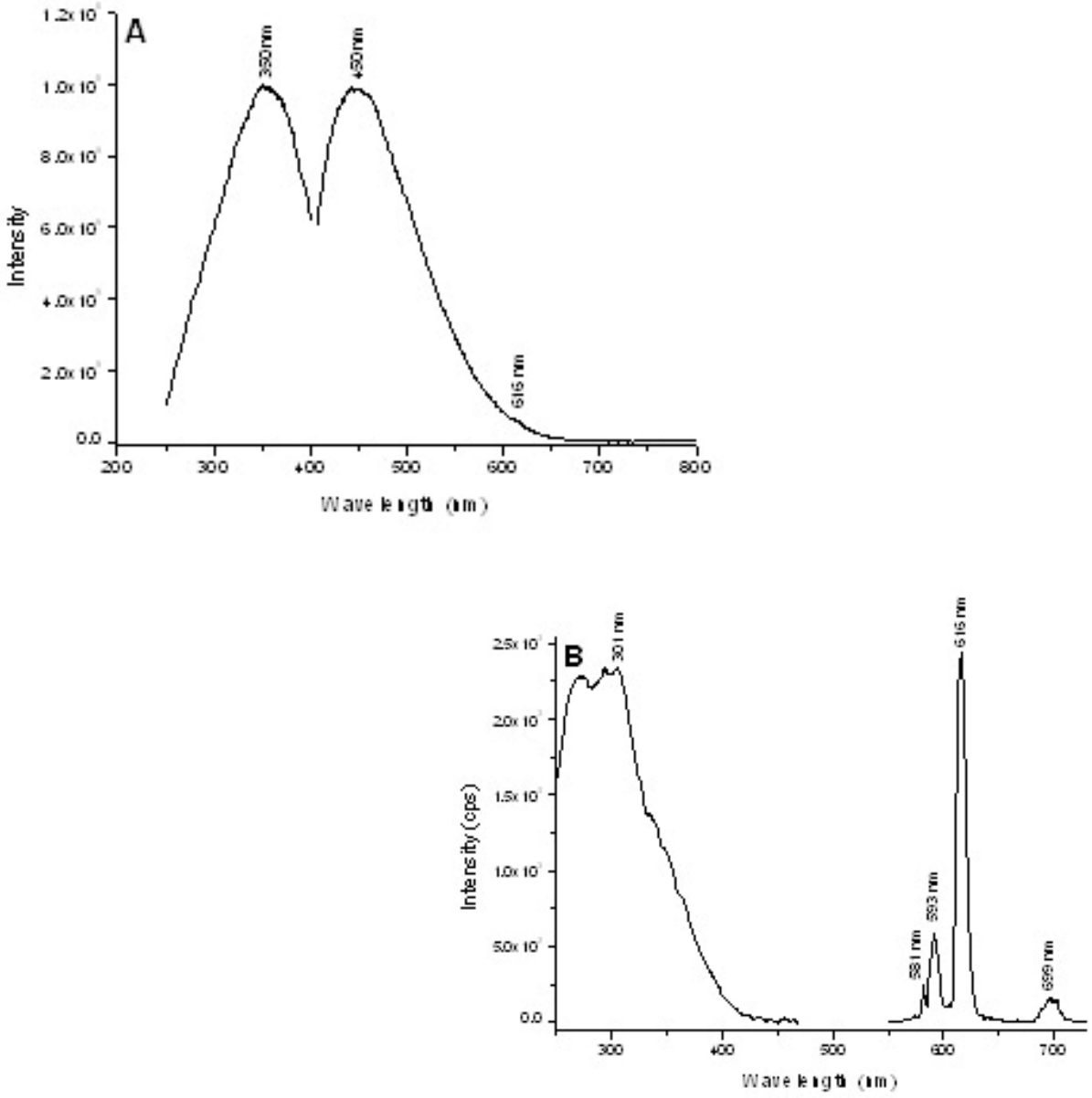

Figure 5.1. Excitation and emission spectra of EDTA-5As-Eu^{3+} incorporated into polymerized liposomes recorded under SS (A) and TR (B) conditions.

SS spectra were recorded using 7 and 2 nm excitation and emission band-pass, respectively at $\lambda_{exc}/\lambda_{em}$ = 350/450 nm. TR spectra were recorded using 30 and 2 nm excitation and emission band-pass, respectively at $\lambda_{exc}/\lambda_{em}$ = 301/616 nm. Delay and gate times were 0.15 and 1 ms, respectively. A cutoff filter was used at 450 nm to avoid second-order emission.

Figure 5.2 A shows the TR excitation-emission matrix (EEM) of the polymerized liposomes. Although the strongest excitation occurs between 275 and 325 nm, a wide excitation range is available to promote luminescence from the lanthanide ion. This versatility provides ample opportunity for finding an appropriate excitation wavelength with minimum or no matrix interference. Figure 5.2 B compares the luminescence emitted by the lanthanide ion upon excitation at 298 nm, 326 nm (the maximum wavelength of the sensitizer (see Figure 4.1), and 395, i.e., a wavelength for the direct excitation of Eu^{3+} (see Figure 3.1). The best signal to background ratio (S/B) away from protein absorption was clearly obtained via energy transfer from the antenna. This excitation wavelength (326 nm) was the one used for all further studies.

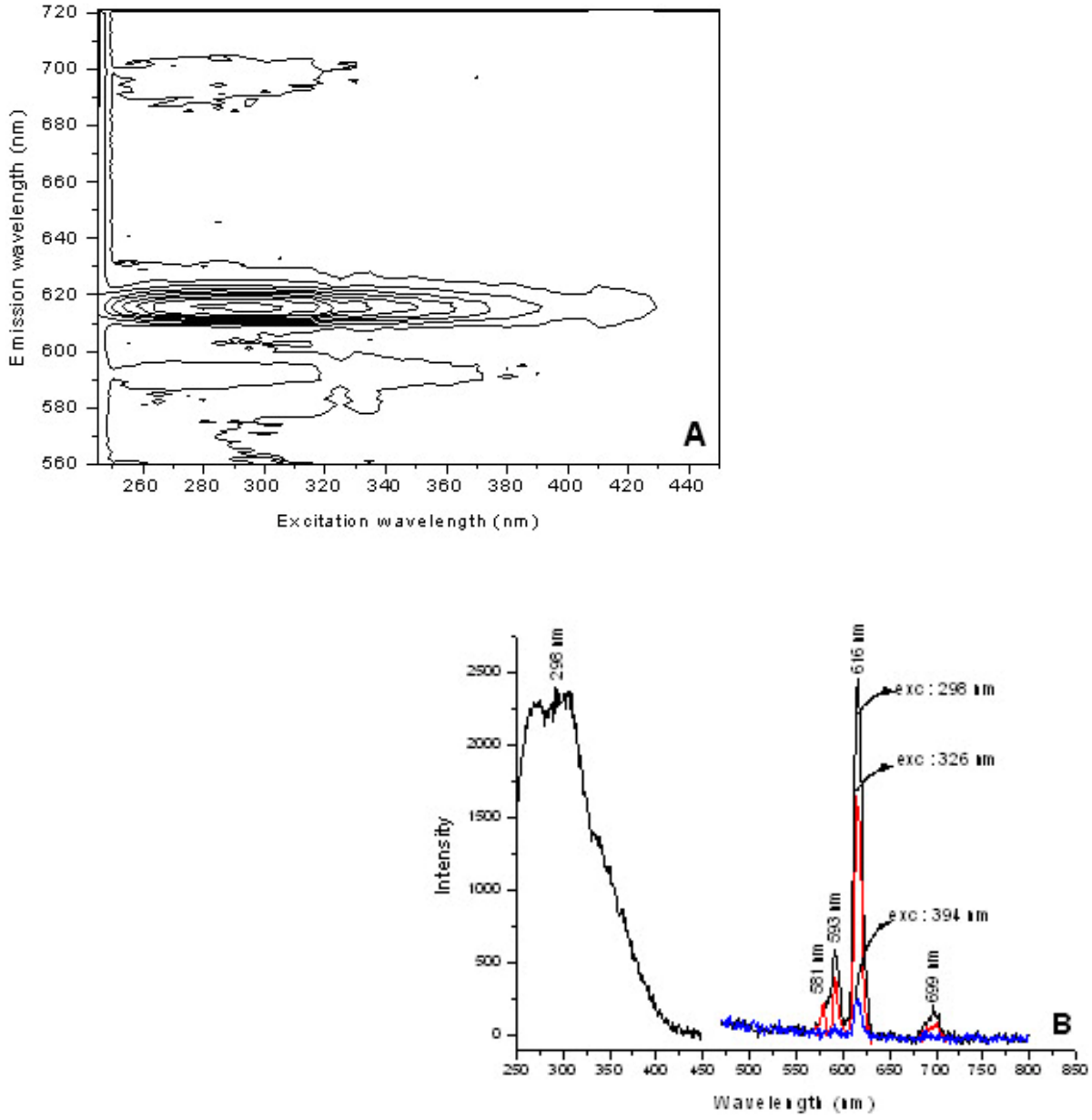

Figure 5.2. (A) TREEM and (B) TR luminescence spectra (500-800 nm) recorded at three excitation wavelengths from a 92.3 mg/L polymerized liposome solution prepared in 25 mM HEPES.

All spectra were recorded using 30 and 2 nm excitation and emission band-pass, respectively. Other acquisition parameters were 0.15 ms delay and 1 ms integration time. A cutoff filter was used at 450 nm to avoid second-order emission. (B) Excitation spectrum (250-450 nm) was recorded monitoring the luminescence intensity at 615 nm.

5.3 Concentration of 5As-EDTA-Eu^{3+} in polymerized liposomes

Initial studies tested the batch-to batch reproducibility of the liposome signal. Signal variations within one order of magnitude were observed from batch to batch. The lack of reproducibility results from different final concentrations of 5As-EDTA-Eu^{3+} in the original liposome batch. A convenient way to eliminate batch-to-batch variability was to work with appropriate amounts of liposome that provided the same 5As-EDTA-Eu^{3+} concentration in all analytical samples. The selected working concentration was 5×10^{-6} M. At this concentration, the S/B was 20 and the relative standard deviation (RSD) of sixteen determinations ($N = 16$) was 2.6 %. Liposome working solutions were prepared upon appropriate dilutions with HEPES buffer. The dilution factors were based on the complex concentration in the original liposome sample.

The original concentration was determined with the method of standard additions. This approach was the method of choice to compensate for potential matrix interference. Different volumes of concentrated 5As-EDTA-Eu^{3+} solution were added to several different sample aliquots of the same liposome volume. The volumes of the standard additions were negligible in comparison to the liposome volumes to ensure that the sample matrix was not significantly changed by dilution with the added standards.

Figure 5.3 shows the least-squares fit of the luminescence intensity as a function of effective analyte standard concentration [$nC_sV_s/(V_x+V_s)$] for two different liposomes batches incorporating 5As-EDTA-Eu^{3+}. C_s is the concentration of standard, V_s is the volume of aliquot sample, and n is the number of standard additions (n = 0-5). The luminescence intensities plotted in the graph were subtracted from the blank intensity, which corresponded to the average intensity of six measurements taken from a 25 mM HEPES buffer solution. Similarly, each point in the calibration graph corresponds to the average of six intensity measurements taken from six

individual aliquots of standard solution. The correlation coefficients close to unity, 0.9989 and 0.9982, demonstrate the linear relationship between luminescence intensity and 5As-EDTA-Eu^{3+} complex concentration. The extrapolation of the linear plot to $y = 0$ provides a concentration of Eu^{3+} estimated as 2.32×10^{-4} M and 7.95×10^{-5} M in the polymerized liposomes.

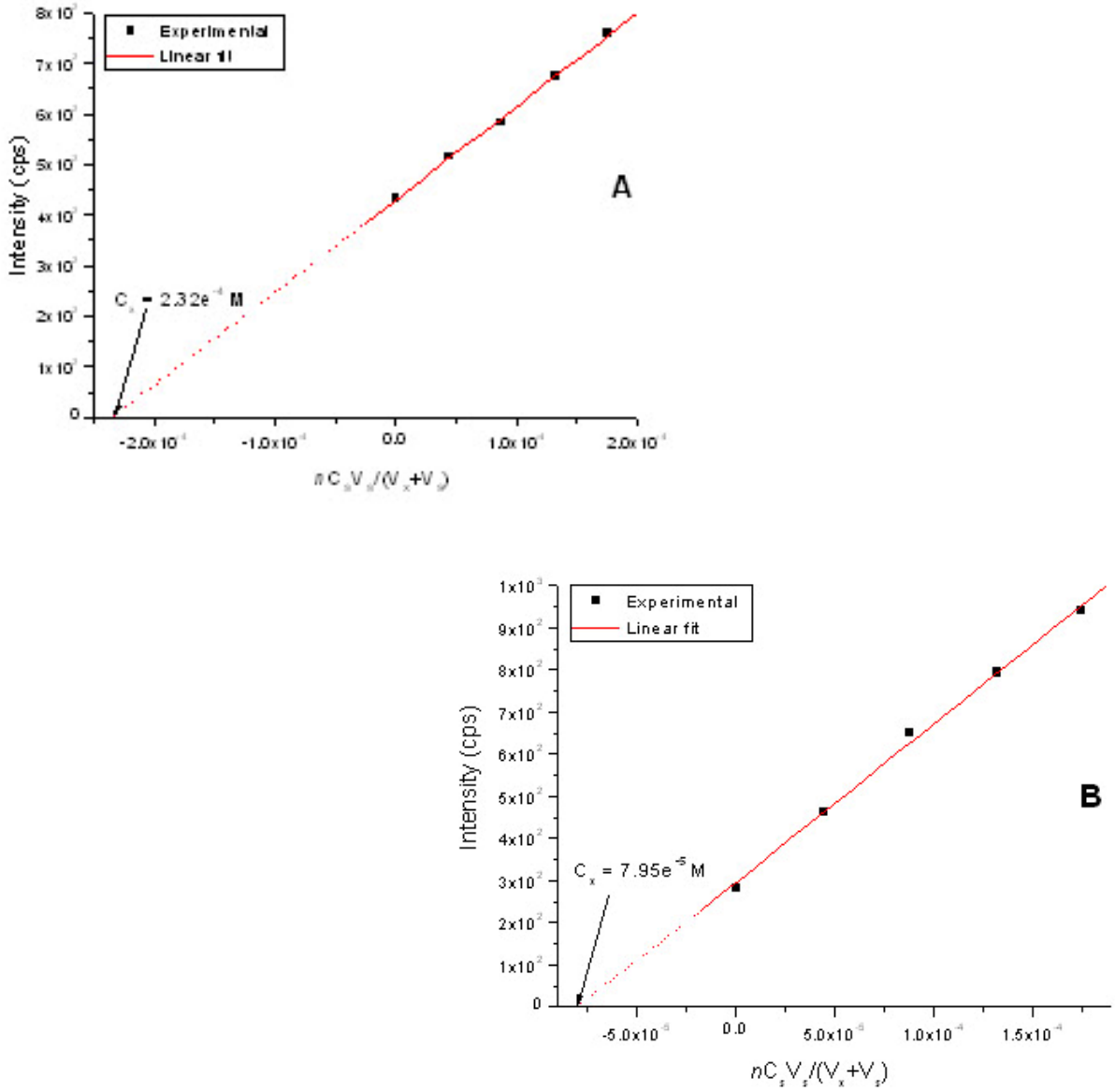

Figure 5.3. Luminescence intensity of two different batches (A and B) of polymerized liposomes incorporating 5As-EDTA-Eu^{3+} as a function of standard addition concentration.

Intensities were recorded at $\lambda_{exc}/\lambda_{em}$ = 326/616 nm with 0.15 and 1 ms delay and gate times, respectively. Excitation and emission band-pass were 20 and 2 nm, respectively. A cutoff filter at 450 nm was used to avoid second-order emission.

5.4 Number of water molecules coordinated to liposome incorporating 5As-EDTA-Eu^{3+} complex

Figure 5.4 shows the reciprocal luminescence lifetime (τ^{-1}) as a function of mole fraction of water (χ_{H2O}) in D_2O-H_2O mixtures for liposomes incorporating 5As-EDTA-Eu^{3+}. All measurements were made at λ_{exc}/ λ_{em} = 326/615 nm. The lifetime in water (τ_{H2O} = 223.0 ± 7 μs) was obtained from the average of six independent measurements directly taken from the polymerized liposomes in aqueous buffer (25 mM HEPES). The D_2O value (τ_{D2O} = 638.8 μs) was obtained from extrapolation of the linear plot between the experimental reciprocal luminescence lifetime (τ^{-1}) and the mole fraction of water (χ_{H2O}) in the H_2O-D_2O mixtures. The number of coordinated water molecules was calculated as 3.06, which is in good agreement with the fact that EDTA was synthesized to coordinate five sites in the first coordination sphere of the lanthanide ion.

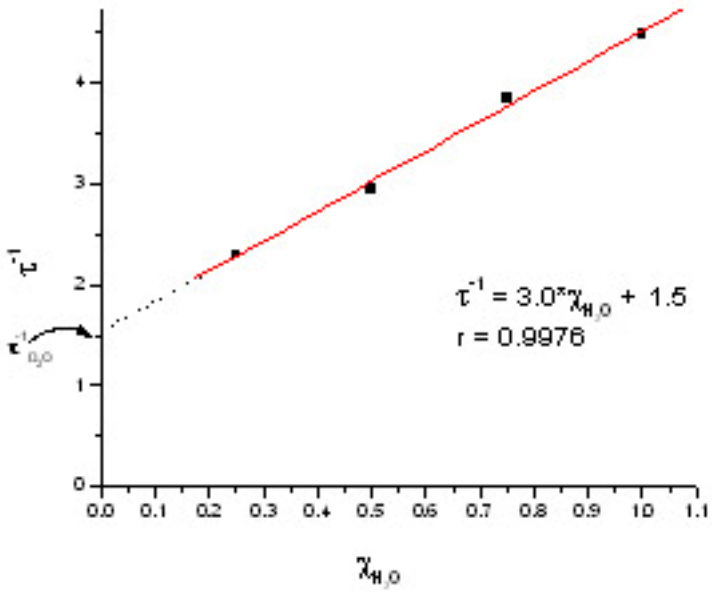

Figure 5.4 . Reciprocal luminescence lifetime (τ^{-1}) in ms^{-1} as a function of mole fraction of water (χ_{H20}) in D_2O-H_20 mixtures in polymerized liposomes incorporating 5As-EDTA-Eu^{3+} solution.

Experimental parameters for wavelength-time matrix collection were the following: λ_{exc}/ λ_{em} = 326/616 nm, time delay = 0.3 ms, gate width = 1 ms, gate step = 0.03 ms, number of accumulations per spectrum = 100 laser pulses, number of kinetic series per wavelength-time matrix = 40, slit width of spectrograph: 5 mm.

5.5 Quantitative analysis with polymerized liposomes

Similar to the expected effect on the luminescence lifetime, the presence of D_2O enhanced the luminescence signal of the polymerized liposomes. The luminescence enhancement was directly proportional to χ_{D2O}. Predicting a similar effect in the presence of the target proteins, the quantitative performance of the proposed sensor was evaluated. Liposome working solutions ([5As-EDTA-Eu^{3+}] = 5×10^{-6} M) were prepared upon appropriate dilutions with HEPES buffer. The dilution factors were based on the complex concentration in the original liposome

sample. Table 5.1 summarizes the AFOM obtained for the three proteins. The luminescence intensities plotted in the calibration graphs are the average of individual measurements taken from three aliquots of the same working solution. The LDR of the calibration curves are based on at least five protein concentrations. The correlation coefficients (R) are close in unity, demonstrating a linear relationship between protein concentration and signal intensity. The relative standard measurements of six aliquots of the same working solution, demonstrate the excellent precision of measurements.

Table 5.1. AFOM[a] obtained with the liposome sensor.

protein	LDR (mg/L)	R	LOD (mg/L)
HSA	1.8-27.0	0.9990	1.8
CA	1.7-24.5	0.9992	1.7
γ-globulins	0.9-18.0	0.9991	0.9

[a] Measurements were made in 25 mM HEPES using excitation and emission wavelengths of 326 and 616 nm, respectively. Delay and gate times were 0.15 and 1 ms, respectively. A cutoff filter was used at 450 nm to avoid second-order emission.

5.6 Qualitative potential of polymerized liposomes

Because no spectral shift is observed in the presence of proteins, extracting qualitative information from the luminescence spectrum of the liposome is not possible. However, the replacement of O-H oscillators by the O-D variety causes a significant change to the luminescence lifetime of the liposome ($\Delta\tau = 415.8 \pm 17.9$ μs). Assuming a similar effect upon protein binding, and knowing that the luminescence lifetime is usually sensitive to the

microenvironment of the luminophor, the feasibility of using this parameter for qualitative analysis of proteins was investigated. The experiments were carried out in batch (25 mM HEPES) with a fixed concentration of liposome ([5As-EDTA-Eu^{3+}] = 5×10^{-6} M). The exponential decays were collected at λ_{exc}/ λ_{em} = 326/615 nm after 15 min of protein mixing. Protein concentrations in the final mixtures were at the upper limit concentration of their respective LDR (see Table 5.1). Single exponential decays with excellent fittings were observed in all the measurements. Table 5.2 compares the reference lifetime (absence of protein) to the lifetimes in the presence of the target proteins. For a confidence level of 95 % (α = 0.05; $N_1 = N_2$ = 6),[53] the reference value was statistically different to the lifetime in the presence of proteins, demonstrating that the lifetime of the liposomes is sufficiently sensitive to probe the presence of a target protein on the bases of lifetime analysis. The lifetime in the presence of CA was statistically different (α = 0.05, $N_1 = N_2$ = 6)[53] to the lifetimes in the presence of the other two proteins. It is possible, therefore, to use the liposome sensor to identify CA against HSA and γ-globulins. On the other end, HSA and γ-globulins provided statistically equivalent (α = 0.05, N_1 = N_2 = 6) lifetimes. The inability to differentiate between these two proteins shows the need for an additional parameter to improve the selectivity of the proposed sensor toward a target protein.

Table 5.2. Comparison of luminescence lifetimes measured with the liposome sensor in the absence and the presence of proteins.

Protein[a]	Lifetimes[b] (μs)	RSD (%)
—	233.0 ± 7.0	3.1
HSA	294.0 ± 7.6	2.6
γ–globulins	301.0 ± 8.0	2.6
CA	353.3 ± 7.5	2.1

[a]Protein solutions were mixed with 5×10^{-6} M 5As-EDTA-Eu^{3+} to provide the following final concentrations: 27 mg/L HSA, 24.5 mg/L CA, and 18.0 mg/L γ-globulins. All solutions were prepared in 25 mM HEPES.
[b]Lifetimes are the average values of six measurements taken from six aliquots of sample solution. Experimental parameters for wavelength-time matrix collection were the following: λ_{exc}/ λ_{em} = 326/616 nm, time delay = 0.3 ms, gate width = 1 ms, gate step = 0.03 ms, number of accumulations per spectrum = 100 laser pulses, number of kinetic series per wavelength-time matrix = 40, slit width of spectrograph: 5 mm.

5.7 Conclusions

The feasibility of using the luminescence response of 5As-EDTA-Eu^{3+} incorporated into polymerized liposomes to monitor protein concentrations in aqueous media was demonstrated. The energy transfer needed for the sensitization of the lanthanide ion was obtained from the antenna and/or liposome, providing a reproducible reference signal for protein determination at the parts per million level. Quantitative analysis is based on the linear relationship between the luminescence signal of the liposome and protein concentration. The luminescence enhancement is attributed to the removal of water molecules from the coordination sphere of Eu^{3+} upon protein interaction. Qualitative analysis is based on the luminescence lifetime of the liposome. This

parameter follows well-behaved single exponential decays in the absence and the presence of proteins. Because the lifetime of the liposome changes significantly upon protein interaction, the potential for protein identification on the bases of lifetime analysis exists. However, the fact that two of the target proteins showed statistically equivalent lifetimes (HSA and γ-globulins) demonstrates the need for additional selectivity. With regard to these two proteins, the use of the liposome presents a drawback compared to free 5As-EDTA-Eu^{3+} which provided discrimination via lifetime analysis.

CHAPTER 6. LIPOSOMES INCORPORATING EDTA-LANTHANIDE^{3+} (NO SENSITIZER) AS LUMINESCENT PROBES FOR QUALITATIVE AND QUANTIVATIVE ANALYSIS OF PROTEINS

6.1 Introduction

Luminescence excitation above 320 nm wavelength is highly desirable in biological matrixes because it avoids inner filter effects from main protein absorption. Chapters 4 and 5 exploit 5As-EDTA-Eu^{3+} as the luminescence probe. With this complex, sample excitation is accomplished at 320nm, an appropriate wavelength to achieve efficient energy transfer from the antenna (5-aminosalicylic acid) to the lanthanide ion. The presence of the antenna overcomes an inherent limitation of the lanthanide ion, which is the rather weak absorption of excitation energy above 300nm. The comparison among the fluorescence of the complex 5As-EDTA-Eu^{3+} when it is incorporated into the liposome (Figure 5.1 A) and when it is free in solution (Figure 4.3 A) reveals that liposomes emit fluorescence when excited in the 250-400 nm range. In this chapter, we focus on the possibility of using the liposome fluorescence for lanthanide ion sensitization.

We investigate the analytical potential of polymerized liposomes incorporating the complexes EDTA-Eu^{3+} and EDTA-Tb^{3+} without sensitizer. We will show that the liposome backbone provides a wide tunable excitation range for lanthanide excitation that extends all the way up to ~ 400nm. Although the luminescence intensity of Eu^{3+} is considerably lower in the absence of the antenna (5As), liposome excitation above 320nm still provides an analytically useful signal (S/B $\geq$ 3) for protein analysis. Upon sample excitation at wavelengths with minimum inner filter effects, excellent AFOM are presented for the analyzed proteins. Distinct

luminescence lifetimes upon protein-liposome interaction demonstrate the feasibility to using the liposome sensor for qualitative analysis of proteins.

6.2 Spectral characterization of liposomes incorporating EDTA-Eu^{3+} and EDTA-Tb^{3+} complexes

Figure 6.1 depicts the SS excitation and emission spectra of the polymerized liposomes incorporating EDTA-Eu^{3+} (A) and EDTA-Tb^{3+} (B). The broad excitation and emission bands correspond to the fluorescence of the liposome backbone. The luminescence contribution of Eu^{3+} appears in the form of a shoulder (592 nm) and a small peak (616 nm). As well, Tb^{3+} luminescence emerges at 546 nm.

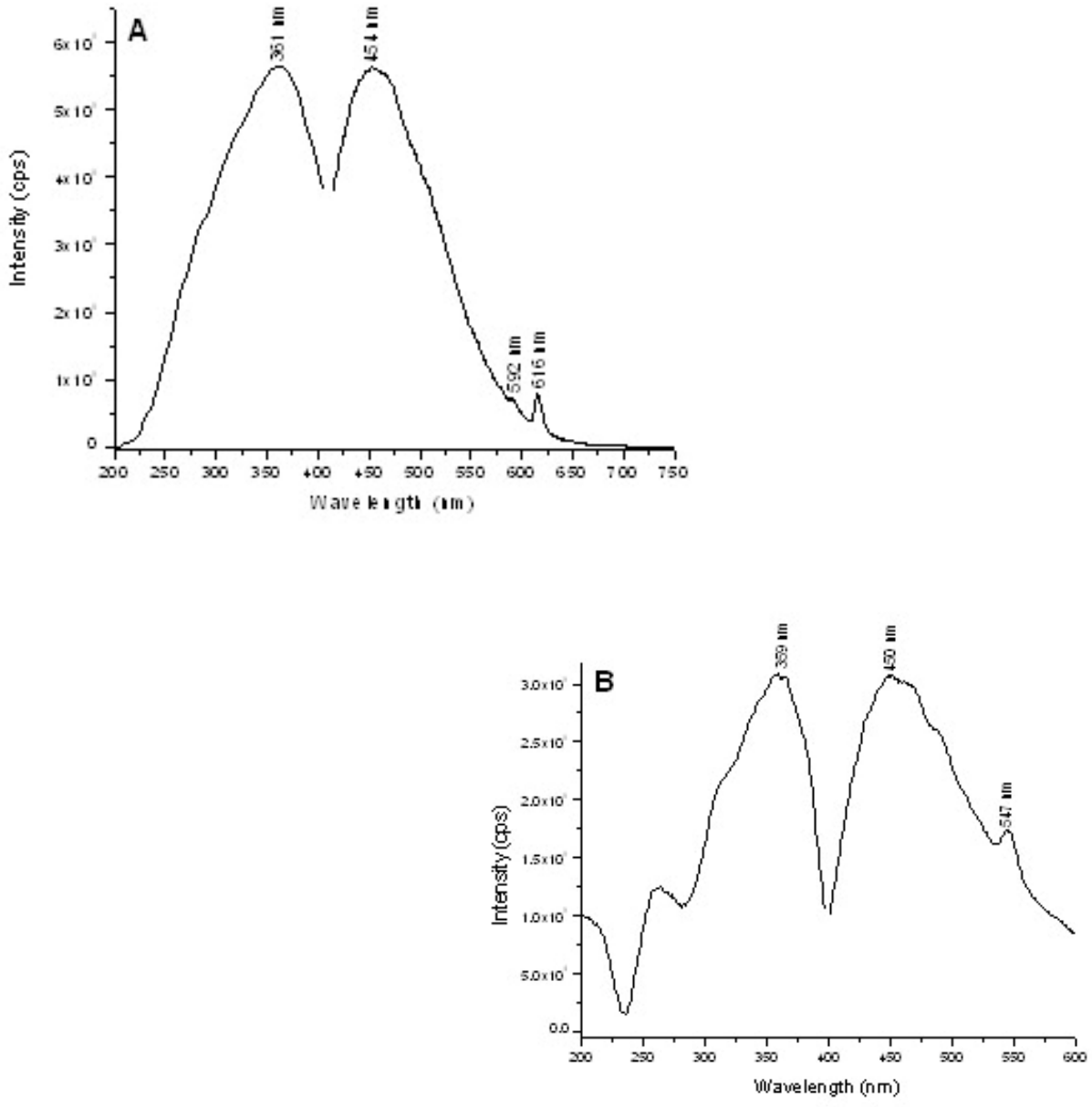

Figure 6.1. SS excitation and emission spectra of the polymerized liposomes incorporating EDTA-Eu^{3+} (A) and EDTA-Tb^{3+} (B).

Both solutions were prepared in 25 mM HEPES. The concentrations of polymerized liposome were 71.3 mg/L (A) and 45.3 mg/L (B). Spectra were recorded using 10 nm excitation and emission band-pass.

The TR excitation and emission spectrum of the liposomes confirms the presence of Eu^{3+} (Figure 6.2 A) and Tb^{3+} (Figure 6.2 B). A 90 μs delay removes the strong fluorescence from the liposome backbone and reveals the luminescence from the lanthanide ion. The luminescence bands are characteristic of the corresponding lanthanide ions.

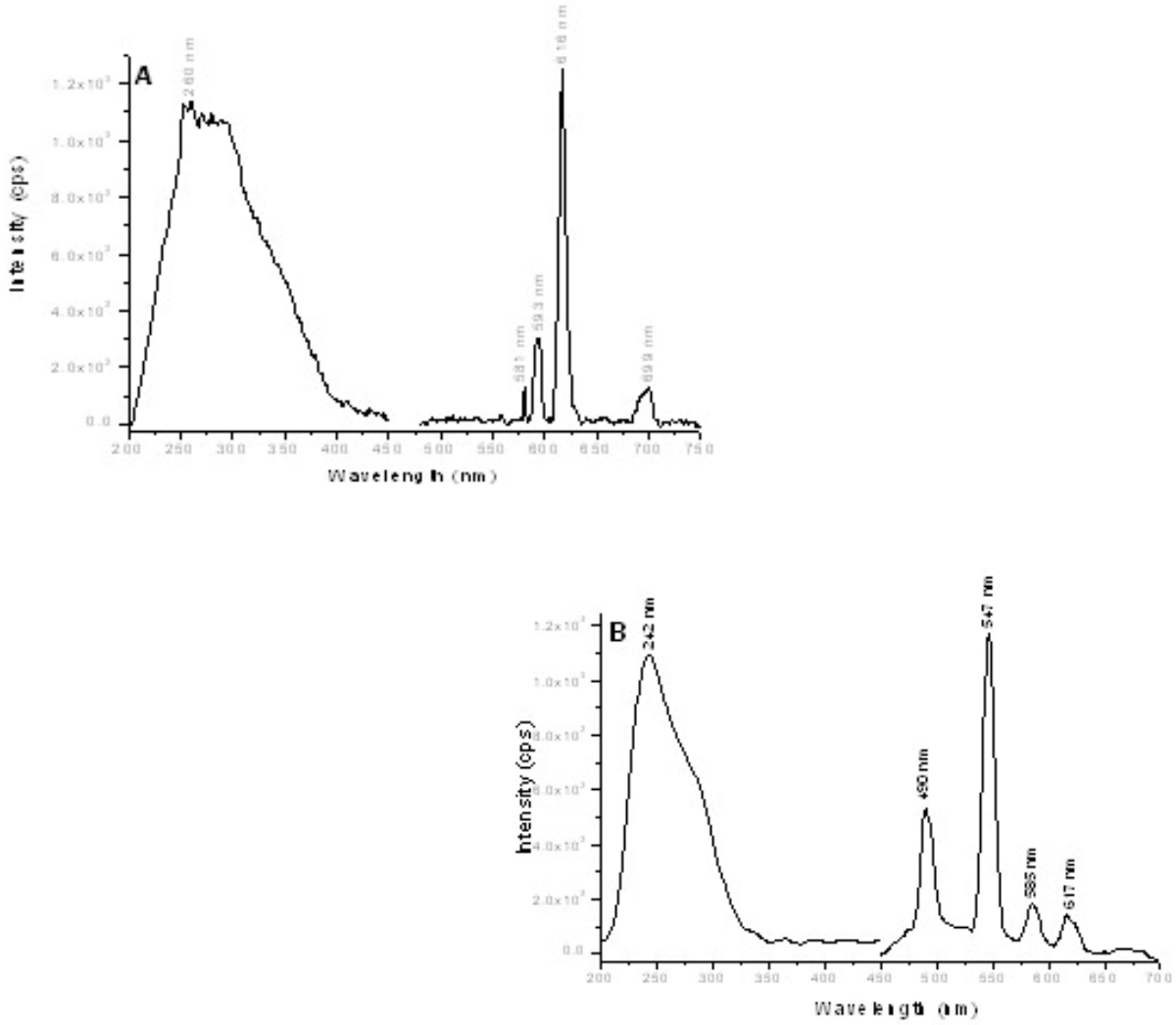

Figure 6.2. TR spectra of polymerized liposomes incorporating EDTA-Eu^{3+} (A) and EDTA-Tb^{3+} (B).

Spectra were recorded using the following parameters: 40 and 7 nm excitation and emission band-pass, respectively. Delay and gate times were 0.9 and 1 ms, respectively. Both solutions were prepared in 25 mM HEPES. The concentrations of polymerized liposome were 71.3 mg/L (A) and 45.3 mg/L (B).

Figure 6.3 depicts the TREEM of the polymerized liposomes incorporating EDTA-Eu^{3+} (A) and EDTA-Tb^{3+} (B). Even though the strongest excitation occurs between 260 nm and 310 nm for both lanthanides, a wide excitation range is available to promote luminescence from the lanthanide ion. This versatility provides ample opportunity of finding an appropriate excitation wavelength with no matrix interference. Here, it is important to point out that the delay needed to time-resolve the fluorescence of the EDTA-Eu^{3+}-liposome (90 μs) was much shorter than the one (150μs) previously used with the 5As-EDTA-Eu^{3+}-liposome. In the context of analytically useful S/B ratios, i.e. S/B ≥ 3, shorter delays are comparatively advantageous because they collect a larger portion of the initial luminescence decay away from instrumental noise.

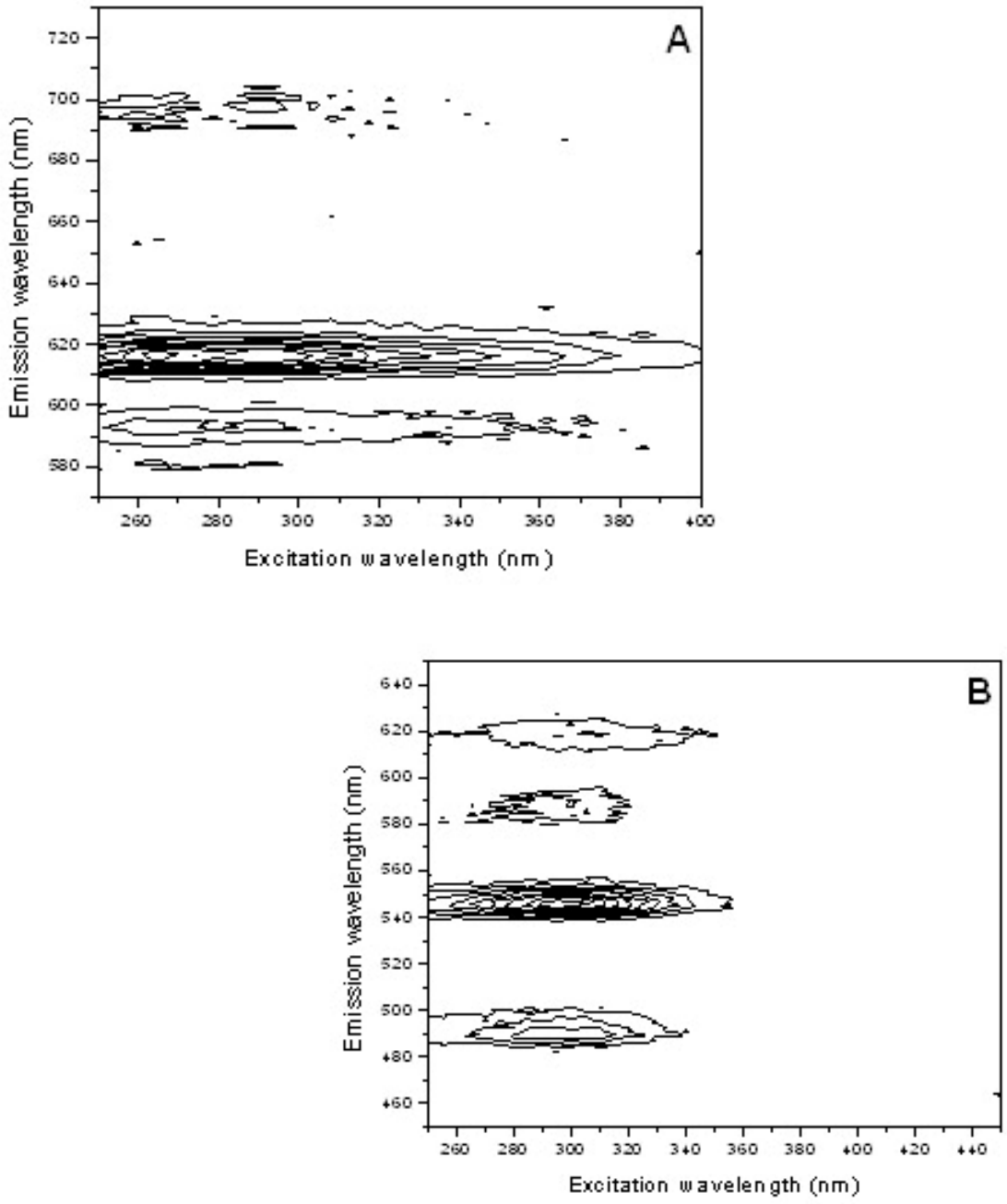

Figure 6.3. TREEM of liposomes incorporating EDTA-Eu^{3+} and EDTA-Tb^{3+}.

Spectra were recorded using the following parameters: 40 and 7 nm excitation and emission band-pass, respectively. Delay and gate times were 0.9 and 1 ms, respectively. Both solutions were prepared in 25 mM HEPES. The concentration of polymerized liposome were 71.3 mg/L (A) and 45.3 mg/L (B).

6.3 Concentration of EDTA-lanthanide^{3+} in polymerized liposomes

As explained in Section 5.3, the original concentration of the complex EDTA-lanthanide^{3+} was determined with the method of standard additions. Following the same approach, which compensates for potential matrix interference, different volumes of concentrated complex solution were added to several different sample aliquots of the same liposome volume. The volumes of the standard additions were insignificant in comparison to the liposome volumes to guarantee that the sample matrix was not considerably altered by dilution with the added standards.

Figure 6.4 shows the least-squares fit of the luminescence intensity as a function of effective analyte standard concentration [$nC_sV_s/(V_x+V_s)$] for liposomes incorporating EDTA-Eu^{3+} (A) and EDTA-Tb^{3+} (B), where C_s is the concentration of standard, V_s is the volume of aliquot sample, and n is the number of standard additions (n = 0-6). The luminescence intensities plotted in the graph were subtracted from the blank intensity, which corresponded to the average intensity of six measurements taken from a 25 mM HEPES buffer solution (pH = 7.0). Similarly, each point in the calibration graph corresponds to the average of six intensity measurements taken from six individual aliquots of standard solution. The correlation coefficients close to unity (0.9972 for liposome-EDTA-Eu^{3+}, 0.9966 for liposome-EDTA-Tb^{3+}) demonstrate the linear relationship between luminescence intensity and lanthanide ion concentration. The extrapolation of the linear plot to $y = 0$ provides the concentration of Eu^{3+} and Tb^{3+} in the polymerized liposomes (3.25×10^{-3} M and 5.55×10^{-6} M, respectively). Because the liposome-EDTA-Tb^{3+} solution was diluted 10 times, the concentration of Tb^{3+} in the original liposome sample was 5.55×10^{-5} M.

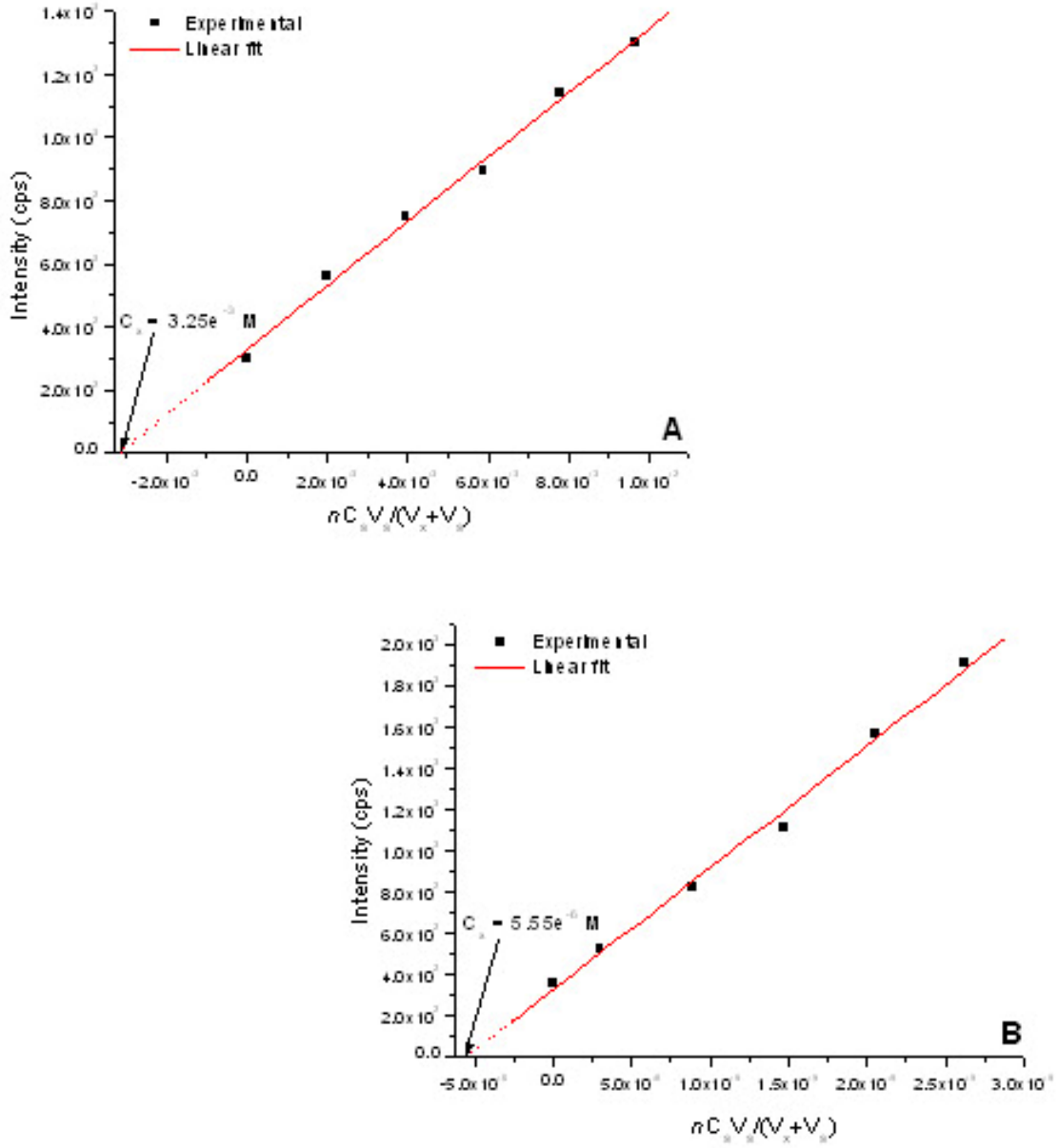

Figure 6.4. Luminescence intensity of polymerized liposomes incorporating EDTA-Eu^{3+} (A) and EDTA-Tb^{3+} (B) as a function of standard addition concentration.

Instrumental parameters were: 0.9 and 1 ms delay and gate times, respectively. Excitation and emission band-pass were 40 and 7 nm, respectively. A cutoff filter at 450 nm was used. Intensities were recorded at $\lambda_{exc}/\lambda_{em}$ = 260/616 nm (A) and $\lambda_{exc}/\lambda_{em}$ = 243/547 nm (B).

Previous knowledge of these concentrations provided the appropriate dilution factors to compensate for batch-to-batch variations of luminescence signal. All analytical samples used for quantitative and qualitative measurements with proteins were then prepared to contain $5x10^{-6}$M EDTA-Eu^{3+} and $3x10^{-7}$M EDTA-Tb^{3+}. The concentrations of lanthanide ions provided useful reference signals for analytical use with relative standard deviations (RSD) below 5 %.

6.4 Number of water molecules coordinated to liposome incorporating EDTA-Eu^{3+} and EDTA-Tb^{3+} complexes

Figure 6.5 shows the reciprocal luminescence lifetime (τ^{-1}) as a function of mole fraction of water (χ_{H2O}) in D_2O-H_2O mixtures for liposomes incorporating EDTA-Eu^{3+} (A) and EDTA-Tb^{3+} (B). Measurements were made with a commercial spectrofluorimeter at the maximum excitation and emission wavelengths (λ_{exc}/ λ_{em}) of the samples; i.e., λ_{exc}/ λ_{em} = 260/615 nm for liposomes incorporating EDTA-Eu^{3+} and λ_{exc}/ λ_{em} = 243/547 nm for liposomes incorporating EDTA-Tb^{3+}. Each lifetime plotted in the graph represents the average of six independent measurements. The number of coordinated water molecules were calculated as 2.95 (liposome-EDTA-Eu^{3+}) and 2.98 (liposome-EDTA-Tb^{3+}). Therefore, the maximum number of available sites for protein-metal interaction can be approximated to three in both types of liposomes. These results are in good agreement with the fact that Eu^{3+} and Tb^{3+} can take up to eight or nine molecules in their first coordination sphere and EDTA was synthesized to coordinate five sites of the lanthanide ion.

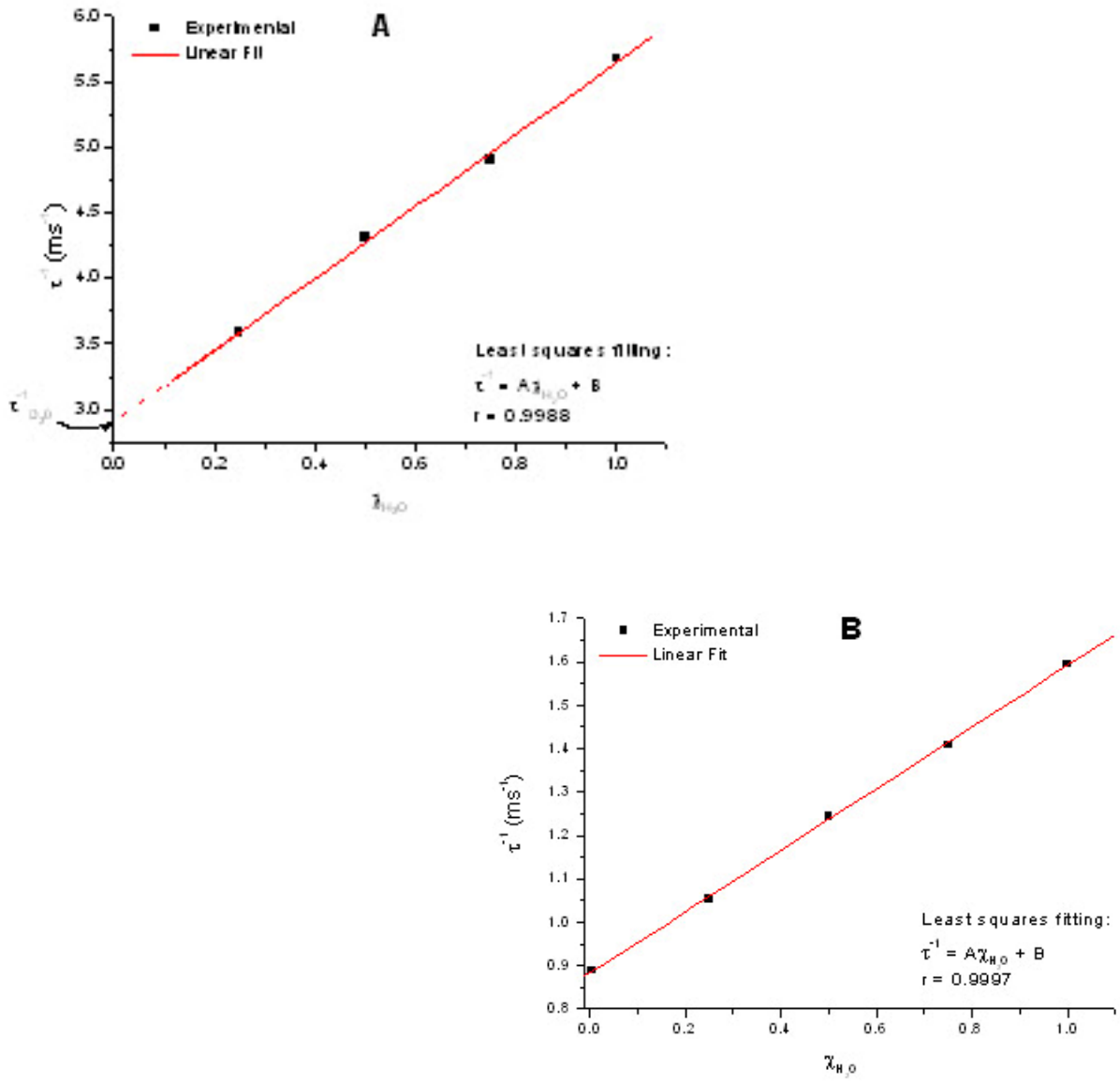

Figure 6.5. Reciprocal luminescence lifetime (τ^{-1}) in ms^{-1} as a function of mole fraction of water (χ_{H20}) in D_2O-H_2O mixtures in polymerized liposomes incorporating 5×10^{-6} M EDTA-Eu^{3+} (A) and 3×10^{-7} M EDTA-Tb^{3+} (B).

Experimental parameters for wavelength-time matrix collection were the following: time delay = 0.3 ms, gate width = 1 ms (A), 3 ms (B), gate step = 0.03 ms, number of accumulations per spectrum = 100 laser pulses, number of kinetic series per wavelength-time matrix = 40, slit width of spectrograph: 5 mm.λexc/λem = 260/616 nm (A), and λexc/λem = 260/547 nm (B).

6.5 Liposomes incorporating EDTA-Eu^{3+} as probes for protein analysis

6.5.1 Quantitative analysis with the liposomes incorporating EDTA-Eu^{3+}

Upon protein interaction with the polymerized liposome, the luminescence intensity of the lanthanide ion experiences a considerable enhancement. Within a certain range of protein concentrations, the magnitude of the luminescence enhancement correlates linearly with protein concentration. Figure 6.6 shows the observed titration curves when the luminescence signal of the liposome sensor was monitored as a function of increasing protein concentrations. All measurements were made in batch (25mM HEPES) after 15 minutes of protein mixing. In the case of HSA (Figure 6.6 A) and Thermolysin (Figure 6.6 B), the luminescence intensity of Eu^{3+} reached a plateau after a certain protein concentration. The behavior of CA is different as it presents a linear correlation within the entire range of studied concentrations (Figures 6.6 C). In the case of γ-globulins (Figure 6.6 D), the luminescence intensity of the lanthanide ion drastically dropped after reaching the upper limit of the LDR. It is important to note that all luminescence intensities were corrected for inner filter effects.

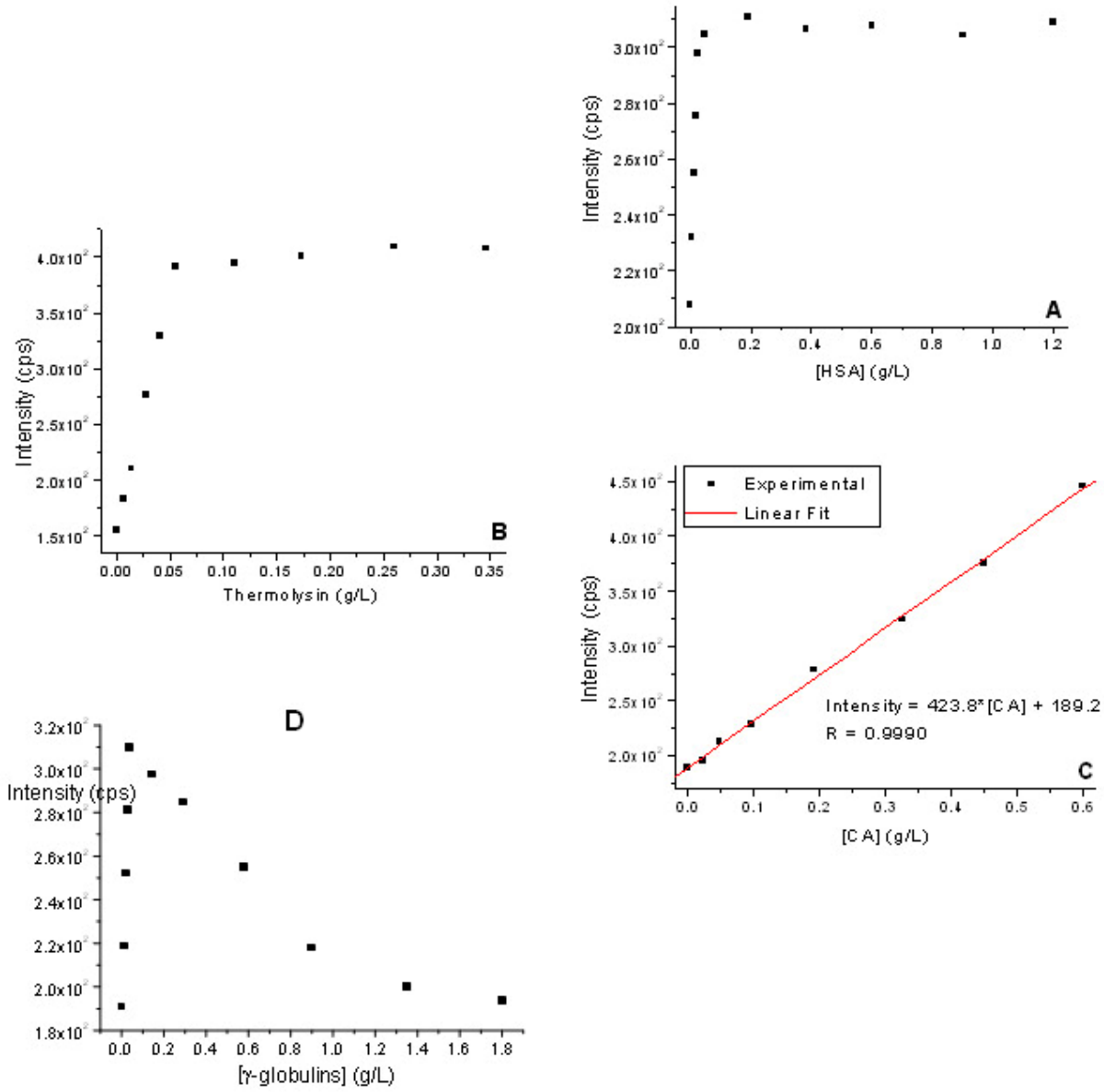

Figure 6.6. Titration curves for HSA (A), Thermolysin (B), CA (C), and γ-globulins (D) obtained with polymerized liposomes incorporating 5×10^{-6} M EDTA-Eu^{3+}.

Intensity measurements were done at λ_{exc}/ λ_{em} = 266/616 nm using 90 μs and 1000 μs delay and gate times, respectively. Excitation and emission band-pass were 40 and 5, respectively. A cutoff filter was used at 400 nm to avoid second-order emission.

Figure 6.7 shows the "least squares fitting" of the linear portions of the titration curves of HSA (A), Thermolysin (B), and γ-globulins. The luminescence intensities plotted in the calibration graphs are the averages of individual measurements taken from three aliquots of the same working solution. Excellent fittings were obtained for all the studied proteins.

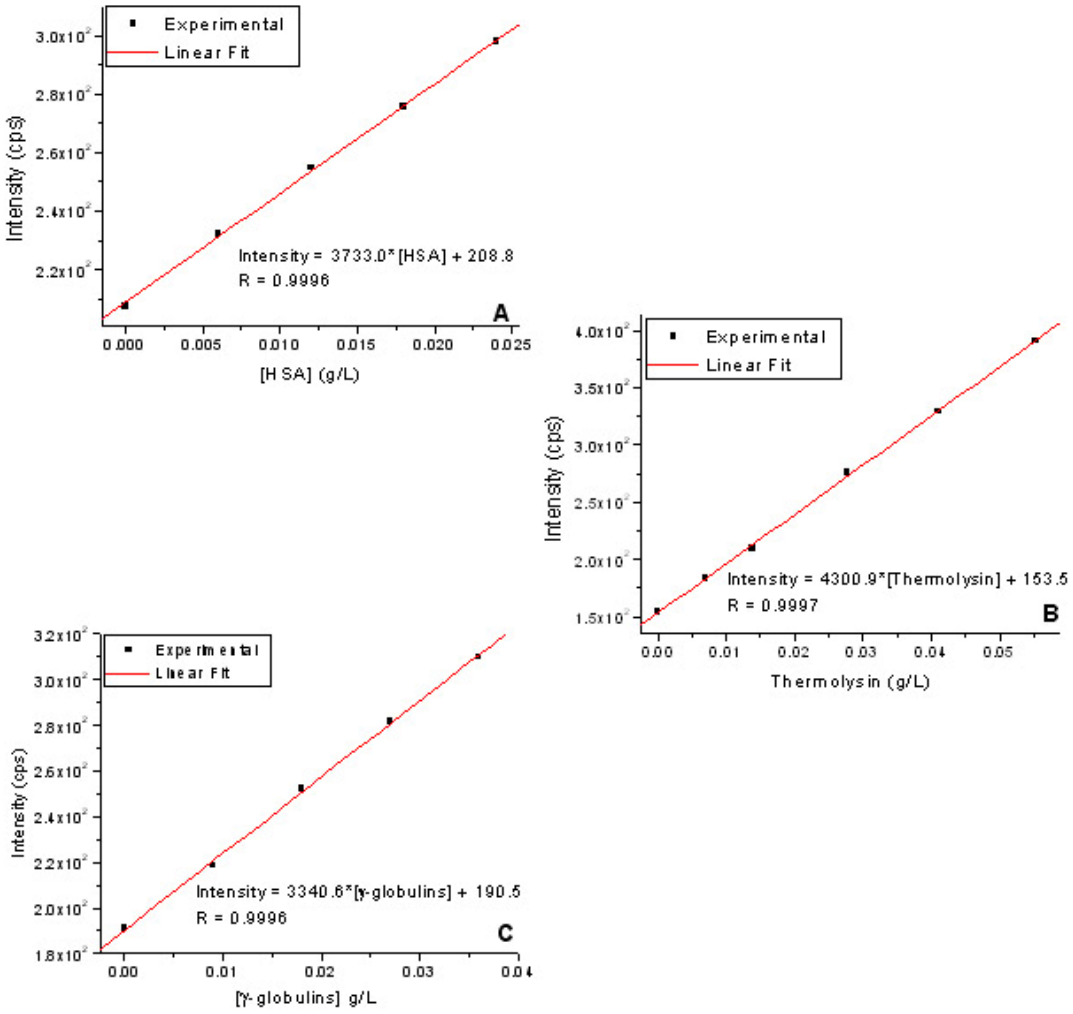

Figure 6.7. Calibration curves for HSA (A), Thermolysin (B), and γ-globulins (C) obtained with polymerized liposomes incorporating 5×10^{-6} M EDTA-Eu^{3+}.

Measurements were performed under instrumental conditions stated in Figure 6.6.

Table 6.1 summarizes the AFOM obtained with the liposome sensor for the four studied proteins. The LDR of the calibration curves are based on at least five protein concentrations. All correlation coefficients were close to unity showing excellent potential for quantitative analysis of proteins. Two excitation wavelengths were used for LOD determination. Excitation at 266 nm provides the highest intensity of the reference signal as it directly excites the lanthanide ion at its maximum excitation wavelength. In this case, the intensity of the reference signal was corrected for protein absorption. Excitation at 320nm provides an excitation wavelength above the main protein absorption region and, therefore, extremely desirable for bio-analytical work. The obtained LOD, which were in the parts per million (ppm) range for any given protein at both excitation wavelengths demonstrate the feasibility to perform sensitive protein detection at relatively long wavelength. A straightforward comparison with reported LOD for these four proteins is difficult because different instrumental set ups, experimental and mathematical approaches have been used for their determination. However, we can safely state that our levels of detection are of the same order of magnitude as those previously reported with most sensitive methods.[15-17]

Table 6.1. AFOM[a] obtained with the liposomes incorporating EDTA-Eu^{3+}

Protein	LDR (mg/L)	R	LOD (mg/L) (λ_{exc} = 266 nm)	LOD (mg/L) (λ_{exc} = 320 nm)
HSA	1.5-24.0	0.9996	1.5	6.8
CA	19.2-600.0	0.9989	19.2	56.2
γ-globulins	2.5-36.0	0.9996	2.5	7.5
Thermolysin	1.6-55.4	0.9997	1.6	6.5

[a] Measurements were performed under instrumental conditions stated in Figure 6.6.

6.5.2 Qualitative analysis with liposomes incorporating EDTA-Eu^{3+}

Previous work with polymerized liposome incorporating 5As-EDTA-Eu^{3+} (Chapter 4) has shown a significant change on the luminescence lifetime of the lanthanide ion upon protein interaction with the liposome sensor. Similar to the effect observed with D_2O, protein interaction increases the lifetime of the luminescence decay. Because the luminescence lifetime is sensitive to the microenvironment of the lanthanide ion, the feasibility of using this parameter for qualitative analysis of proteins was investigated. Similar studies were performed here. Lifetime measurements were performed along the entire LDR of the studied proteins. Single exponential decays with excellent fittings are observed in all cases. Table 6.2 compares the reference lifetime (absence of protein) to the lifetimes in the presence of the target proteins. Protein concentrations corresponded to their respective asymptotic values. For a confidence level of 95% ($\alpha = 0.05$; $N_1 = N_2 = 6$)[53] the reference value was statistically different from the lifetime in the presence of

proteins, demonstrating that the lifetime of the liposome is sufficiently sensitive to probe the presence of a target protein on the bases of lifetime analysis. In addition, all the lifetimes in the presence of proteins were statistically different ($\alpha = 0.05$, $N_1 = N_2 = 6$)[53], showing the feasibility to differentiate these four proteins on the bases of lifetime analysis. These results show an advantage over the liposome incorporating 5As-EDTA-Eu^{3+}, which was incapable to distinguish between HSA and γ-globulins (Section 3.5.).

Table 6.2. Comparison of luminescence lifetimes measured with the liposomes incorporating in the absence and the presence of proteins.

Protein[a]	Lifetime[b] (μs)	RSD (%)
—	177.3 ± 4.4	2.5
HSA	223.1 ± 4.0	1.8
CA	276.7 ± 10.2	3.7
γ-globulins	248.4 ± 5.2	2.1
Thermolysin	370.1 ± 17.7	4.8

[a]Protein solutions were mixed with polymerized liposomes incorporating 5×10^{-6} M EDTA-Eu^{3+} to provide the following final concentrations: 24.0 mg/L HSA, 600.0 mg/L CA, 36.0 mg/L γ-globulins, and 55.4 mg/L Thermolysin. All solutions were prepared in 25 mM HEPES. [b]Lifetimes are the average values of six measurements taken from six aliquots of sample solution. Experimental parameters for wavelength-time matrix collection were the following: $\lambda_{exc}/\lambda_{em}$ = 266/616 nm, time delay = 0.09 ms, gate width = 1 ms, gate step = 0.03 ms, number of accumulations per spectrum = 100 laser pulses, number of kinetic series per wavelength-time matrix = 40, slit width of spectrograph: 10 mm.

6.6 Liposomes incorporating EDTA-Tb^{3+} as a probe for protein analysis

6.6.1 Quantitative analysis with liposoms incorporating EDTA-Tb^{3+}

Batch titrations of HSA, CA, and γ-globulins were unsuccessfully attempted with this system. On the other hand, the sensor was sensitive to the presence of Thermolysin and α-amylase. Figure 6.8 A and B show the resulting titration curves. All experiments were performed in batch (25 mM HEPES) and signal intensities were measured after 15 min of protein mixing. Linear correlations were observed below 8.65 mg/L for Thermolysin (see Figure 6.8 C) and 50 mg/L for α-amylase (see Figure 6.8 D).

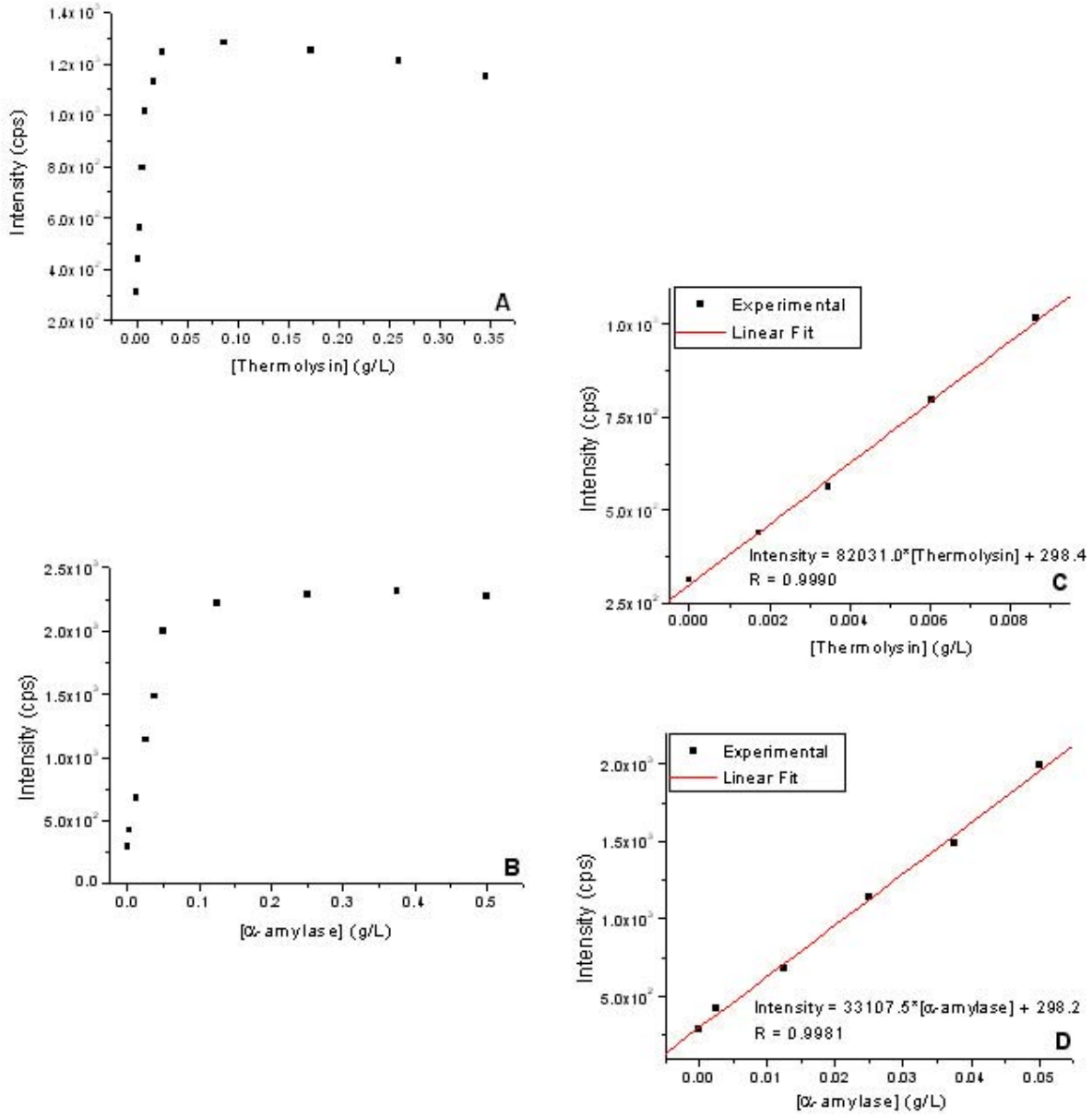

Figure 6.8. Titration curves for Thermolysin (A,C) and α-amylase (B,D) obtained with polymerized liposomes incorporating 3×10^{-7} M EDTA-Tb^{3+}.

Intensity measurements were done at λ_{exc}/ λ_{em} = 266/547 nm using 90 μs and 1000 μs delay and gate times, respectively. Spectra were recorded using 40 and 6 nm excitation and emission band-pass, respectively. A cutoff filter was used at 400 nm to avoid second-order emission.

Table 6.3 summarizes the AFOM obtained with the liposome sensor for the two proteins. The LDR of the calibration curves are based on at least five protein concentrations. All correlation coefficients were close to unity showing excellent potential for quantitative analysis of proteins. Emission intensity was corrected for protein absorption when exciting at 266 nm. The LOD (ppm) obtained for Thermolysin and α-amylase at both wavelengths prove the ability of the sensor to quantify these proteins at low concentration levels. The higher LOD values at 320 nm reflect the poorer reproducibility of measurements of the reference signal.

Table 6.3. AFOM[a] obtained with the liposomes incorporating EDTA-Tb^{3+}

Protein	LDR (mg/L)	R	LOD (mg/L) (λ_{exc} = 266 nm)	LOD (mg/L) (λ_{exc} = 320 nm)
α-amylase	2.1 – 50.0	0.9981	2.1	58.6
Thermolysin	0.4 – 8.7	0.9990	0.4	33.1

[a] Measurements were performed under instrumental conditions stated in Figure 6.8.

6.6.2 Qualitative analysis with the liposome-EDTA-Tb^{3+} sensor

Lifetime measurements were performed along the entire LDR of the two proteins. Single exponential decays with excellent fittings were observed in all cases. Table 6.4 compares the reference lifetime (absence of protein) to the lifetimes in the presence of the target proteins. For a confidence level of 95% ($\alpha = 0.05$; $N_1 = N_2 = 6$)[53] the reference value was statistically different

to the lifetime in the presence of proteins, demonstrating that the lifetime of the liposome is sufficiently sensitive to probe the presence of these two proteins.

Table 6.4. Comparison of luminescence lifetimes measured with the liposomes incorporating EDTA-Tb^{3+} in the absence and the presence of proteins.

Protein[a]	Lifetimes[b] (μs)	RSD (%)
—	511.8 ± 15.8	3.1
α-amylase	891.3 ± 22.3	2.5
Thermolysin	1293.7 ± 51.7	4.0

[a]Protein solutions were mixed with polymerized liposomes incorporating 3×10^{-7} M EDTA-Tb^{3+} to provide the following final concentrations: 50.0 mg/L α-amylase, and 8.7 mg/L Thermolysin. All solutions were prepared in 25 mM HEPES. [b]Lifetimes are the average values of six measurements taken from six aliquots of sample solution. Experimental parameters for wavelength-time matrix collection were the following: λ_{exc}/ λ_{em} = 266/616 nm, time delay = 0.09 ms, gate width = 3 ms, gate step = 0.03 ms, number of accumulations per spectrum = 100 laser pulses, number of kinetic series per wavelength-time matrix = 40, slit width of spectrograph: 10 mm.

In comparison to its EDTA-Eu^{3+} counterpart, this liposome presents the advantage of being sensitive toward the presence of α-amylase. On the other hand, liposomes incorporating EDTA-Tb^{3+} were not sensitive to the presence of HSA, CA, and γ-globulins.

6.7 Conclusions

The feasibility to using the luminescence response of polymerized liposomes incorporating EDTA-Eu^{3+} or EDTA-Tb^{3+} for monitoring protein concentrations in aqueous

media has been demonstrated. Two excitation wavelengths - 266 and 320nm - were used for LOD determination. Excitation at 266nm directly excites the luminescence of the lanthanide ion at its maximum excitation wavelength and, therefore, provides the highest S/B ratio for the reference signal. Because there is a direct correlation between liposome and protein concentration and protein traces are detected only with relatively low lanthanide concentrations, there is the possibility to lowering the liposome concentration to reach even better LOD. The main disadvantage of sample excitation at 266nm is the need to correct for protein absorption. In a matrix of unknown protein composition, the inadvertently use of inappropriate correction factors might significantly affect the accuracy of analysis. Excitation at 320nm provides an excitation wavelength above the main protein absorption region and, therefore, extremely desirable for bio-analytical work. In this case, however, the relatively low intensity of the reference signal (S/B = 3) excludes the possibility to lower liposome concentration for LOD improvement.

The liposome incorporating EDTA-Eu^{3+} presents a major advantage over its 5As counterpart (Chapter 5), since it is capable to differentiate among HSA and γ-globulins. Offsetting this advantage, its LOD for CA was two orders of magnitude worse than the one obtained with the liposome incorporating 5As- EDTA-Eu^{3+}. The liposome incorporating EDTA-Tb^{3+} presents no improvements over the EDTA-Tb^{3+} complex since the liposomes are capable of detecting only two proteins (α-amylase and Thermolysin).

CHAPTER 7. ANALYTICAL POTENTIAL OF LIPOSOMES INCORPORATING EDTA-LANTHANIDE^{3+} AND IDA-Cu^{2+} TO ANALYZE PROTEINS

7.1 Introduction

Every protein has a unique pattern of histidine residues on its surface. It is then possible to bind transition metal complexes to proteins via histidine residues.[69] Transition metal ions (e.g., Cu^{2+}, Ni^{2+}, etc.) bind to the imidazole side chains of surface exposed histidines of proteins.[70,71] This coordination interaction (M^{2+}-His) has been used for applications in which proteins are distinguished on the basis of their surface histidine contents, such as protein purification by immobilized metal affinity chromatography (IMAC).[72-75] In IMAC, a metal (Cu^{2+}, Ni^{2+} or Zn^{2+}) binary complex is covalently coupled to a permeable solid support such as agarose and packed into a column. The protein under purification is "washed" through the column and selective binding between the basic amino acids (particularly histidine) of the protein and the immobilized binary metal complex occurs. Selective binding allows separation of histidine-rich proteins from other protein material.[72-75] The first report of IMAC used iminodiacetic acid (IDA) as the covalently bound ligand to immobilize the metal ions to the solid support.[76]

With the purpose of increasing the affinity of proteins for liposomes, we investigated the possibility to incorporate IDA-Cu^{2+} to liposomes that also contained the EDTA-Lanthanide^{3+} complex. IDA was chosen as the ligand to chelate the cupric ions because of its strong affinity for Cu^{2+} ($K \approx 10^{12}$ M^{-1}).[77] This strong affinity should prevent the complex to demetalate even at high protein concentrations. Literature reports show that IDA-Cu^{2+} complexes bind to proteins (pH = 7.0) primarily trough histidine residues located on the protein surface.[78] Therefore its affinity for proteins is a well-known phenomenon.

7.2 Spectral characterization of liposomes incorporating IDA-Cu^{2+} and EDTA-lanthanide^{3+} complexes

Figure 7.1 shows the SS excitation and emission spectra of polymerized liposomes incorporating IDA-Cu^{2+} and EDTA-Eu^{3+} (A) or EDTA-Tb^{3+} (B) at neutral pH (25mM HEPES buffer). The broad excitation and emission bands are mostly attributed to the fluorescence of the liposome backbone. The relatively weak luminescence of Eu^{3+} or Tb^{3+} is overwhelmed by the strong fluorescence of the liposome, and their contributions to the SS spectrum of the liposome appear as small shoulders at 616 nm (Eu^{3+}) and 547 nm (Tb^{3+}).

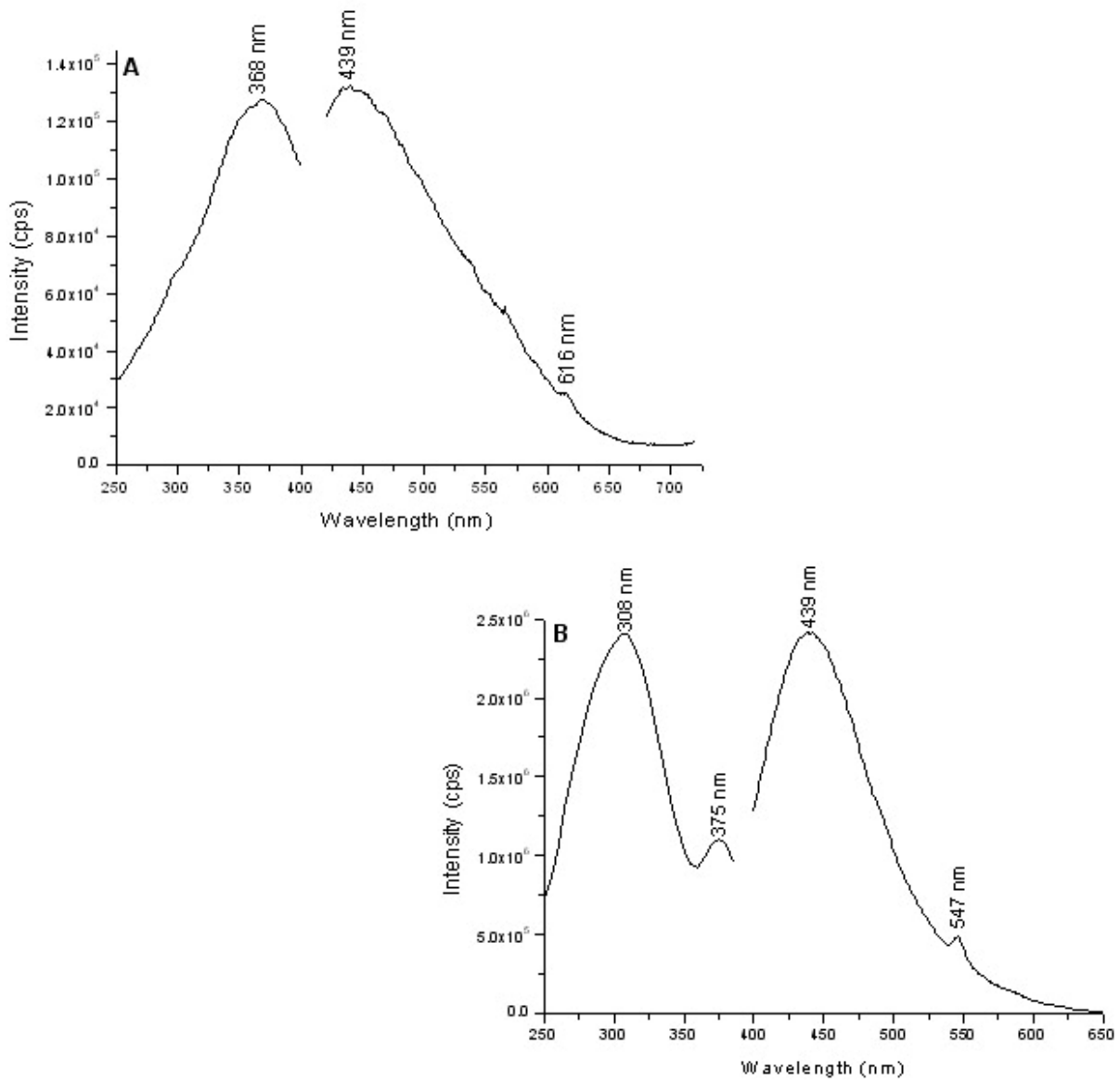

Figure 7.1. SS excitation and emission spectra of polymerized liposomes incorporating IDA-Cu^{2+} and EDTA-Eu^{3+} (A) and EDTA-Tb^{3+} (B).

Both solutions were prepared in 25 mM HEPES. Spectra were recorded using 8 nm excitation and emission band-pass. The concentrations of polymerized liposome were 27.7 mg/L (A) and 84.3 mg/L (B).

The luminescence of Eu^{3+} and Tb^{3+} is clearly distinguished in the TR spectrum of the liposome (see Figure 7.2). A 90 μs delay after the excitation pulse completely removes the

fluorescence contribution from the liposome providing a probe that solely relies on the characteristic peaks of Eu^{3+} (Figure 7.2 A) or Tb^{3+} (Figure 7.2 B).

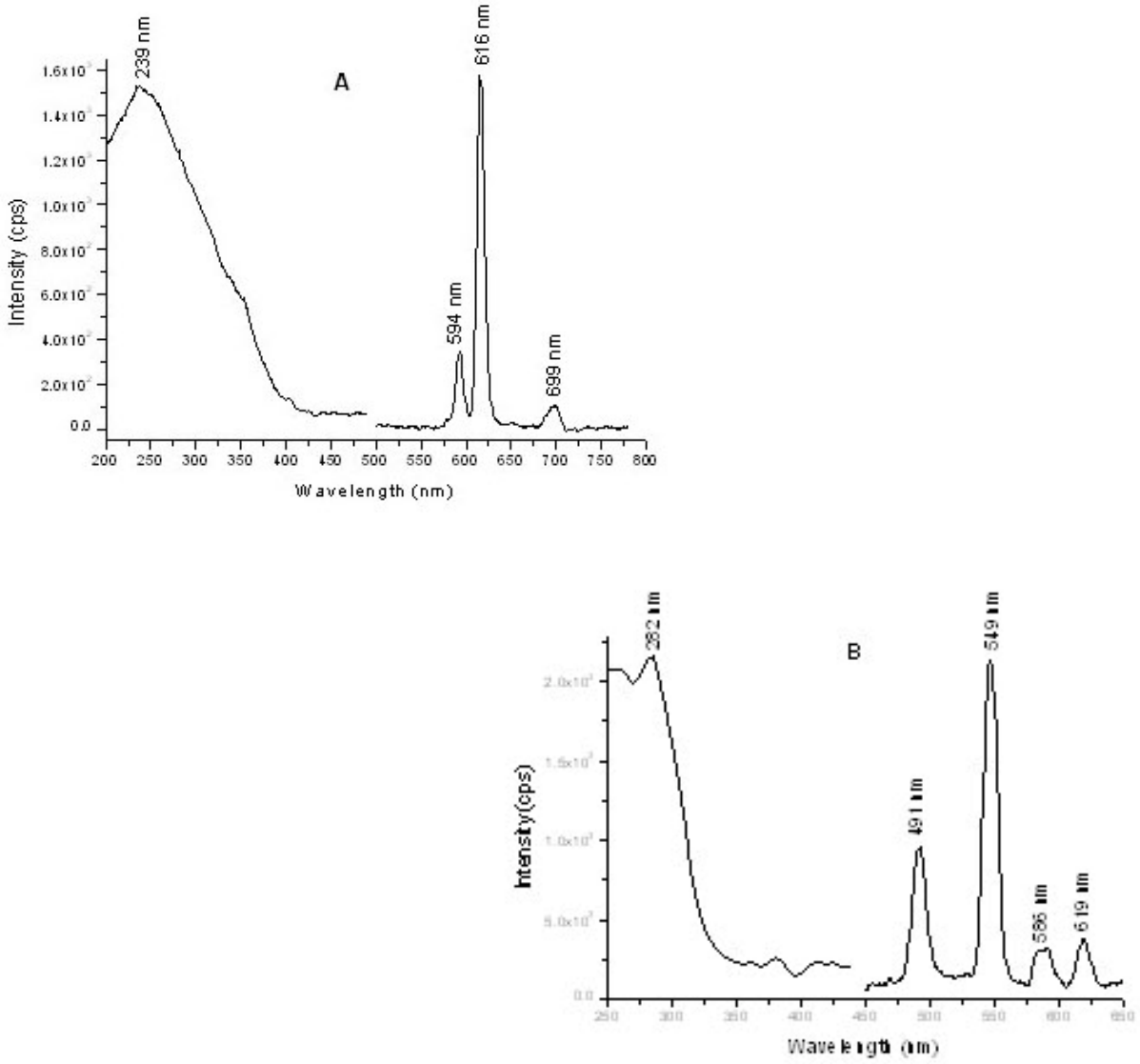

Figure 7.2. TR spectra of liposomes incorporating IDA-Cu^{2+} and EDTA-Eu^{3+} (A) or EDTA-Tb^{3+} (B).

Spectra were recorded using the following parameters: 40 and 8 nm excitation and emission band-pass, respectively. Delay and gate times were 0.9 and 1 ms, respectively. The concentrations of polymerized liposome were 27.7 mg/L (A) and 84.3 mg/L (B). $\lambda_{exc}/\lambda_{em}$ = 239/616 nm (A), and $\lambda_{exc}/\lambda_{em}$ = 282/549 nm (B).

Figure 7.3 depicts the TR excitation-emission matrix (TREEM) of the polymerized liposome. Although maximum excitation occurs at ~ 250nm, a wide excitation range is still available to promote strong luminescence from the lanthanide ions.

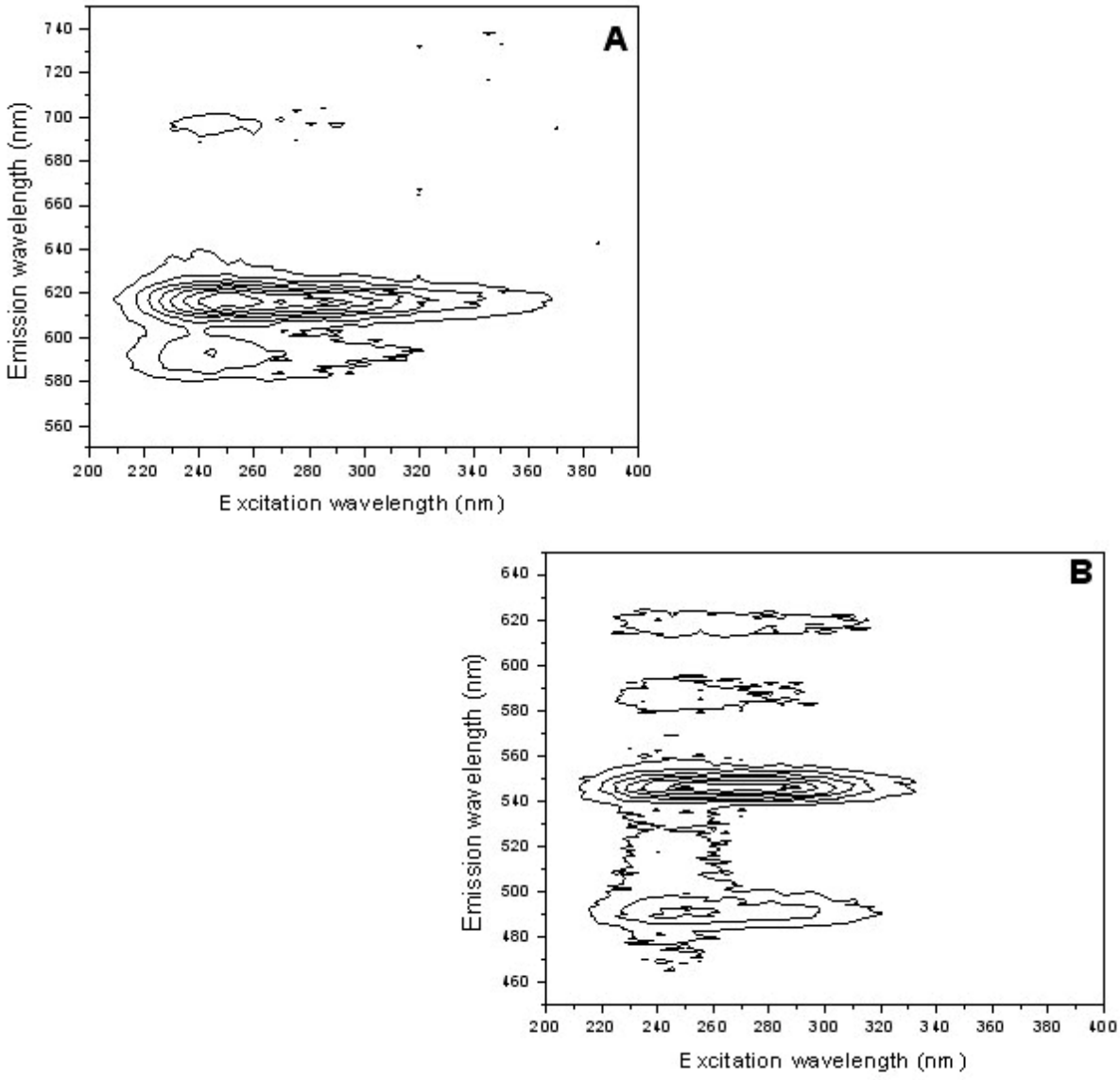

Figure 7.3. TREEM of liposomes incorporating IDA-Cu^{2+} and EDTA-Eu^{3+} (A) or EDTA-Tb^{3+} (B).

Spectra were recorded using the following parameters: 40 and 8 nm excitation and emission band-pass, respectively. Delay and gate times were 0.9 and 1 ms, respectively. The concentrations of polymerized liposome were 27.7 mg/L (A) and 84.3 mg/L (B).

7.3 Concentration of EDTA-Eu^{3+} and EDTA-Tb^{3+} in polymerized liposomes incorporating IDA-Cu^{2+}

As previously shown, irreproducibility of measurements due to batch-to-batch variations of lanthanide concentrations are eliminated by adjusting the final concentration of lanthanide ion in the analytical sample (see Section 5.3). Although the same could be true for the concentration of IDA-Cu^{2+}, our initial studies did not consider this possibility based on the fact that there is no direct correlation between the concentration of IDA-Cu^{2+} and the luminescence signal in the absence of protein (reference signal). Figure 7.4 shows the outcome of the multiple standard additions plots for liposomes incorporating EDTA-Eu^{3+} (A) or EDTA-Tb^{3+} (B). The luminescence intensity of the lanthanide ion is graphed as a function of effective analyte standard concentration [$nC_sV_s/(V_x+V_s)$], where C_s is the concentration of standard, V_s is the volume of standard addition, V_x is the volume of aliquot liposome, and n is the number of standard additions. The volumes of standard additions were negligible in comparison to the liposome volumes to ensure that the sample matrix was not significantly changed by dilution with standards. The extrapolation of the linear plot to y = 0 provides a good approximation of the concentration of lanthanide in the liposomes. For these liposome batches, EDTA-Eu^{3+} and EDTA-Tb^{3+} concentrations were estimated as 2.63×10^{-3} M and 1.31×10^{-3} M, respectively. Since the liposome incorporating EDTA-Eu^{3+} solution was diluted 100 times, the concentration of Eu^{3+} in the original liposome sample was 0.263 M.

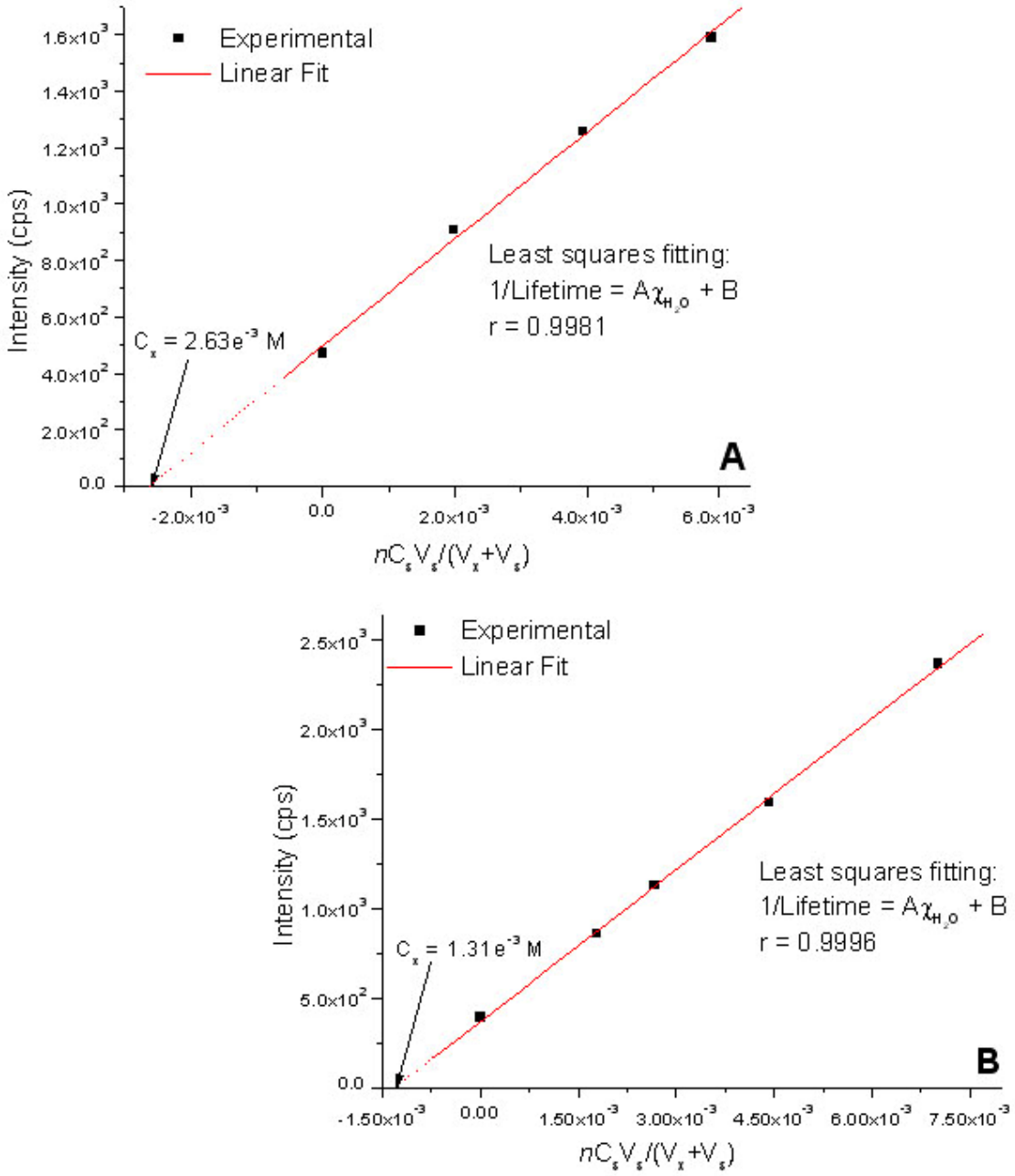

Figure 7.4. Luminescence intensity of polymerized liposomes incorporating IDA-Cu^{2+} and EDTA-Eu^{3+} (A) or EDTA-Tb^{3+} (B) as a function of standard addition concentration.

Instrumental parameters were: 0.9 and 1 ms delay and gate times, respectively. Excitation and emission band-pass were 40 and 8 nm, respectively. A cutoff filter at 450 nm was used. Intensities were recorded at $\lambda_{exc}/\lambda_{em}$ = 239/616 nm (A) and $\lambda_{exc}/\lambda_{em}$ = 282/547 nm (B).

7.4 Number of water molecules coordinated to polymerized liposomes incorporating IDA-Cu^{2+} and EDTA-Eu^{3+} or EDTA-Tb^{3+} complexes

Figure 7.5 shows the reciprocal luminescence lifetime (τ^{-1}) as a function of mole fraction of water (χ_{H2O}) in D_2O-H_2O mixtures for liposomes incorporating IDA-Cu^{2+} and EDTA-Eu^{3+} (A) or EDTA-Tb^{3+} (B). The number of coordinated water molecules was calculated as 2.93 (EDTA-Eu^{3+}) and 2.97 (EDTA-Tb^{3+}). The same result was obtained for the liposomes without IDA-Cu^{2+} complex (Section 6.4), showing that the presence of IDA-Cu2+ does not affect the number of available sites for protein interaction.

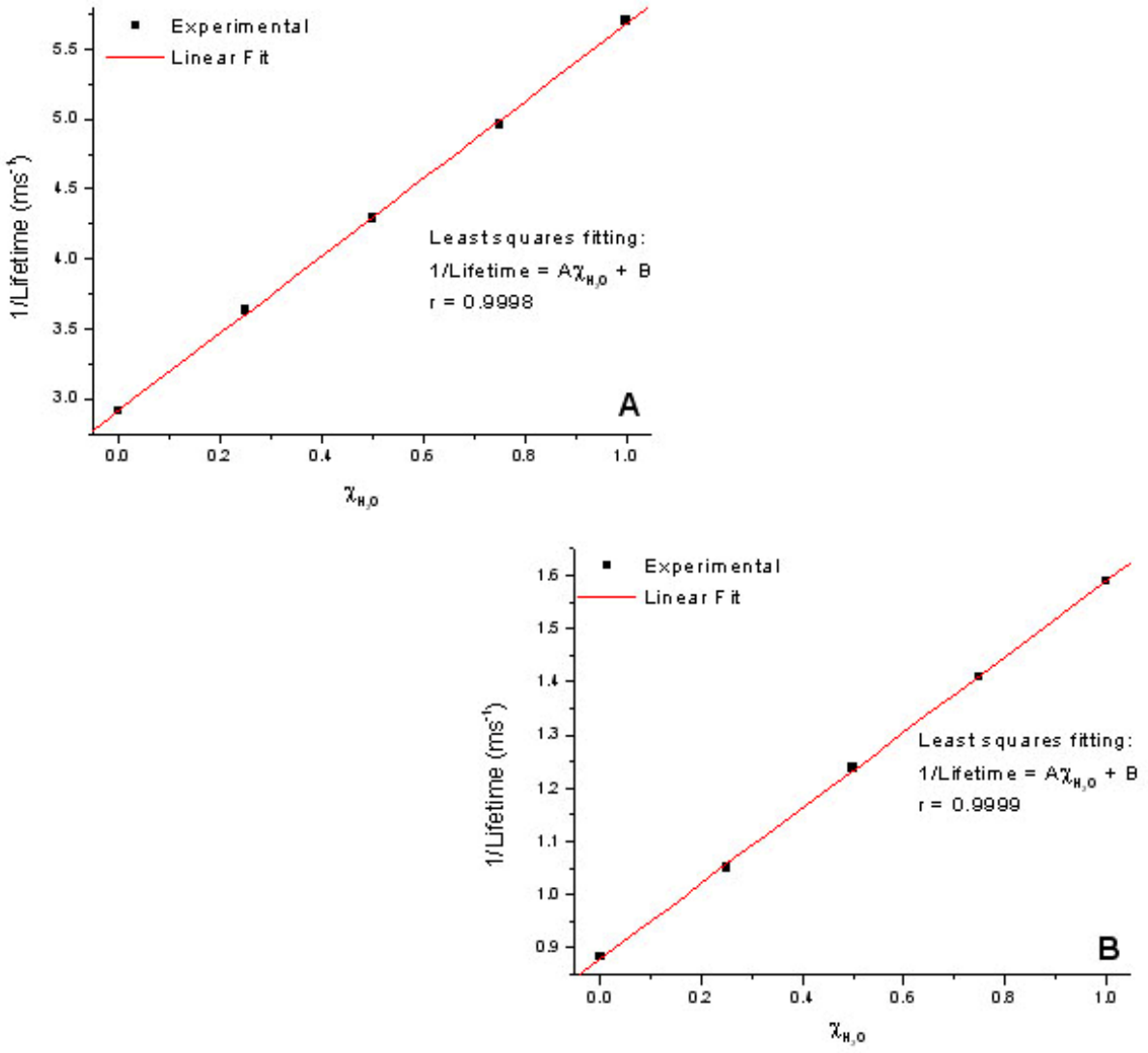

Figure 7.5. Reciprocal luminescence lifetime (τ^{-1}) in ms^{-1} as a function of mole fraction of water (χ_{H20}) in D_2O-H_20 mixtures in polymerized liposomes incorporating IDA-Cu^{2+} and 5×10^{-6} M EDTA-Eu^{3+} (A) and 3×10^{-7} M EDTA-Tb^{3+} (B).

Lifetimes are the average values of six measurements taken from six aliquots of sample solution. Experimental parameters for wavelength-time matrix collection were the following: $\lambda_{exc}/\lambda_{em}$ = 266/616 nm (A), and $\lambda_{exc}/\lambda_{em}$ = 282/549 nm (B), time delay = 0.9 ms, gate width = 1 ms (A) and 3 ms (B), gate step = 0.03 ms, number of accumulations per spectrum = 100 laser pulses, number of kinetic series per wavelength-time matrix = 40, slit width of spectrograph: 5 mm.

7.5 Polymerized liposomes incorporating IDA-Cu^{2+} and EDTA-Eu^{3+} as a probe for protein analysis

7.5.1 Quantitative analysis with the liposome sensor

Figure 7.6 illustrates the experimental titration curves at the liposome's signal as a function of increasing protein concentrations. All measurements were made in batch (25mM HEPES) after 15 minutes of protein mixing.

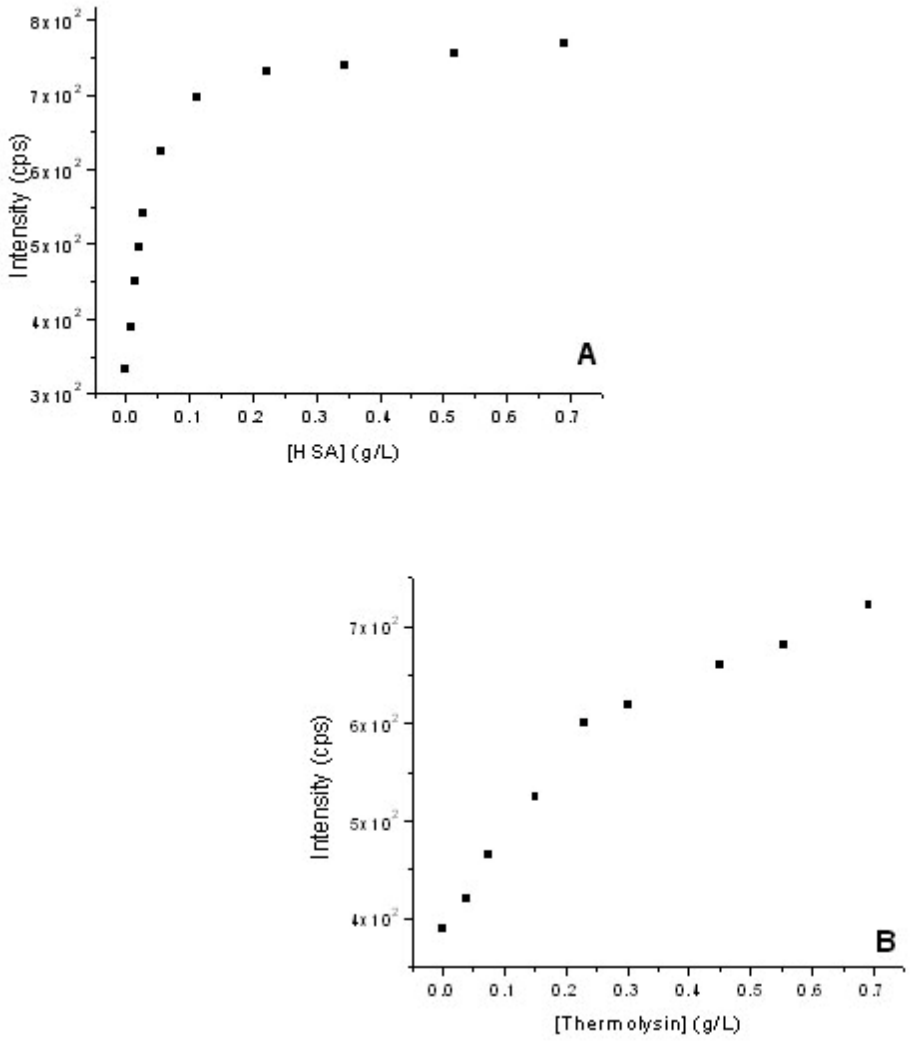

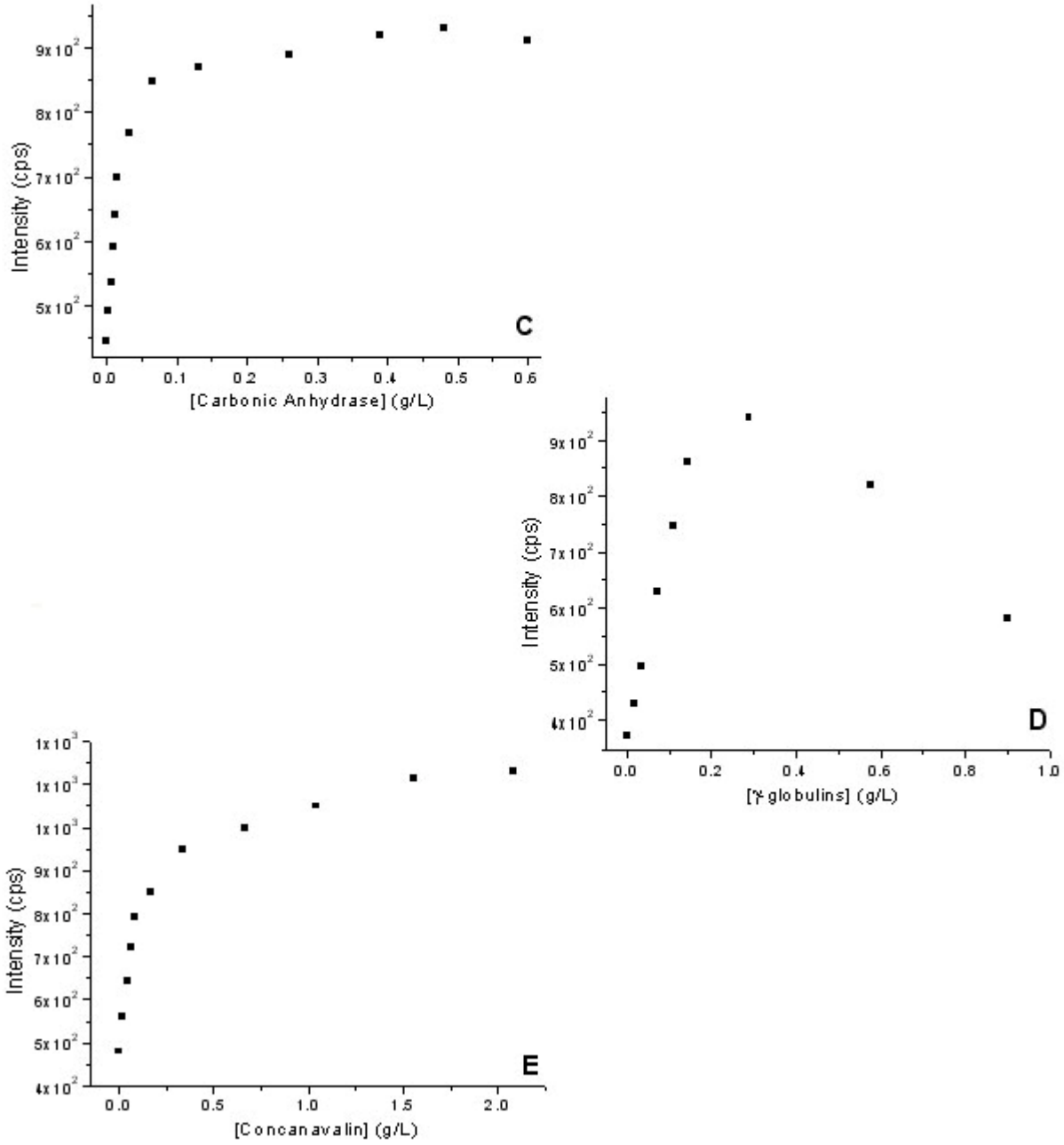

Figure 7.6. Titration curves for HSA (A), Thermolysin (B), CA (C), γ-globulins (D), and Concanavalin A (E) obtained with polymerized liposomes incorporating IDA-Cu^{2+} and 5×10^{-6} M EDTA-Eu^{3+}.

All solutions were prepared in HEPES 25 mM. Intensity measurements were done at λ_{exc}/ λ_{em} = 266/616 nm using 90 μs and 1000 μs delay and gate times, respectively. Spectra were recorded using 40 and 8 nm excitation and emission band-pass, respectively. A cutoff filter was used at 400 nm to avoid second-order emission.

Figure 7.7 shows the "least squares fitting" of the linear portions of the titration curves. The luminescence intensities plotted in the calibration graphs are the averages of individual measurements taken from three aliquots of the same working solution. Excellent fittings were obtained for all the studied proteins.

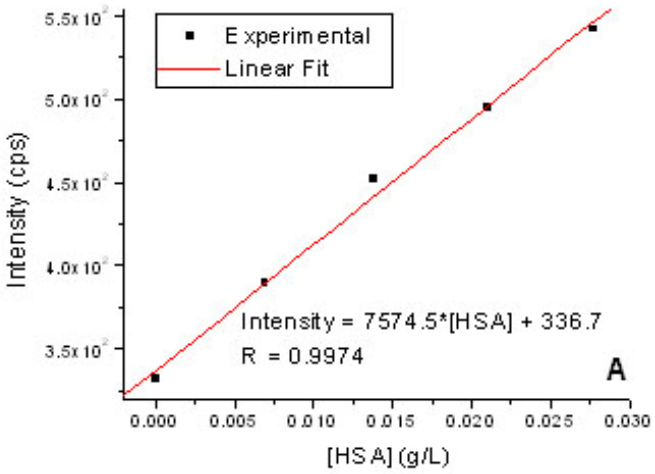

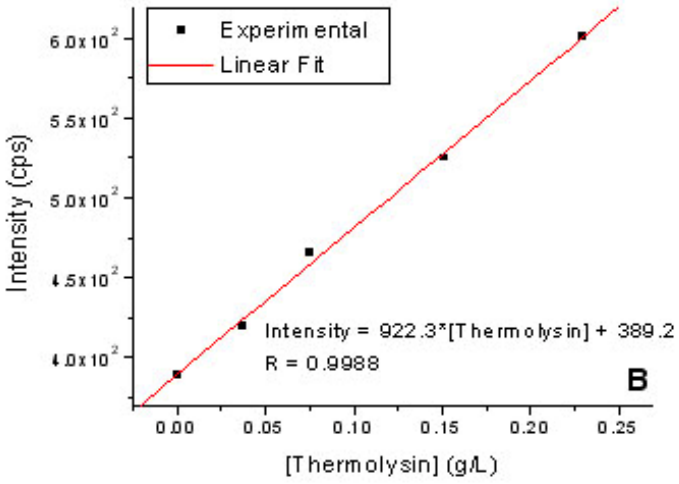

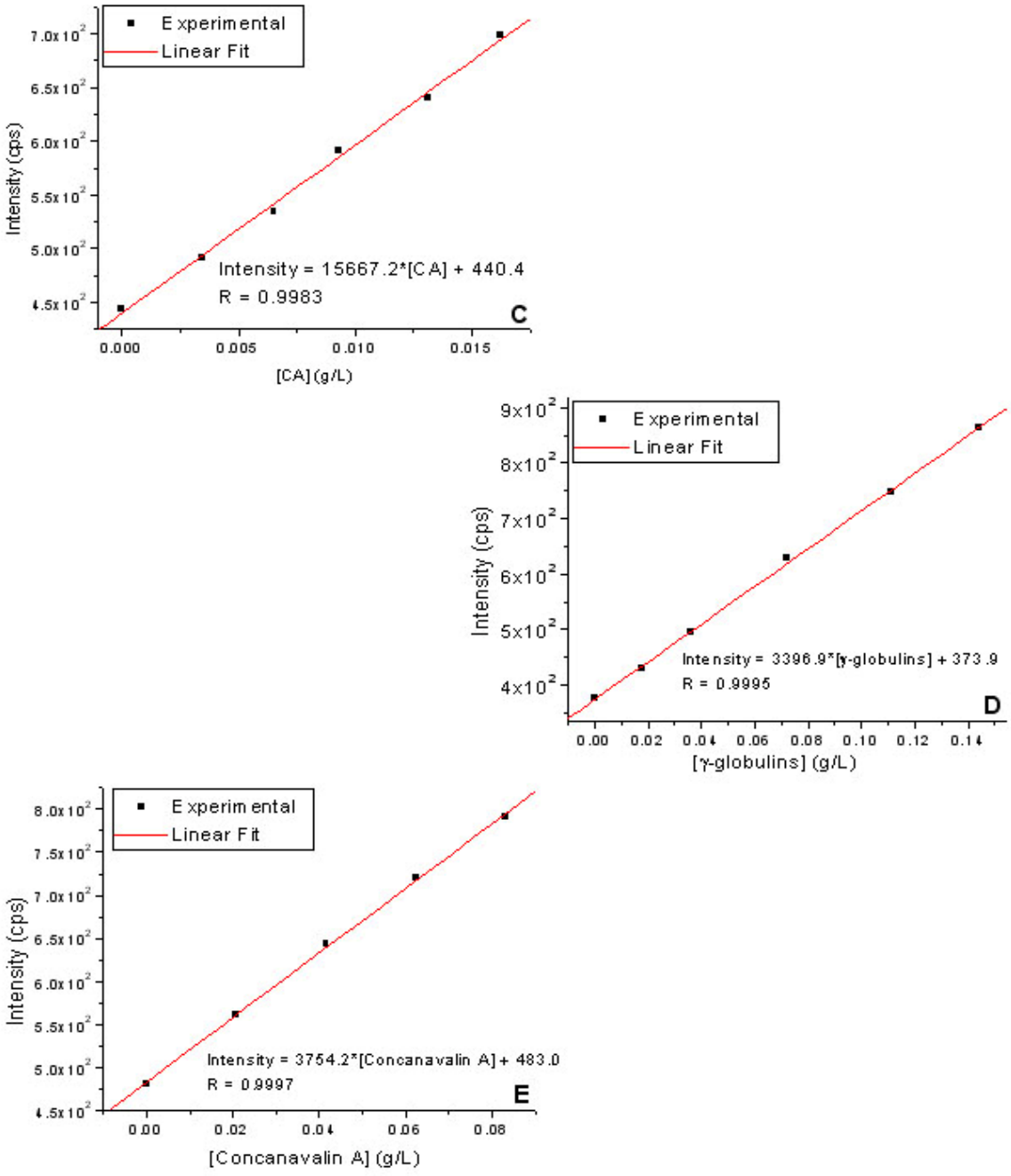

Figure 7.7. Calibration curves for HSA (A), Thermolysin (B), CA (C), γ-globulins (D), and Concanavalin A (E) obtained with polymerized liposomes incorporating IDA-Cu^{2+} and 5×10^{-6} M EDTA-Eu^{3+}.

Measurements were performed under instrumental conditions stated in Figure 7.6.

Table 7.1 summarizes the AFOM obtained with the liposome sensor for the five proteins. The LDR of the calibration curves are based on at least five protein concentrations. All correlation coefficients were close to unity showing excellent potential for quantitative analysis of proteins. Emission intensity was corrected for protein absorption when exciting at 266 nm. The LOD (ppm) at both wavelengths prove the ability of the sensor to quantify these five proteins at low concentration levels.

Table 7.1. AFOM[a] obtained with the polymerized liposomes incorporating IDA-Cu^{2+} and EDTA-Eu^{3+}

Protein	LDR (mg/L)	R	LOD (mg/L) (λ_{exc} = 266 nm)	LOD (mg/L) (λ_{exc} = 320 nm)
HSA	4.1 – 27.7	0.9974	4.1	5.3
CA	2.3 – 16.2	0.9983	2.3	4.4
γ-globulins	13.4 - 144.0	0.9995	13.4	19.3
Thermolysin	44.9 – 229.1	0.9988	44.9	59.9
Concanavalin	9.7 – 83.2	0.9997	9.7	20.1

[a]Measurements were performed under instrumental conditions stated in Figure 7.6.

Liposomes incorporating IDA-Cu^{2+} and EDTA-Eu^{3+} present two major advantages in comparison to liposomes without IDA-Cu^{2+}: i) they are sensitive to the presence of Concanavalin A. When liposomes incorporating only EDTA-Eu^{3+} were titrated with this protein, no change was observed in intensity or lifetime of the luminescence signal; ii) the LOD obtained for CA is two orders of magnitude better than the one obtained with the non-copper liposome.

This LOD improvement is attributed to the presence of six histidines residues in the CA surface, which can bind to IDA-Cu^{2+} and enhance lanthanide-protein interaction.[69]

7.5.2 Qualitative potential of liposomes with IDA-Cu^{2+} and EDTA-Eu^{3+}.

Lifetime measurements were made in the absence and in the presence of protein. Single exponential decays with excellent fittings were observed with the five proteins. Table 7.2 compares the reference lifetime (absence of protein) to the lifetimes in the presence of the target proteins. For a confidence level of 95% ($\alpha = 0.05$; $N_1 = N_2 = 6$)[53] the reference value is statistically different to the lifetime in the presence of proteins. In addition, all the lifetimes are statistically different which demonstrates the feasibility to using this liposome to analyze target proteins on the basis of lifetime measurements.

Table 7.2. Comparison of luminescence lifetimes measured with the polymerized liposomes incorporating IDA-Cu^{2+} and EDTA-Eu^{3+} in the absence and the presence of proteins.

Protein[a]	Lifetime[b] (μs)	RSD (%)
–	159.0 ± 3.4	2.1
HSA	206.3 ± 4.2	2.0
CA	188.8 ± 4.8	2.5
γ-globulins	195.8 ± 3.1	1.6
Thermolysin	261.6 ± 8.5	3.2
Concanavalin	168.2 ± 2.7	1.6

[a]Protein solutions were mixed with polymerized liposomes incorporating IDA-Cu^{2+} and 5×10^{-6} M EDTA-Eu^{3+} to provide the following final concentrations: 27.7 mg/L HSA, 16.2 mg/L CA, 144.0 mg/L γ-globulins, 229.1 mg/L Thermolysin, and 83.2 mg/L Concanavalin A. All solutions were prepared in 25 mM HEPES buffer.
[b]Lifetimes are the average values of six measurements taken from six aliquots of sample solution. All measurements were made at at λ_{exc}/ λ_{em} = 266/616 nm using time delay = 0.9 ms, gate width = 1 ms, gate step = 0.03 ms, number of accumulations per spectrum = 100 laser pulses, number of kinetic series per wavelength-time matrix = 40, slit width of spectrograph: 5 mm.

7.6 Polymerized liposomes incorporating IDA-Cu^{2+} and EDTA-Tb^{3+} as a probe for protein analysis

7.6.1 Quantitative analysis with the liposome sensor

Figure 7.8 illustrates the experimental titration curves obtained by monitoring the luminescence signal of the liposome as a function of increasing protein concentrations. All measurements were made in batch (25mM HEPES) after 15 minutes of protein mixing.

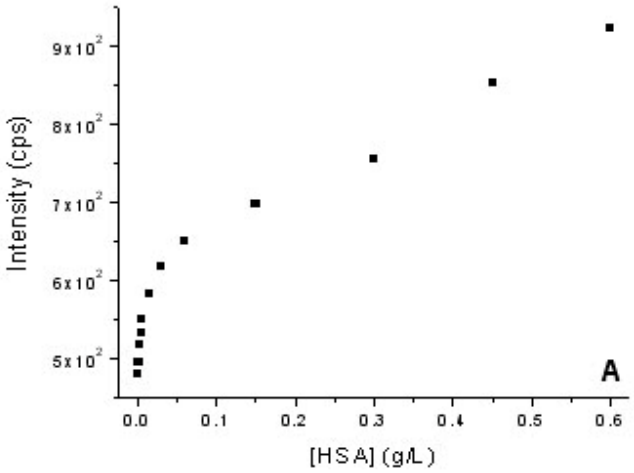
Intensity (cps)
9x10²
8x10²
7x10²
6x10²
5x10²
0.0
0.1
0.2
0.3
0.4
0.5
0.6
[HSA] (g/L)
A

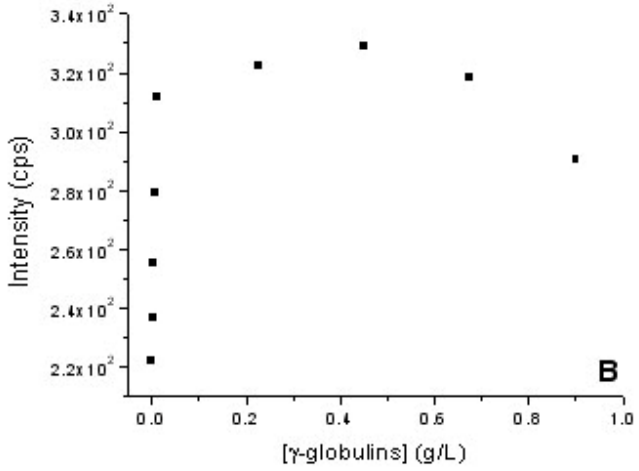
Intensity (cps)
3.4x10²
3.2x10²
3.0x10²
2.8x10²
2.6x10²
2.4x10²
2.2x10²
0.0
0.2
0.4
0.6
0.8
1.0
[γ-globulins] (g/L)
B

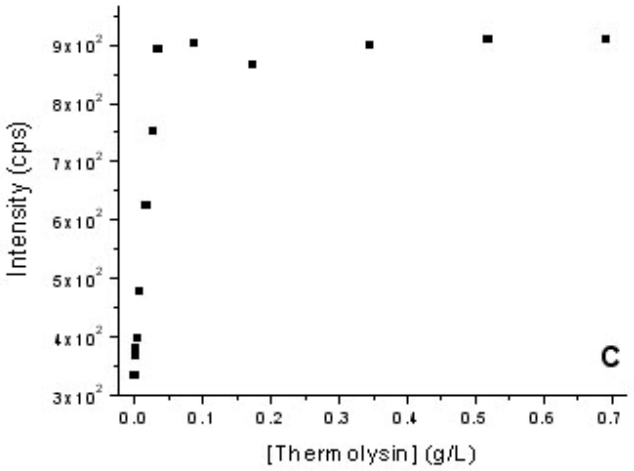
Intensity (cps)
9x10²
8x10²
7x10²
6x10²
5x10²
4x10²
3x10²
0.0
0.1
0.2
0.3
0.4
0.5
0.6
0.7
[Thermolysin] (g/L)
C

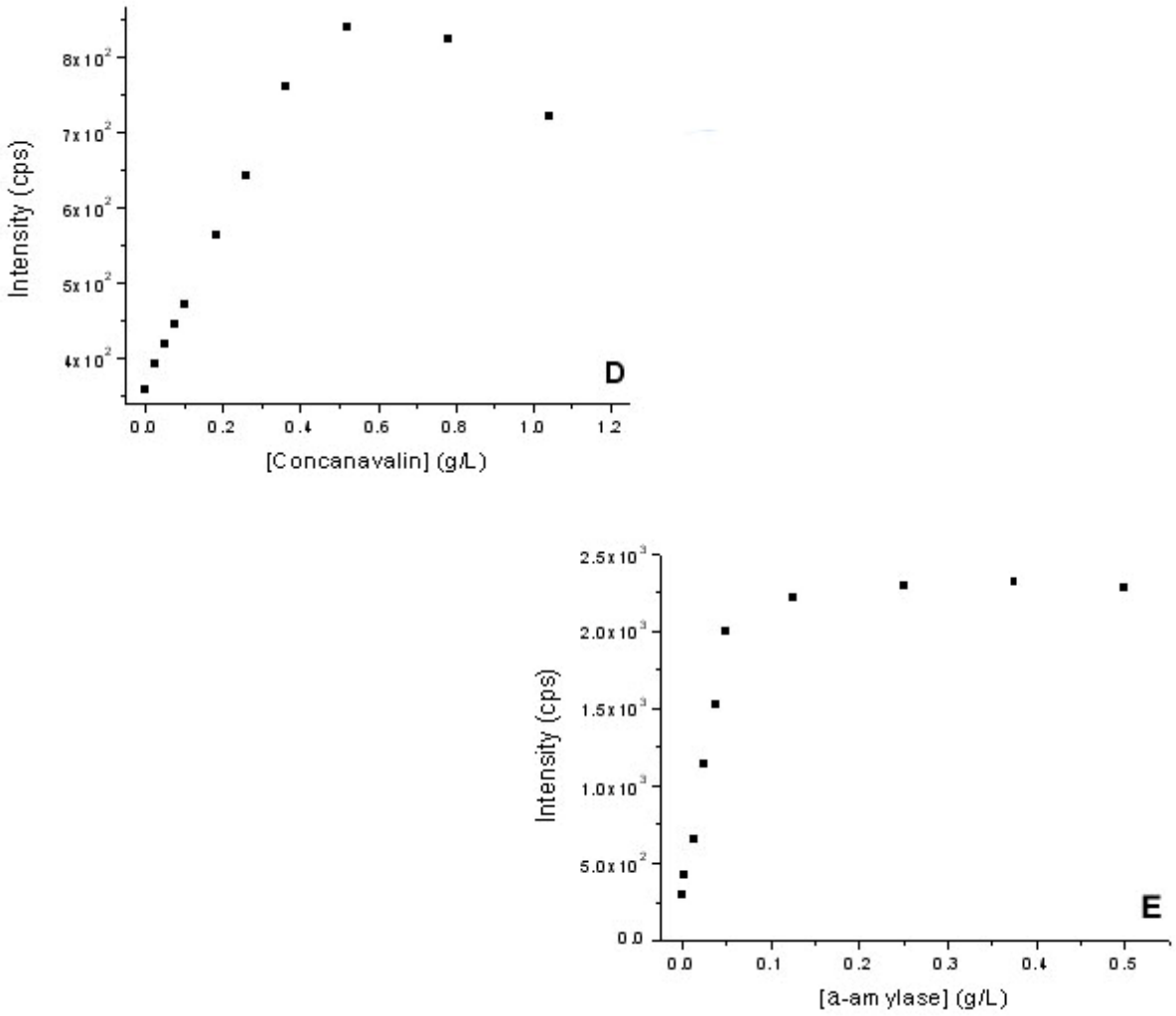

Figure 7.8. Titration curves for HSA (A), γ-globulins (B), Thermolysin (C), Concanavalin A (D), and α-amylase (E) obtained with polymerized liposomes incorporating IDA-Cu^{2+} and 3×10^{-7} M EDTA-Tb^{3+}.

Intensity measurements were done at $\lambda_{exc}/\lambda_{em}$ = 266/547 nm using 90 μs and 1000 μs delay and gate times, respectively. Excitation and emission band-pass were 40 and 7, respectively. A cutoff filter was used at 400 nm to avoid second-order emission.

Figure 7.9 shows the "least squares fitting" of the linear portions of the titration curves. The luminescence intensities plotted in the calibration graphs are the averages of individual

measurements taken from three aliquots of the same working solution. Excellent fittings were obtained for all the proteins.

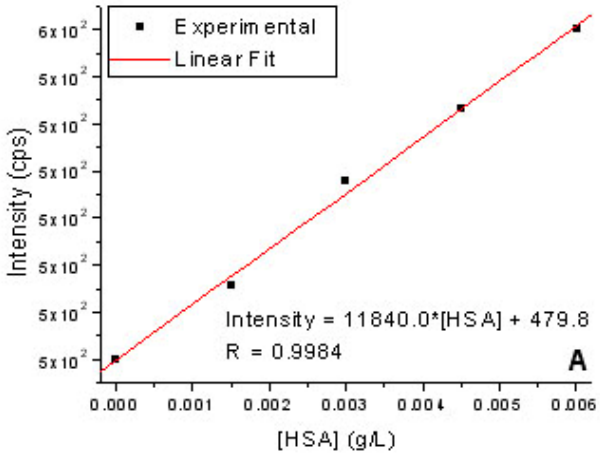

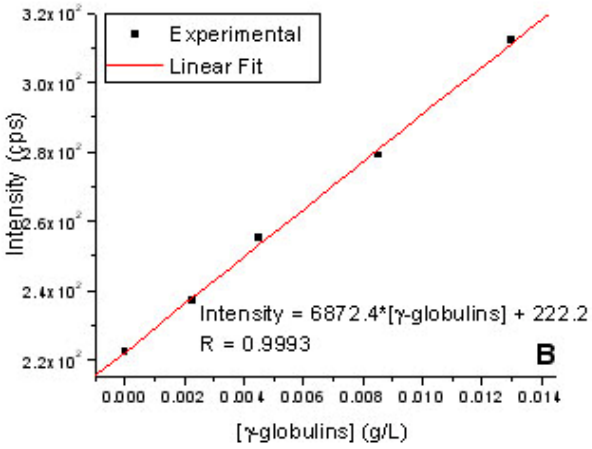

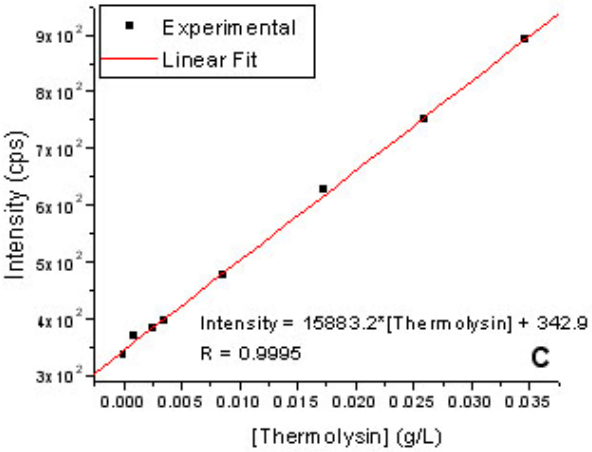

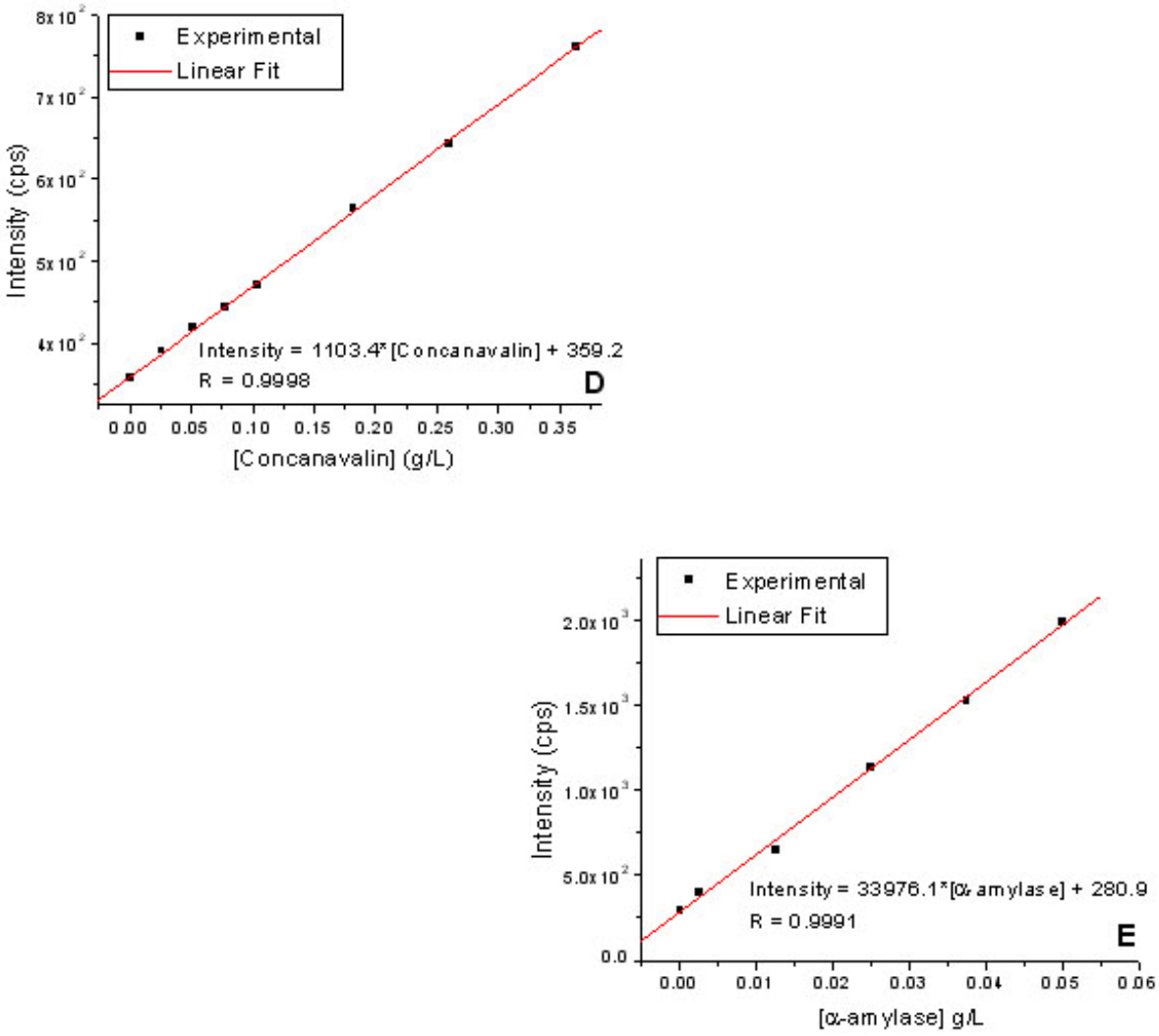

Figure 7.9. Calibration curves for HSA (A), γ-globulins (B), Thermolysin (C), Concanavalin A (D), and α-amylase (E) obtained with polymerized liposomes incorporating IDA-Cu^{2+} and 3×10^{-7} M EDTA-Tb^{3+}. Measurements were performed under instrumental conditions stated in Figure 7.8.

Table 7.3 summarizes the AFOM obtained for the five proteins. The LDR of the calibration curves are based on at least five protein concentrations. All correlation coefficients are close to unity showing excellent potential for quantitative analysis of proteins. Emission

intensity was corrected for protein absorption when exciting at 266 nm. The LOD at both wavelengths prove the ability of the sensor to quantify these five proteins at the ppm level.

Table 7.3. AFOM[a] obtained with the polymerized liposomes incorporating IDA-Cu^{2+} and EDTA-Tb^{3+}

Protein	LDR (mg/L)	R	LOD (mg/L) (λ_{exc} = 266 nm)	LOD (mg/L) (λ_{exc} = 320 nm)
HSA	3.2 – 6.0	0.9984	3.2	6.1
α-amylase	1.3 – 50.0	0.9991	1.3	1.9
γ-globulins	4.9 – 13.0	0.9993	4.9	8.6
Thermolysin	2.6 – 34.6	0.9995	2.6	3.7
Concanavalin	29.9 – 364.0	0.9998	29.9	36.4

[a]Measurements were performed under instrumental conditions stated in Figure 7.8.

When compared to the liposome with no IDA-Cu^{2+}, the liposome with EDTA-Tb^{3+}/ IDA-Cu^{2+} presents the unique ability to detect HSA, γ-globulins, and Concanavalin A. Considering its ability to also detect α-amylase and Thermolysin, the presence of IDA-Cu^{2+} in the liposome appears to favor the interaction of Tb^{3+} with a wider range of proteins.

7.6.2 Qualitative potential of the liposome sensor

Table 7.4 compares the reference lifetime (absence of protein) to the lifetimes in the presence of the target proteins at their asymptotic concentrations. Single exponential decays with excellent fittings are observed in all cases. For a confidence level of 95% ($\alpha = 0.05$; $N_1 = N_2 =$

6)[53], all lifetimes were statistically different, which shows the capability to differentiate these proteins on the bases of lifetime analysis.

Table 7.4. Comparison of luminescence lifetimes measured with the polymerized liposomes incorporating IDA-Cu^{2+} and EDTA-Tb^{3+} in the absence and the presence of proteins.

Protein[a]	Lifetime[b] (μs)	RSD (%)
–	630.0 ± 6.9	1.1
HSA	753.2 ± 12.0	1.6
α-amylase	848.9 ± 12.7	1.5
γ-globulins	815.1 ± 11.7	1.4
Thermolysin	1259.6 ± 25.2	2.0
Concanavalin A	717.4 ± 13.6	1.9

[a]Protein solutions were mixed with polymerized liposomes incorporating IDA-Cu^{2+} and 5×10^{-6} M EDTA-Tb^{3+} to provide the following final concentrations: 6.0 mg/L HSA, 50.0 α-amylase, 13.0 mg/L γ-globulins, 34.6 mg/L Thermolysin, and 364.0 mg/L Concanavalin A. All solutions were prepared in 25 mM HEPES buffer.
[b]Lifetimes are the average values of six measurements taken from six aliquots of sample solution. All measurements were made at at λ_{exc}/ λ_{em} = 266/547 nm using time delay = 0.9 ms, gate width = 3 ms, gate step = 0.03 ms, number of accumulations per spectrum = 100 laser pulses, number of kinetic series per wavelength-time matrix = 40, slit width of spectrograph: 5 mm.

7.7 Conclusions

The incorporation of IDA-Cu^{2+} to EDTA-Eu^{3+} liposomes provides an overall improvement on sensing performance. Liposomes containing the Cu^{2+} complex are sensitive to five studied proteins. The LOD obtained for CA and HSA were two and one orders of magnitude better, respectively. The lifetime values in the presence of Thermolysin, HSA, CA, γ-globulins

and Concanavalin A were statistically different, showing the capability of this type of liposome to act as "universal sensor" for the five studied proteins. The incorporation of IDA-Cu^{2+} to EDTA-Tb^{3+} liposomes extended the sensing capability of the former liposomes to three additional proteins, namely HSA, γ-globulins and Concanavalin A. In general, the RSD of intensity and lifetime measurements were better in the presence of IDA-Cu^{2+}. The overall improvements are attributed to the ability of the Cu2+ complex to provide a "tighter interaction" between proteins and liposome platforms.

CHAPTER 8. SIMULTANEOUS DETERMINATION OF BINARY MIXTURES OF PROTEINS

8.1 Simultaneous determination of HSA and γ-globulins in binary mixtures using 5As-EDTA-Eu^{3+}

8.1.1 Introduction

Our approach performs quantitative analysis of proteins based on the linear relationship between signal intensity and protein concentration. Because there is no spectral shift upon protein interaction, the qualitative parameter for protein identification is the luminescence lifetime. Unless the target protein is the only protein in the analytical sample, these two parameters should be simultaneously considered to achieve accurate qualitative and quantitative analysis. In this section, the feasibility of determining the concentration of HSA and γ-globulins in binary mixtures is demonstrated. This is achieved by using a chemometric model to simultaneously process signal intensity and lifetime data.

A variety of linear regression methods for multicomponent analysis have been proposed, among which the most popular is PLS. De facto, PLS has become the standard for multivariate calibration because of the quality of the calibration models, the ease of implementation, and the availability of commercial software.[39,40] In addition, PLS uses full data points, which is critical for the spectroscopic resolution of complex mixtures of analytes. It allows for a rapid determination of components, usually with no need for prior separation. An additional advantage of PLS is that calibration can be performed by ignoring the concentrations of all other components except the analyte of interest. PLS regression has already been used to predict the concentration of HSA and and γ-globulins in binary mixtures, but protein determination was

based on the differences observed in second-derivative near-infrared spectra.[17,18] In our case, PLS uses the luminescence lifetimes as discriminatory parameters and regresses the luminescence decays onto the concentrations of the standards.

8.1.2 Results and discussion

The calibration set for chemometric analysis was built with a nine-sample set. The component concentrations corresponded to a three-level full factorial design with protein concentrations ranging from 10 to 30 mg/L HSA and from 10.0 to 20.0 mg/L γ-globulins. Protein solutions were mixed with 5×10^{-6} M 5As-EDTA-Eu^{3+} to provide final concentrations in the mentioned ranges. All solutions were prepared in 25 mM HEPES.

The validation set was also built with a nine-sample three-level full-factorial design, but the component concentrations were different from those used for the calibration set. The decays for all sets were recorded in random order with respect to protein concentrations at $\lambda_{exc}/\lambda_{em}$ = 312/615 nm.

Table 8.1 shows the time windows (or regions) of the luminescence decays and the optimum number of factors used for calibration, the root-mean-square error of prediction (REP %). The optimum number of factors -which allows one to model the system with the optimum data volume avoiding overfitting- was determined with the cross validation procedure (Section 1.6.2.3). This procedure removes one training sample at a time and uses the remaining samples to build the latent factors and regression.[29]

Table 8.1. Statistical parameters obtained by PLS 1

Parameters	HSA	γ-globulins
Region (μs)	30-3000 (50 data points)	30-3000 (50 data points)
Factors[a]	2	2
RMSECV[b] (μg/mL)	1.94	1.47
REP (%)[c]	9.9	10.1

[a]Factors were selected following the criterion described in Section 1.6.2.3

[b] $$RMSECV = \sqrt{\frac{\sum_{1}^{I}\left(C_{act} - C_{pred}\right)^2}{I}}$$

[c] $$REP\ (\%) = RMSECV \cdot \frac{100}{\overline{C}_{act}}$$

C_{act} is the actual concentration in the calibration samples, C_{pred} is the predicted concentration with the PLS model and $\overline{C}_{act}$ is the average concentration in the calibration set.

Table 8.2 shows the experimental results obtained from several binary samples with the optimized calibration set. The agreement between the predicted and the actual protein concentrations is excellent for both proteins, demonstrating the potential of the method to simultaneously distinguish and quantify both proteins in the studied concentration range.

Table 8.2. Comparison of predicted and actual protein concentrations in binary mixtures

Validation samples	HSA (mg/L)			γ-Globulins (mg/L)		
	Actual	Predicted	Recovery (%)	Actual	Predicted	Recovery (%)
1	15.0	14.4	96.0	12.5	11.1	88.8
2	15.0	16.3	108.7	12.5	11.7	93.6
3	15.0	15.3	102.0	12.5	13.9	111.2
4	20.0	18.5	92.5	15.0	14.5	96.7
5	20.0	21.2	106.0	15.0	15.3	102.0
6	20.0	20.6	103.0	15.0	15.8	105.5
7	25.0	21.5	86.0	17.5	16.4	93.7
8	25.0	27.6	110.4	17.5	15.0	85.7
9	25.0	26.6	106.4	17.5	18.0	102.9
Average recovery (%)			**101.2**			**97.8**
Std. Dv.			**8.1**			**8.3**
RSD			**0.080**			**0.084**

8.2 Comparison of two chemometric models for the direct determination of CA and HSA in a binary mixture using polymerized liposomes incorporating EDTA-Eu^{3+}

8.2.1 Introduction

In the previous section, the feasibility to using a multivariate calibration method - partial-least squares (PLS) - to simultaneously process lifetime and intensity data was demonstrated.

HSA and γ-globulins were accurately determined in synthetic mixtures without previous separation using 5As-EDTA-Eu^{3+}. This approach is here applied to the direct determination of HSA and CA in binary mixtures using polymerized liposomes incorporating EDTA-Eu^{3+}. Its ability to provide accurate protein determination is compared to the performance of a non-linear calibration technique, ANN.

Unless deviations from linearity are suppressed by including additional modeling factors, PLS tends to give large prediction errors and calls for more suitable models.[56,57] As many other non-linear calibration techniques,[56, 58-62] ANN is particularly useful when modeling complex and overlapped signals. Within the ANN context, the so-called multilayer feed-forward networks[60,65] is often used for prediction as well as for classification. The present approach to ANN modelling consists of three layers of neurons or nodes: the basic computing units; the input layer with a number of active neurons corresponding to the predictor variables in regression; and one hidden layer with a number of active neurons. The input and the hidden layer numbers are optimized during training, and the output layer has just one unit. The neurons are connected in a hierarchical manner, i.e. the outputs of one layer of nodes are used as inputs for the next layer and so on. In the hidden layer the sigmoid function $f(x) = 1 / (1+e^{-x})$ is used. Linear functions are used in both the input and output layers. Learning is carried out through the back-propagation rule (Section 1.6.2.4). The remarkable advantage of this rule is that there is no need to know the exact form of the analytical function on which the model should be built. Thus, neither the functional type nor the number of parameters in the model needs to be given to the program.[65]

Qualitative analysis with the liposome sensor is based on the luminescence lifetime of the lanthanide ion, which is sensitive to the nature of the interacting protein. Quantitative analysis relies on the linear relationship between luminescence intensity and protein concentration. In any

given sample, therefore, the direct determination of a specific protein requires the simultaneous consideration of both luminescence lifetime and signal intensity. PLS and ANN use the luminescence lifetimes as discriminatory parameters and regress the luminescence decays onto the concentrations of the standards.

8.2.2 Results and discussion

The calibration set for chemometric analysis was built with a thirteen samples set performing ten replicates for each sample (130 luminescence decay curves). The component concentrations corresponded to a three level full factorial design with five center samples in order to obtain an orthogonal design. HSA and CA concentrations ranged from 7.7 to 15.4 mg/L and from 75.4 to 261.9 mg/L, respectively. Protein solutions were mixed with polymerized liposomes incorporating EDTA-Eu^{3+} (final concentration of EDTA-Eu^{3+} in each sample: 5×10^{-6} M). All solutions were prepared in 25 mM HEPES. The validation set was built with seven samples. The component concentrations were different from those used for the calibration set. The fact that the component concentrations spanned between the concentrations ranges of the calibration set allowed us to draw conclusions on the predictive ability of the implemented models. The luminescence decays for all sets were recorded in random order with respect to protein concentrations. Measurements were performed at $\lambda_{exc}/\lambda_{em}$ = 320/615nm using the same time window (90 -1390 μsec; 24 points in total per sample) for both methods.

Table 8.3 summarizes the optimum number of factors used for calibration and the relative error of prediction (REP %) for both, calibration and validation sets. The optimum number of factors – which allows one to model the system with the optimum data volume avoiding over

fitting – was determined with the cross validation procedure (Section 1.6.2.3). The large REP % values clearly show the difficulty to finding a common set of calibration parameters good enough for both proteins.

A calibration set of 130 samples was used to train ANN. A randomized 30 % of this 130 sample calibration set was used as monitoring set. The seven sample PLS-validation set was used as the test set for checking the predictive ability of ANN and for comparison between both calibration models. The number of neurons in the input hidden layers was optimized by trial and error. The finally selected architecture for both components is displayed in Table 8.3. The numbers between brackets indicate how many active neurons are employed in each layer. This means that the employed architecture has 3 input neurons, 3 hidden neurons and a single output neuron for both components. In order to find the best model, each ANN was trained with the randomized 30 % sub-set of the calibration set, but it was subsequently stopped before it learned the idiosyncrasies present in the training data. This was achieved by searching the minimum value of the root mean square error for the monitoring set. The number of adjustable weights was ($4\times4\times1 = 16$). These figures were obtained after considering the number of input and hidden layers plus one bias neuron on each layer. Table 8.4 compares the results obtained with PLS and ANN for the seven samples validation set. The prediction improvement obtained with ANN (c.a. 50 %) demonstrates the power of this method for both modelling non-linear data and solving overlapped signals. The agreement between the predicted and the actual protein concentrations demonstrates the potential of the method to simultaneously distinguish and quantify both proteins in the studied concentration range.

Table 8.3. Statistical parameters when applying both PLS-1 and ANN analyses

Figures	Carbonic anhydrase		HSA	
	PLS-1	**ANN**	**PLS-1**	**ANN**
Region (μsec)	240 – 1390			
PLS-1 factors	3	–	3	–
ANN model	–	(3,3,1)	–	(3,3,1)
REP(CV) (%)[a]	27.8	12.1	29.3	15.5
REP(Val) (%)[a]	15.8	8.4	17.4	7.5

[a] $REP(\%) = \frac{\bar{x}}{100}\left[\frac{1}{I}\sum_{1}^{I}(c_{\text{act}} - c_{\text{pred}})^2\right]^{1/2}$ **, (CV) corresponds to the calibration set when cross validation is applied and (Val) corresponds to the validation set,** $\bar{x}$ **is the average concentration of calibration or validation sets and** I **is the number of samples.**

Table 8.4. Prediction on the validation set when applying PLS-1 and ANNs analyses

	CA			HSA		
Validation			**(mg/L)**			
samples	**Actual**	**PLS_1[a]**	**ANN[a]**	**Actual**	**PLS_1[a]**	**ANN[a]**
1	75.4	100.5 (14.7)	83.8 (4.2)	7.7	8.3 (1.2)	7.4 (0.1)
2	136.1	186.3 (27.2)	186.4 (14.7)	7.7	10.5 (0.9)	7.9 (0.3)
3	230.4	243.0 (10.5)	230.4 (6.7)	12.0	13.7 (0.6)	13.4 (0.3)
4	230.4	222.0 (12.6)	215.7 (8.4)	12.0	15.4 (1.3)	12.6 (0.4)
5	241.0	247.3 (23.1)	238.8 (14.7)	13.6	14.5 (1.7)	13.2 (0.7)
6	241.0	238.9 (4.2)	222.0 (6.3)	15.4	16.0 (0.5)	14.6 (0.3)
7	261.9	255.6 (6.3)	243.0 (6.3)	15.4	15.4 (0.9)	14.0 (0.3)
Recovery average (%)		110.3	103.8		113.8	99.8
Std. Dv.		17.4	16.4		13.4	6.9

[a] Average of three replicates. Standard deviation between parenthesis.

8.3 Conclusions

The efficacy of 5As-EDTA-Eu^{3+} to determine binary mixtures of proteins was demonstrated. The combination of luminescence intensities and decays with a PLS calibration model made feasible the simultaneous determination of HSA and γ-globulins at concentration levels typically found in human blood tests.[66]

Also, the effectiveness of polymerized liposomes incorporating EDTA-Eu^{3+} to resolve binary mixtures of proteins was proved. The combination of luminescence intensities and decays

with PLS-1 and ANN calibration models made feasible the direct determination of HSA and CA in binary mixtures. The considerable prediction improvement obtained with ANN (c.a. 50 %) is attributed to its ability to modelling non-linear data and solving overlapped signals.

CHAPTER 9. CONCLUSIONS

We have demonstrated the capability of Eu^{3+} and Tb^{3+} for protein sensing on the bases of luminescence analysis. Liposomes incorporating IDA-Cu^{2+} provide the best lipophilic platform for protein-lanthanide interaction. At the present stage of our research, the main limitation of this type of liposome for the analysis of complex samples is the lack of chemical specificity towards a target protein. Our approach should remove this limitation by incorporating the lanthanide ions into templated, polymerized liposomes specifically designed to recognize the target protein in the complex sample.

Significant improvements towards selectivity are also expected from instrumentation and mathematical approaches. Instrumental techniques based on multivariate calibration analysis have shown improvements over classical methods, but still lack the selectivity for the problem at hand. Isolating the contribution of a target protein from the total sample signal of a biological matrix requires the application of advanced data processing methods. Particularly relevant to the nature of this project is the existence of chemometric methods applicable to second order and third order data.[83]

Traditional luminescence (fluorescence and/or phosphorescence) spectra belong to first order data. EEM and TREEM are examples of second and third order data, respectively. As previously shown in this dissertation, an EEM is obtained by measuring luminescence intensities for different combinations of luminescence emission and excitation frequencies within a certain wavelength interval. Since the excitation and emission wavelengths may be scanned over a wide wavelength range, comprehensive information on the luminescence components of the sample is

obtained. The ultimate selectivity for chemical analysis is obtained with TREEM, which combine spectral and lifetime information.[84]

Previous work in our group has fully developed the experimental and the instrumentation to successfully apply multidimensional luminescence spectroscopy to the direct analysis of target proteins in complex biological fluids.[63] Our research with polymerized liposomes incorporating only one type of lanthanide ion demonstrated the sensitization of lanthanide luminescence via fluorescence excitation of the liposome backbone.[5,27,63,66,85] The naturally broad excitation band of the liposome provides the protein sensing probe with a wide excitation range for EEM and TREEM collection. However, on the emission side EEM and TREEM are restricted to a few narrow wavelength intervals resulting from the luminescence signature of Eu^{3+} or Tb^{3+}. Future studies shall remove this restriction by incorporating more than one type of lanthanide ion into the polymerized liposome. The combination of luminescence signatures of Eu^{3+} and Tb^{3+} will expand the emission range of the probe. The possibility to collect a larger number of "data points" per EEM and/or TREEM increases the selectivity of the probe. An additional advantage results from the luminescence decays of Eu^{3+} and Tb^{3+}. The experimental results in this dissertation demonstrate significant differences between the lifetimes of the two lanthanide ions for the same protein. These facts add selectivity to the temporal dimension of the probe. Such a liposome will be an excellent probe to explore the full potential of multidimensional luminescence spectroscopy in protein analysis.

APPENDIX A: ABSORBANCE SPECTRA OF PROTEINS

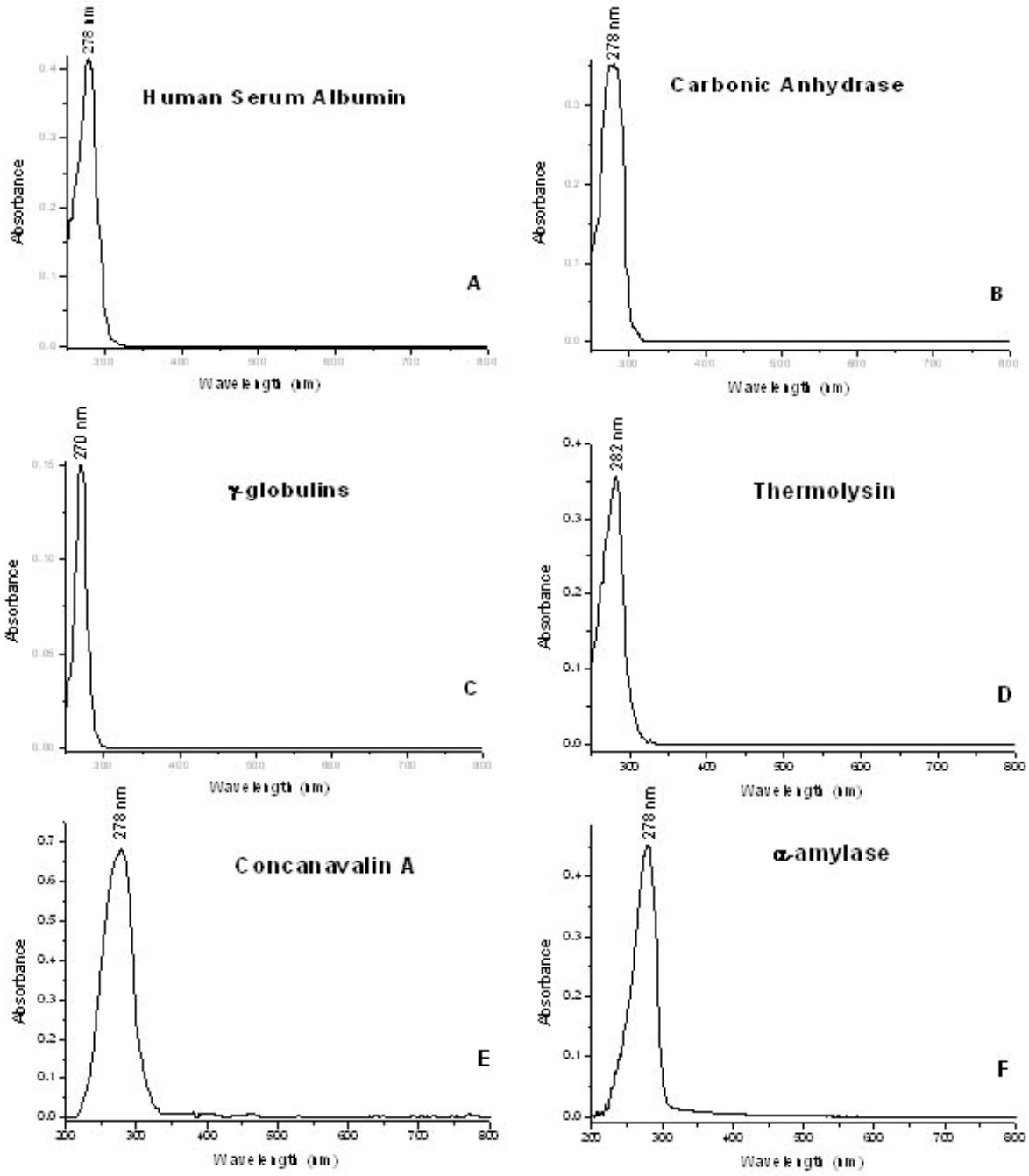

Figure A. 1. UV-vis absorption spectra of 0.6 g/L HSA (A), 0.3 g/L CA (B), 0.9 γ/L g-globulins (C), 0.3 g/L Thermolysin (D), 1.1 g/L Concanavalin A (E), 0.5 g/L α-amylase (F) in 25 mM HEPES buffer.

Measurements were done with a commercial standard spectrophotometer (Cary 50) consisting of a single crystal of dysprosium-activated yttrium aluminum garnet mounted in a cuvette-size holder.

APPENDIX B: FLUORESCENCE SPECTRA OF PROTEINS

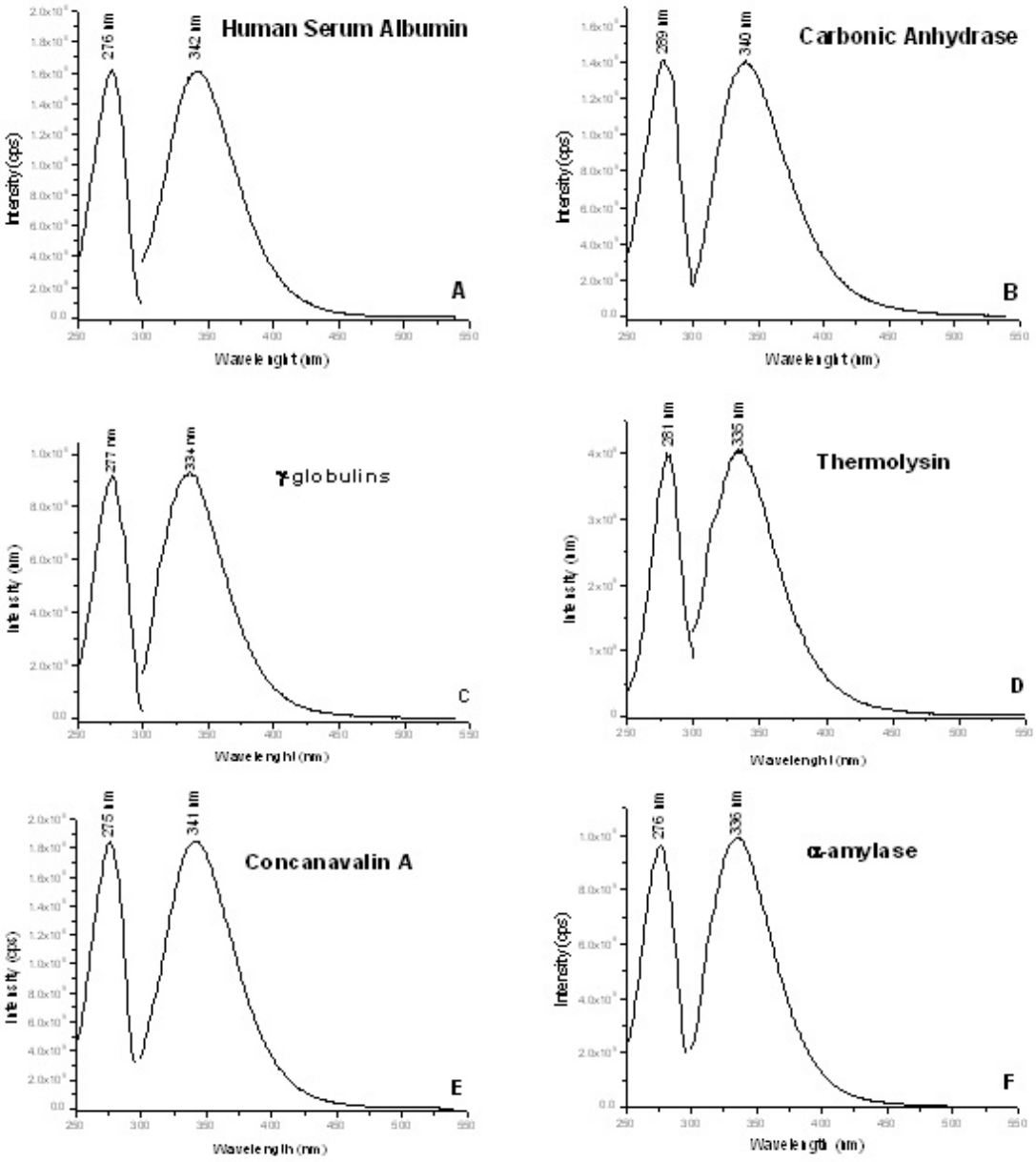

Figure B. 1. Excitation and emission fluorescence spectra of 0.6 g/L HSA (A), 0.3 g/L CA (B), 0.9 γ/L g-globulins (C), 0.3 g/L Thermolysin (D), 1.1 g/L Concanavalin A (E), 0.5 g/L α-amylase (F) in 25 mM HEPES buffer.

Excitation and emission band-pass were 5 nm. Excitation spectra (250-300 nm) were recorded monitoring the fluorescence intensity at emission maximum wavelengths. Emission spectra (300-550 nm) were recorded using excitation maximum wavelengths.

APPENDIX C: CHEMICAL STRUCTURES

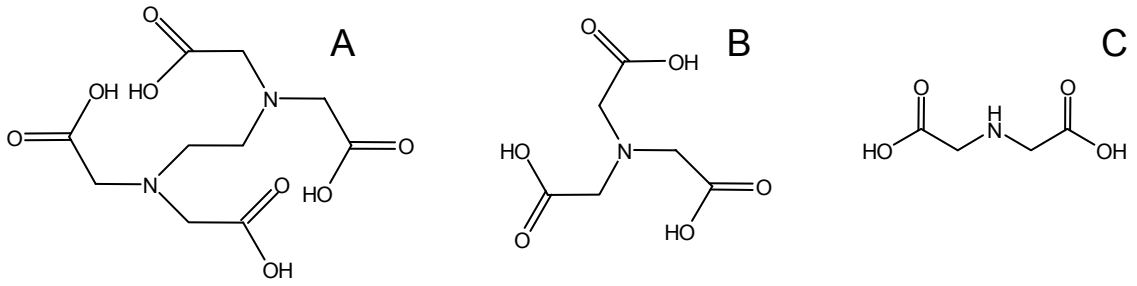

Figure C. 1. EDTA (A), NTA (B) and IDA (C).

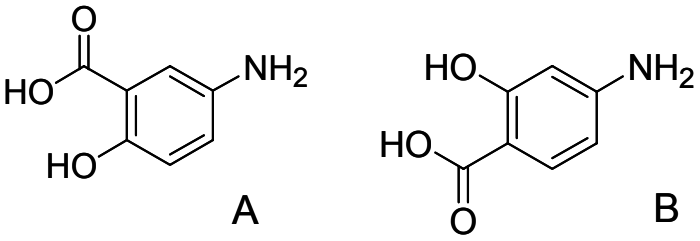

Figure C. 2. 5As (A) and 4As (B).

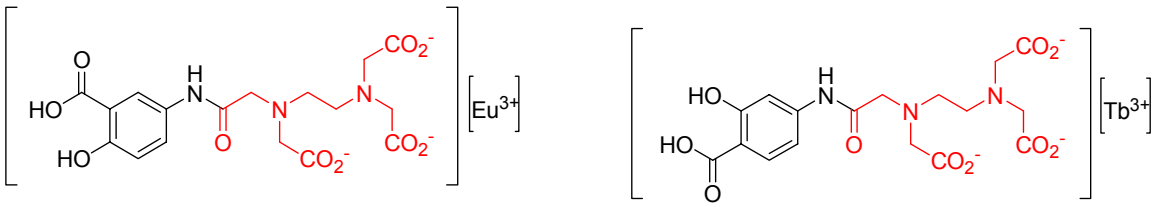

Figure C. 3. 5As-EDTA-Eu^{3+} and 4As-EDTA-Tb^{3+}.

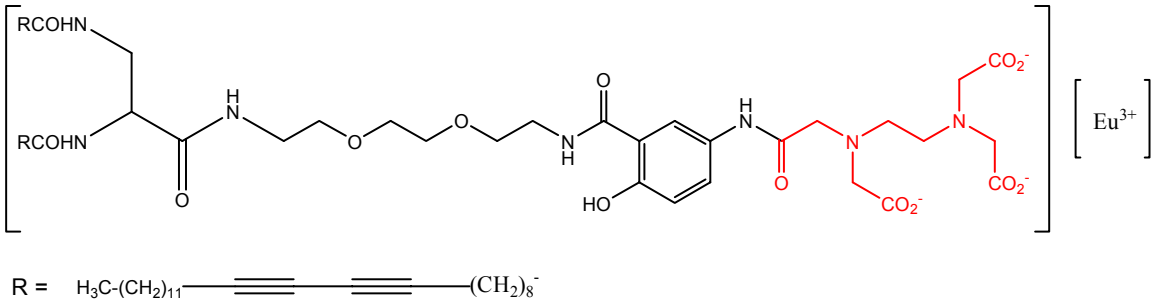

Figure C. 4. Structure of the metal-chelating lipid used to form the polymerized liposomes incorporating 5As-EDTA-Eu^{3+}.

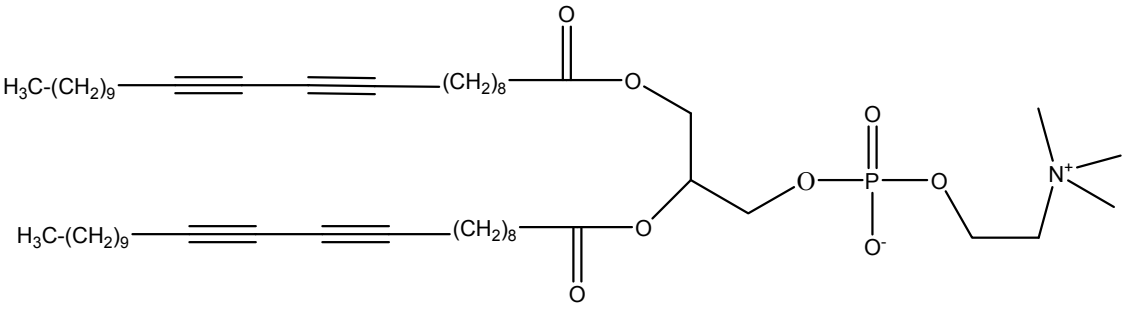

Figure C. 5. Commercially available polymerizable phosphocholine (PC1) used to form the polymerized liposomes.

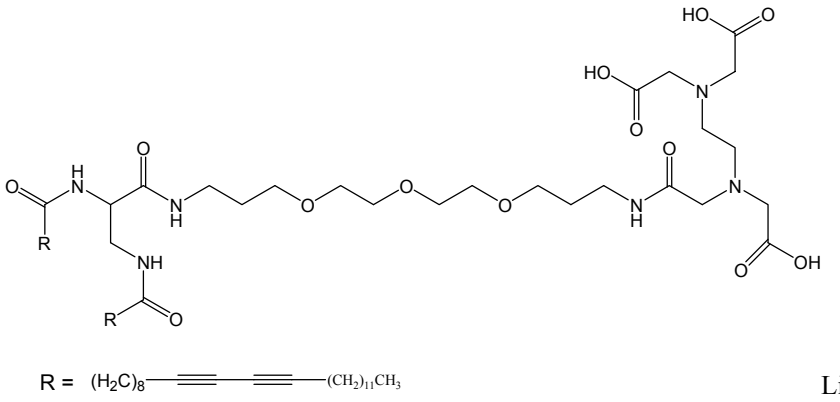

R = $(H_2C)_8$—≡—≡—$(CH_2)_{11}CH_3$ Lipid 1

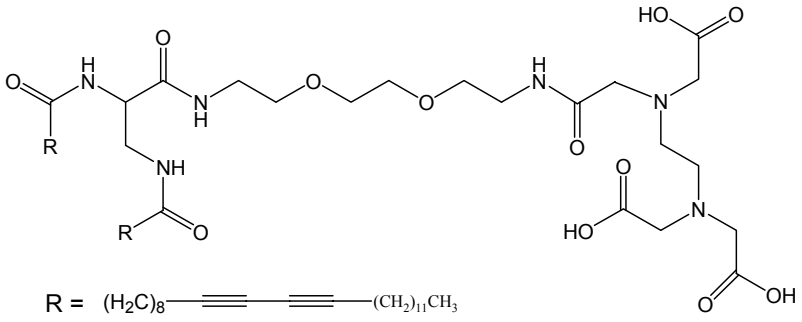

R = $(H_2C)_8$—≡—≡—$(CH_2)_{11}CH_3$ Lipid 2

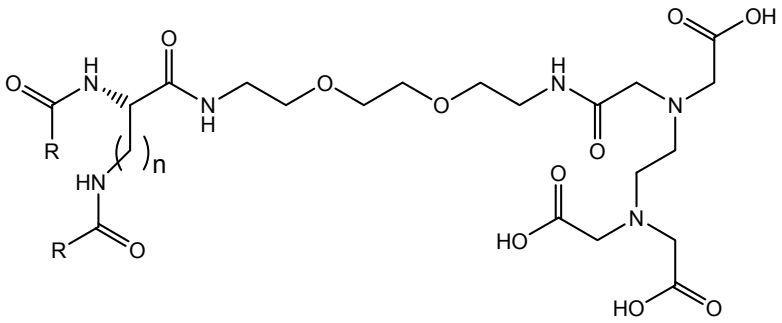

n = 3: Lipid 3: R = —$(CH_2)_{16}CH_3$

Lipid 4: R = —$(CH_2)_8$—≡—≡—$(CH_2)_{11}CH_3$

n = 4: Lipid 5: R = —$(CH_2)_{16}CH_3$

Lipid 6: R = —$(CH_2)_8$—≡—≡—$(CH_2)_{11}CH_3$

Figure C. 6. Structures of the metal-chelating lipids used to form the polymerized liposomes incorporating EDTA-lanthanide^{3+}.

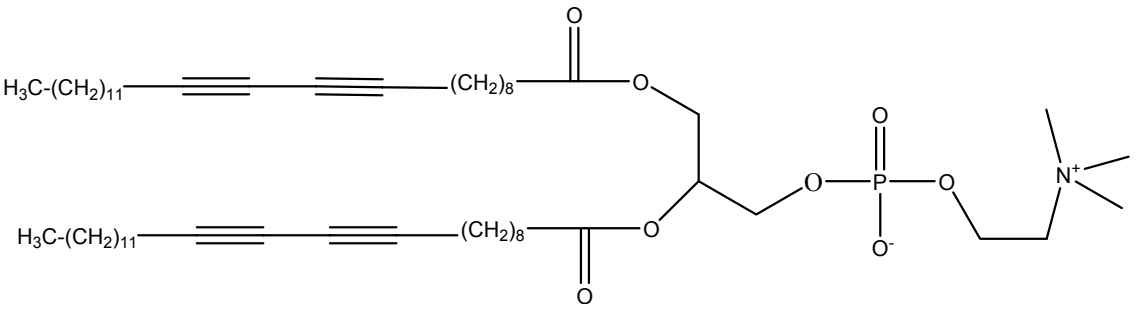

Figure C. 7. Commercially available polymerizable phosphocholine (PC1) used to form the polymerized liposomes incorporating EDTA-lanthanide^{3+}.

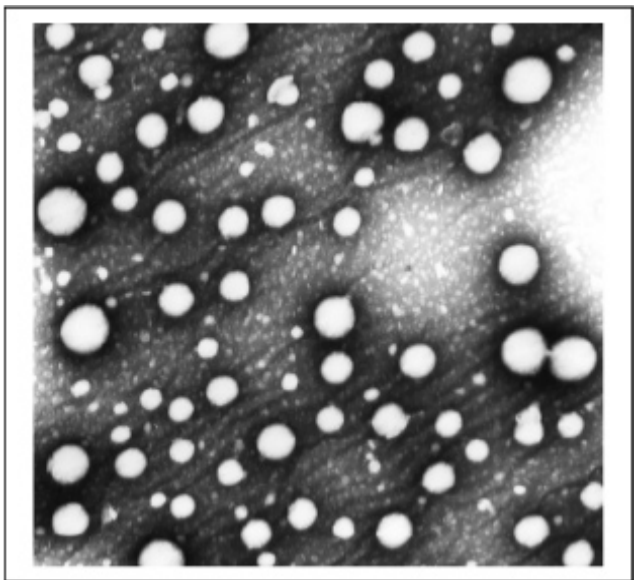

Figure C. 8. Transmission electron micrograph of the polymerized liposomes incorporating 10% (by weight) of lipid 2-Eu^{3+} and 90 % of PC1 (1 mm in the picture corresponds to 21 nm).

The average diameter was found to be ~ 1000 Å.

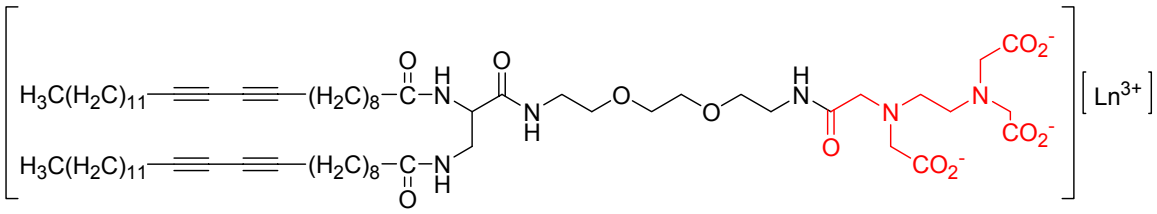

Figure C. 9. Structures of the metal-chelating lipids used to form the polymerized liposomes incorporating EDTA-Ln^{3+} and IDA-Cu^{2+}.

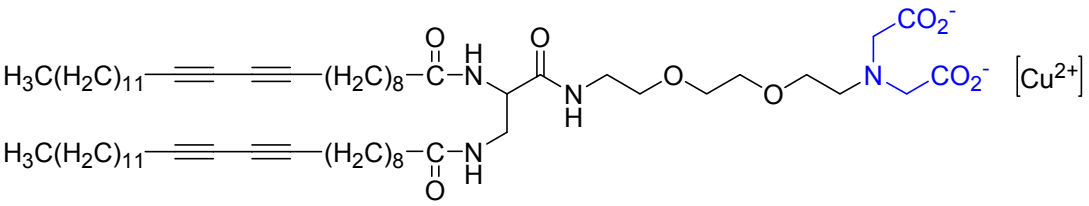

Figure C. 10. Structures of the metal-chelating lipids used to form the polymerized liposomes incorporating IDA-Cu^{2+} and EDTA-Ln^{3+}.

LIST OF REFERENCES

1. M.S. Wolfe, *J. Med. Chem.* **44** (2001) 2039-2060.

2. J.A.A. Ho, and R.D. Wanchope *Anal. Chem.* **74** (2002) 1493-1496.

3. A.K. Deising, M. Thompson *Analyst* **127** (2002) 567-581.

4. I. Arzyl, T. Renault, A. Thebanlt, and A. Gerard *Virus Res.* **84** (2002) 151-160.

5. M. Santos, B.C. Roy, H.C. Goicoechea, A.D. Campiglia, and S. Mallik *J. Am. Chem. Soc.* **126** (2004) 10738-10745.

6. T. Kodadek *Trends Biochem. Sci.* **27** (2002) 295-300.

7. T. Kukar, S. Eckenrode, Y. Gu, W. Lian, M. Meggison, J.X. She, and D. Wu *Anal. Biochem.* **306** (2002) 50-54.

8. H. Lin, and V.W. Cornish *Angew. Chem., Int. Ed.* **41** (2002) 4402-4425.

9. L.Y. Wang, Y.Y. Zhou, L. Wang, C.Q. Zhu, and Y.X. Li, F.Gao *Anal. Chim. Acta* **466** (2002) 87-92.

10. O.H. Lowry, N.J. Rosebrough, A.L. Farr, and R.J. Randall *J. Biol.* Chem. **193** (1951) 265-275.

11. L.P. Kirazov, L.G. Venkov, and E.P. Kirazov *Anal. Biochem.* **208** (1993) 44-48.

12. M.A. Bradford *Anal. Biochem.* **72** (1976) 248-254.

13. M. Tal, A. Silberstein, and E. Nusser, *J. Biol. Chem.* **260** (1985) 9976-9980.

14. A.G. Splittgerber, and J. Sohl *Anal. Biochem.* **179** (1989) 198-201.

15. C.X. Yang, Y.F. Li, and C.Z. Huang *Anal. Sci.* **19** (2003) 1483–1486.

16. L.J. Dong, R.P. Jia, and Q.F. Li *Anal. Chim. Acta* **459** (2002) 313–322.

17. K. Murayama, K. Yamada, R. Tsenkova, Y. Wang, and Y. Ozaki *Vib. Spectrosc.* **18** (1998) 33–40.

18. S. Kasemsumran, Y.P. Du, K. Murayama, M. Huehne, and Y. Ozaki *Anal. Chim. Acta* **512** (2004) 223–230.

19. D.D. Lasic *Liposomes: From Physics to Applications* (1993) Elsevier: New York.

20. *Handbook on the Physics and Chemistry of Rare Earths* (1979) North-Holland Publishing Company

21. P.G. Sammes, and G. Yahioglu *Nat. Prod. Rep.* **13** (1996) 1-28.

22. C. Turro, P.K. Fu, and P.M. Bradley *Met. Ions Biol. Syst.* **40** (2003) 323-353.

23. D. Parker, and J.A. Gareth Williams *J. Chem. Soc., Dalton Trans.* (1996) 3613-3628.

24. J.R. Lackowitz *Principles of Fluorescence Spectroscopy* (1999) New York: Kluwer Academic/Plenum.

25. N.S. Baek, M.K. Nah, Y.H. Kim, S.G. Roh, and H.K. Kim *Bull. Korean Chem. Soc.* **25** (2004) 443-444.

26. W.D. Horrocks Jr., D.R. Sudnick *Acc. Chem. Res.* **14** (1981) 384-392

27. B.C. Roy, M. Santos, S. Mallik, and A.D. Campiglia *J. Org. Chem.* **68** (2003) 3999-4007.

28. V. Torchilin, and V. Weissig Eds. *Liposomes-A Practical Approach* (2003) Oxford University Press: New York.

29. C. Turner, N. Weir, C. Catterall, T.S. Baker, and S. Malcom *J. Liposome Res.* **12** (2002) 45-50.

30. Y. Barenholz, and D.D. Lasic Eds. *Handbook of Nonmedical Applications of Liposomes* (1996) CRC Press: Boca Raton, Fl.

31. Z. Li, Y. Wan, and A. Kutateladze *Langmuir* **19** (2003) 6381-6391.

32. C.H. Reylonds, N. Annan, K. Beshah, J.H. Huber, S.H. Shaber, R.E.Lenkinski, and J.A. Wortman *J. Am. Chem. Soc.* **122** (2000) 8940-8945.

33. F.M. Megli, M. Selvaggi, S. Liemann, E. Quagliariello and R. Huber *Biochemistry* **37** (1998) 10540-10546.

34. D.R. Shnek, D.W. Pack, D.Y. Sasaki, and F.H. Arnold *Langmuir* **10** (1994) 2382-2388.

35. H. Kitano, N. Kato, and N. Ise *Biotechnol. Appl. Biochem.* **14** (1991) 192-201.

36. H. Kitano, K. Sohda, and A. Kosaka *Bioconjugate Chem.* **6** (1995) 131-164.

37. D.S. Johnston, L.R. McLean, M.A. Whittam, A.D. Clark, and D. Chapman *Biochemistry* **22** (1983) 3194-3202.

38. S. Nadi, M. Santos, M.K. Haldar, B.C. Roy, S. Mallik, and A.D. Campiglia *Inorg. Chem.* **44** (2005) 2234-2244.

39. H. Martens, and T. Naes *Multivariate Calibration* (1989) John Wiley and Sons. Chichester.

40. E.V. Thomas, and D.M. Haaland *Anal. Chem.* **62** (1990) 1091-1099.

41. M.E. Ketterer, J.J. Rescht, and M.J. Peters *Anal. Chem.* **61** (1989) 2031-2040.

42. G. Janatch, J.D. Kruse-Jarres, R. Marbach, H.M. Heise *Anal. Chem.* **61** (1989) 2016-2023.

43. M. Otto, and J.D.R. Thomas *Anal. Chem.* **57** (1985) 2647-2651.

44. W. Lindberg, J. Ohman, S. Wold, and H. Martens *Anal. Chim. Acta* **174** (1985) 41-51.

45. W.P. Carey, L.E. Wangen, and J.T. Dyke *Anal. Chem.* **61** (1989) 1667-1669.

46. M. Otto, W. Wegscheider *Anal. Chem.* **57** (1985) 63-69.

47. E. Stark, K. Luchter, and M. Margoshes *Applied Spectroscopy Rev.* **22** (1986) 335-399.

48. R.G. Brereton *The Analyst* **125** (2000) 2125-2154.

49. R. Manne *Chemom. Intell. Lab. Syst.* **2** (1987) 187-197.

50. A. Lorber, L. Wangen, and B.R. Kowalski *J. Chemom.* **1** (1987) 19-35.

51. H. Martens, R. Karstang, and T. Naes *J. Chemom.* **1** (1987) 201-219.

52. J.R. Catai, H.A. Tervahauta, G.J. de Jong, and G.W. Somsen *J. Chrom. A*, **1083** (2005) 185–192.

53. J.C. Miller, J.N. Miller *Statistics for Analytical Chemistry* (1984) Wiley: New York.

54. S. Wold, N. Kettaneh-Wold, and B. Skagerberg *Chemom.. Intell. Lab. Syst.* **7** (1989), 53–65.

55. D.M. Haaland and E.V. Thomas *Anal. Chem.* **60** (1988) 1193-1202.

56. P.J. Gemperline, J.R. Long, and V.G. Gregoriou *Anal. Chem.* **63** (1991) 2313–2323.

57. S. Sekulic, M.B. Seasholtz, Z. Wang, B.R. Kowalski, S.E. Lee, and B.R. Holt *Anal. Chem.* **65** (1993) 835A–845A.

58. S. Wold, N. Kettaneh-Wold, and B. Skagerberg *Chemom. Intell. Lab. Syst.* **7** (1989) 53–65.

59. S. Wold *Chemom. Intell. Lab. Syst.* **14** (1992) 71–84.

60. F. Despagne, and D.L. Massart *Analyst* **11** (1998) 157R–178R.

61. R.M. Carvalho, C. Mello, and L.T. Kubota *Anal. Chim. Acta* **420** (2000) 109–121.

62. Q. Li, X. Yao, X. Chen, M. Liu, R. Zhang, X. Zhang, and Z. Hu *Analyst* **11** (2000), 2049–2053.

63. A.D. Campiglia, A.J. Bystol, and S. Yu *Anal. Chem.* **78** (2006) 484–492.

64. MATLAB 6.0, The Math Works Inc., Natick, MA, (2000).

65. J. Zupan, and J. Gasteiger *Neural Networks in Chemistry and Drug Design* (1999) Wiley-VCH, 2nd edition, Weinheim.

66. H.C. Goicoechea, B.C. Roy, M. Santos, A.D. Campiglia, and S. Mallik *Anal. Biochem.* **336** (2005) 64-74.

67. D.A. Skoog, F.J. Holler, and T.A. Nieman *Principles of Instrumental Analysis* Fifth Ed. (1998) Brooks/Cole US.

68. T. Moeller, D.F. Martin, L.C. Thompson, R. Ferrus, G.R. Feistel, and W.J. Randall *Chem. Rev.* **65** (1965) 1-50.

69. Md. A. Fazal, B.C. Roy, S. Sun, S. Mallik, and K.R. Rodgers *JACS* **123** (2001) 6283-6290.

70. W. Bal, J. Christodolou, P.J. Sadler, and A.J. Tucker *Inorg. Biochem.* **70** (1998) 33-39.

71. P.J. Sadler, and J.H. Viles *Inorg. Biochem.* **35** (1996) 4490-4496.

72. G. Changa, D.E. Bochkariov, G.G. Jokhadze, J. Hopp, and P. Nelson *J. Chromatogr*., *A* **864** (1999) 247-256.

73. U. Sideneus, O. Farver, O. Jons, B. Gamelgaard J. Chromatogr., B 735 (1999) 85-91.

74. M.Y. Wang, Y.Y. Kau, M.S. Lee, S.R. Doong J.Y. Ho, and L.H. Lee Biotechnol. Bioeng. 67 (2000) 104-111.

75. H.P. Wu, and D.F. Bruley Biotechnol. Prog. 15 (1999) 928-931.

76. P.J. Carlsson, I. Olsson, and G. Befrage Nature 258 (1975) 598.

77. A.E. Martell, and P.M. Smith Critical Stability Constants (1975) Plenum Press: New York, Vol. 2.

78. W. Jiang, B. Graham, L. Spiccia, and M.T.W. Hearn *Anal. Biochem*. **255** (1998) 47-58.

79. E. Rohde, A.J. Tomlinson, D.H. Johnson and S. Naylor *J. Chrom. B.* **713** (1998) 301-311.

80. J.R. Catai, H.A. Tervahauta, G.J. de Jong, and G.W. Somsen *J. Chrom. A.* **1083** (2005) 185-192.

81. G.E. Smolka, E.R. Birnbaum, and D.W. Darnall *Biochem.* **10** (1971) 4556-4561.

82. A.D. Sherry, A.D. Newman, and C.G. Gutz *Biochem.* **14** (1975) 2191-2196.

83. H.C. Goicoechea, S. Yu, A. C. Olivieri, and A.D. Campiglia *Anal.Chem.* **77** (2005) 2608 – 2616.

84. S. Yu and A. D. Campiglia. *Anal.Chem* **77** (2005) 1440 – 1447.

85. M. Santos, S. Nadi, H.C. Goicoechea, M. K. Haldar, A. D. Campiglia, and S. Mallik *Anal. Biochem., in press* (2006).